Perovskite Oxides Prepared by Hydrothermal and Solvothermal Synthesis: a Review of Crystallisation, Chemistry, and Compositions

Richard I. Walton*[a]

[a] Department of Chemistry, University of Warwick, Gibbet Hill Road, Coventry CV4 7AL, UK. Email r.i.walton@warwick.ac.uk

Abstract

Perovskite oxides with general composition ABO_3 are a large group of inorganic materials that can contain a variety of cations from all parts of the Periodic Table and that have diverse properties of application in fields ranging from electronics, energy storage to photocatalysis. Solvothermal synthesis routes to these materials have become increasingly investigated in the past decade as a means of direct crystallisation of the solids from solution. These methods have significant advantages leading to adjustment of crystal form from the nanoscale to the micron-scale, the isolation of compositions not possible using conventional solid-state synthesis and in addition may lead to scalable processes for producing materials at moderate temperatures. These aspects are reviewed, with examples taken from the past decade's literature on the solvothermal synthesis of perovskites with a systematic survey of B-site cations, from transition metals in Groups 4-8 and main group elements in Groups 13, 14 and 15, to solid solutions and heterostructures. As well as hydrothermal reactions, the use of various solvents and solution additives are discussed and some trends identified, along with prospects for developing control and predictability in the crystallisation of complex oxide materials.

1. Introduction

Multinary metal oxides are compounds of oxygen and two or more metallic elements. They are long-studied materials that form the basis of a large variety of important technological applications, ranging from materials in advanced electronic devices to industrial catalysts. This makes use of solid-state properties such as electronic conductivity, ionic conductivity, magnetism, ferroelectricity, oxygen storage and redox

activity. Commonly encountered examples of multinary oxides include ferroelectric titanates such as $BaTiO_3$ and $Pb(Ti_{1-x}Zr_x)O_3$ (PZT) used as dielectrics in capacitors and piezoelectric sensors, lithium cobalt oxides, used as cathodes in rechargeable lithium-ion batteries, and barium ferrite used in magnetic data storage. With the contemporary need for new efficient materials for energy-related applications the focus on the design of new solid-state materials is intense.[1] In addition to application as electrodes in batteries, there is a pressing need for new electrolyte materials, not only for cation transport in the same batteries, but in other devices such as solid-oxide fuel cells, where anion transport is required, and multinary oxide materials are likely candidates. In the field of catalysis, emerging work relies on oxide materials in areas such as electrocatalysis[2] photocatalysis,[3] or combinations of both in photoelectrochemical devices,[4] for energy-efficient splitting of water, where a judicious choice on component metals in the oxide allows electronic structure to be fine-tuned. All of these applications rely on the stability of oxides, and this spans thermal stability, mechanical robustness, resilience towards aqueous acidic or alkali conditions, and also towards atmospheric conditions, and this stability is far superior to many other classes of solid materials.

An important aspect of the development of multinary oxides for practical applications is exploration of synthesis conditions. As with all solid-state materials that possess infinitely connected structures in 1-, 2-, or 3-dimensions, the synthesis and crystallisation of oxides essentially occur in one single step. This is unlike molecular substances where the synthesis, even if in one step (but commonly multiple steps for complex organic molecules), is performed in solution from which crystallisation (usually) is a separate, subsequent operation. Furthermore, unlike the case of molecular solids that can be recrystallised or subject to separation procedures to remove impurities, extended solid materials must be produced as phase-pure samples as there is little scope for purification, unless any impurity happens to be conveniently soluble or volatile. This makes synthesis of extended solid structures challenging and means that careful exploration of a wide variety of conditions (temperature, time, pressure), with a large choice of reagents, and many possible reaction media (solvents, molten salts, solid-gas mixtures, *etc.*). Jansen compared the investigative synthesis of inorganic solids to the exploration of a landscape: in this case an energetic landscape where interesting materials lie not just in valleys but at peaks.[5] He thus proposed that a wide

variety of conditions need to be studied to access all possible phases, and that this must be underpinned by theory to provide models of the energy of a system, to then predict ultimately the conditions for synthesis. These ideas were laid out almost 20 years ago but are still very relevant now and although the idea of rational design of new materials remains elusive and computational prediction of synthesis conditions has rarely been attempted, there have been significant advances in prediction of candidate materials.

Of all the methods for the formation of ternary, or higher, oxide materials,[6] the use of a solution phase in synthesis provides a rich set of reagents and conditions for exploration of chemistry leading to novel solids, even if predictability of the outcome of reaction is uncertain. Solvothermal chemistry[7] is now well developed as a tool for the synthetic chemist: the principle is simply to heat a mixture of reagents and solvent close to or above the boiling point of the solvent to bring about chemical reaction. When water is used then hydrothermal conditions are implied and these have been long studied in materials science, initially for the preparation of silicate zeolites, mimicking conditions in the Earth's crust for the formation of minerals,[8] or for the crystal growth of dense materials like quartz.[9] The properties of water when heated in a sealed vessel to generate autogeneous pressure are well defined and for synthetic chemistry, parameters like ionic strength, viscosity, dielectric constant and density can affect the solubility of reagents, the rate of nucleation and the kinetics of crystal growth.[10] While these solvent properties vary greatly above the critical point (374 °C and 218 atm for water), even under much lower temperatures the reaction medium is modified from under ambient conditions so that dissolution and reaction takes place to allow the crystallisation of complex materials. Indeed, much hydrothermal synthesis reported in the chemistry literature use temperatures below 250 °C. Rabenau first reviewed the role of hydrothermal chemistry in preparative chemistry and showed its applicability to many classes of materials from oxides, halides, nitride, chalcogenides, to metals.[10]

In the case of oxide materials, several groups have highlighted the role of hydrothermal chemistry in synthesis.[11] Others have emphasised the use of non-aqueous solvents.[12] The advantages of solvothermal synthesis of oxides can be summarised as: (1) the formation of fine powders with access to various morphologies from the nano-scale to the micron-scale, (2) the isolation of metastable compositions and structures not seen under conventional, high temperature synthesis, and (3) access to solid-solutions and substitutional variants of familiar structure types, not otherwise seen.[13] More specific

works have highlighted the use of the solvothermal method for preparation of electroceramics,[14] thus emphasising the application of the synthesis route for the production of functional materials.

In this review article we will focus on the solvothermal synthesis of one oxide structure type: the perovskite structure. This provides a set of materials that represents a significant family with many contemporary applications in fields such as electronics, photocatalysis and energy storage/conversion. As will be seen, the review illustrates the power of solution synthesis for accessing useful materials as well as the scope for control in their formation and the prospects it offers to access novel functional solids. We will focus only on the case where the solvothermal method has been used for the materials crystallisation, rather than cases where a solvothermal step has been used to prepare a precursor that is subsequent annealed to induce crystallisation: *i.e.*, we draw a distinction between solvothermal *synthesis* and *processing* and discuss only the former. Following an introduction to the perovskite structure, the review will be divided by chemistry, classifying the materials by the B-site constituent of the perovskite, and finishing with the growing work on complex-solid solutions and heterostructures. Our focus will be on the literature in the past 10 years, following from an earlier review article published in 2010.[15]

2. Perovskites

The perovskite chemical composition is ABO_3, where A and B are cations with appropriate charge to achieve neutrality, commonly, $A^{+}B^{5+}$, $A^{2+}B^{4+}$, $A^{3+}B^{3+}$.[16] Other possible combinations exist, as well as cation- or anion-deficient forms, as will be described below with specific examples. The ideal, primitive-cubic unit-cell of perovskite can be visualised as an A-centred or B-centred cell, Figures 1a and 1b, illustrating how the A cation adopts coordination number 12, while the smaller B cation adopts octahedral coordination. A more convenient representation is that of three-dimensional network of corner-shared $[BX_6]$ octahedra that form a network in which the larger A cations reside, Figure 1c. The versatility in the structure lies in its structurally flexibility, in particular distortions of the structure are possible to accommodate a range of relative ionic sizes. The most common of such distortions are concerted rotations of the corner-shared octahedra to maintain their connectivity, while lowering the coordination number of the A-site cations, Figure 1d. Another often found

distortion is displacement of the B-site cations within their octahedra. This can give rise to polar properties, exploited in ferroelectric devices.

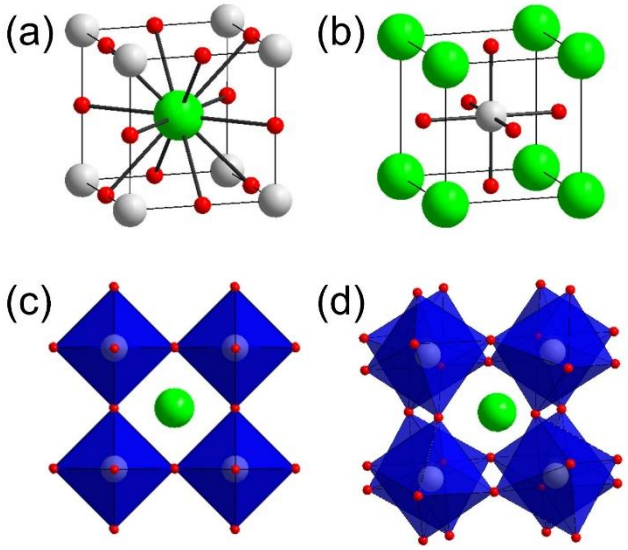

Figure 1: Representations of the perovksite structure: (a) the A unit cell, (b) the B unit cell, (c) the [BO_6] octahedral network of the ideal cubic structure with red spheres oxide ions, green 12-coordinate A cation, and grey octahedral B cations, (d) a distorted orthorhombic unit cell as found for $YFeO_3$ where the octahedra are tilted with respect to each other,

The ABO_3 composition is found in other structure types, some of which are named as perovskites, even though they have different atomic connectivity. One example is the hexagonal structure found for $YMnO_3$, Figure 2a and 2b, with five-coordinate Mn centres connected to give layers, and another, the family of hexagonal materials containing chains of face-sharing octahedra, illustrated by 4H-$SrMnO_3$, Figure 2c, and 2H-$BaMnO_3$, Figure 2d.

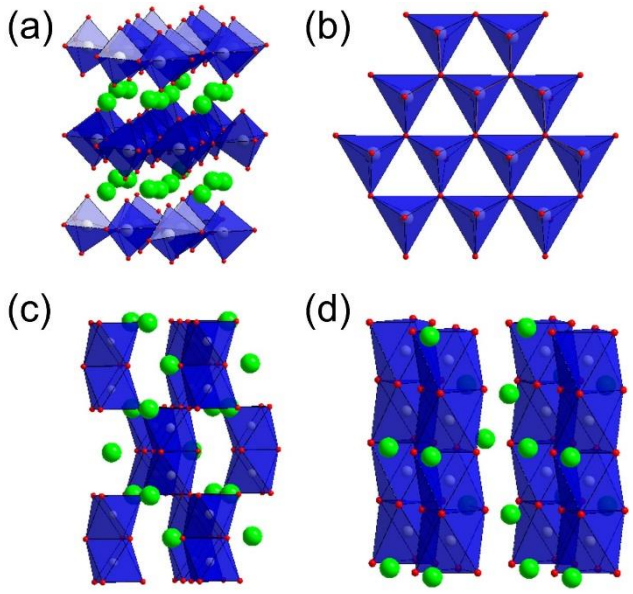

Figure 2: Examples of hexagonal perovskites (a) the hexagonal layered $YMnO_3$ structure with (b) showing a view perpendicular to the layers, (c) 4H-$SrMnO_3$ and (d) 4H-$BaMnO_3$. In all cases the blue octahedra are [BO_6] with red oxide vertices, and the green spheres are the A cations.

The properties of perovskites will be illustrated in the examples chosen in the following sections, and many of these are long established, such as the dielectric properties of $Pb(Zr_{1-x}Ti_x)O_2$ used in capacitors in many electronic devices. But many properties are still being investigated and discovered, such as complex magnetism and superconductivity. The use of perovskites in heterogeneous catalysis is also becoming the focus of growing attention,[17] in areas such as photocatalysis for water splitting and pollutant abatement.[18] This growing emphasis on bulk materials' properties leads to a need for innovative chemical synthesis for perovskites, not only for convenience, but that may offer a higher level of tuning of properties from crystal morphology or novel compositions. One example is in the formation of nanocrystalline forms of perovskites that may have properties different from bulk materials, particularly those prepared by conventional high temperature annealing methods.[19]

3. Survey of perovskites isolated under solvothermal conditions

3.1 Titanates, zirconates and hafnates

$BaTiO_3$ is a material long-studied as the prototypical dielectric and ferroelectric oxide and its properties find use in a range of applications in electronic devices including

multilayer capacitors, transducers, transistors, thermistors actuators, and has related properties such as electrooptical activity, electromechanical, and for dynamic random-access memory devices.[20] The hydrothermal synthesis of $BaTiO_3$ was reported in patents in 1940s,[21] and described briefly by Flaschen in a 1955 paper.[22] Since that time numerous studies of the hydrothermal, and more generally solvothermal, synthesis of $BaTiO_3$ have been reported and this provides a model system for understanding the solution-mediated crystallisation of multinary oxides, as highlighted in our earlier review article, where aspects of crystal growth mechanism and control of crystal morphology was highlighted.[15]

For practical applications, solution-mediated synthesis of $BaTiO_3$ also gives significant advantages, particularly for device fabrication, and this has become more intensely investigated in the past decade. As well as growth of thin films, recent attention has focussed on the preparation of nanoscale powders of $BaTiO_3$, since this is relevant for the miniaturisation of devices, and for the preparation of nanocomposites, where oxide particles are dispersed in, for example, a polymer matrix.[23] The fabrication of polymer composite materials requires the surface of particles to be functionalised to ensure compatibility and the advantage of solution-produced oxide particles is often the prevalence of surface hydroxide moieties for easy chemical modification.[24] The use of high aspect ratio particles is of particular interest in the production of polymer nanocomposites as the resultant properties may be significantly different than those of the individual components. For example, Feng *et al.* prepared nanowires of $BaTiO_3$ by a hydrothermal reaction in the presence of polyethylene glycol (PEG 6000) and then fabricated a composite with poly(vinylidene fluoride-trifluoroethylene) that showed a higher dielectric constant than a similar composite prepared using nanoparticles of $BaTiO_3$.[25] Tu *et al.*, prepared nanowire $BaTiO_3$ using nanowires of $Na_2Ti_3O_7$ as a precursor in a hydrothermal conversion, and then were able to disperse the $BaTiO_3$ fibres in the thermo-polymer poly(arylene ether nitrile) to give a composite with energy storage density appropriate for application in film capacitors.[26]

There is also continued fundamental interest in studying the effect of nanoscale confinement on the phase transitions and resulting dielectric response. It was established earlier that the high temperature cubic polymorph of $BaTiO_3$ may be stabilised in small particles prepared by hydrothermal chemistry, but that this may also be due to the presence of trapped defects, such as hydroxyl groups.[27] Interestingly, the

addition of chloride to the hydrothermal synthesis solution produced the expected tetragonal polymorph,[28] and hydrothermal reactions in the presence of ethylene glycol also gave the tetragonal phase.[29] Hongo *et al.* proved that the ethylene glycol modified synthesis gave a level of hydroxide three times higher than in conventional aqueous synthesis and then used a combination of powder X-ray diffraction and modelling to identify likely locations of hydroxide defects in $BaTiO_3$.[30] This work ascribed the stabilisation of the tetragonal perovskite, to a *trans* orientation of substituent hydroxide ions in the oxide sublattice. Defects have been reported in more complex titanate perovskites from hydrothermal synthesis, such as $Na_{0.5}Bi_{0.5}TiO_3$[31] and $NaCe_{1-x}La_xTi_2O_6$ ($0 < x < 1$),[32] where in the former, the piezoelectric properties showed evidence of polarisation pinning due to oxide vacancies after sintering. Recent work has studied hydrothermally prepared $BaTiO_3$ nanocrystals in combination with scanning transmission electron microscopy and showed how different directions of titanium-ion shifts are found near the top surface compared to in the middle of the nanoparticles, Figure 3.[33] This illustrates how the availability of fine powders of the material may allow properties to be tuned, beyond the average crystal structure, with local atomic displacements and their distributions providing novel characteristics.

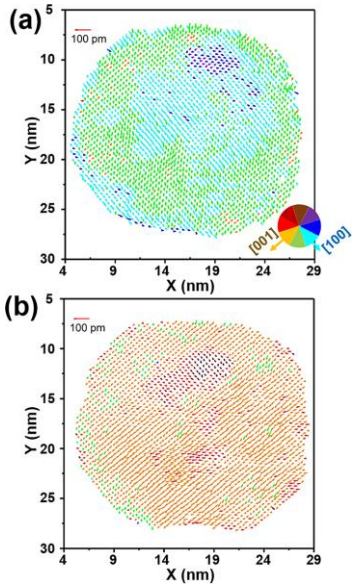

Figure 3: Maps of ferroelectric shift of a $BaTiO_3$ nanoparticle from hydrothermal synthesis derived from scanning transmission electron microscopy imaging at two different focuses showing contrast between (a) surface and (b) centre titanium-ion shift. The positions, directions, and lengths of the arrows indicate the titanium-ion positions and the directions and magnitudes of the shifts. Reprinted with permission from Y.

Sato, M. Aoki, R. Teranishi, K. Kaneko, M. Takesada, H. Moriwake, H. Takashima, Y. Hakuta, *ACS Appl. Nano. Mater.* **2019**, *2*, 5761-5768. Copyright (2019) American Chemical Society.

As well as fundamental studies of properties, and fabrication of devices, there has been continued work on the size and shape control of $BaTiO_3$ particles by solvothermal synthesis. As mentioned above, pre-made $Na_2Ti_3O_7$ nanowires could be used as a 'template' to form nanowires of $BaTiO_3$ upon hydrothermal treatment, [26] and this method was also used by Xie *et al.* who formed $BaTiO_3$ nanowires with length up to tens of micrometres *via* a stirred hydrothermal method, where the stirring speed allowed control over the materials formed.[34] The idea of 'shape memory' of products based on choice of particle morphology of precursors was previously used in $BaTiO_3$ hydrothermal synthesis to prepare various shaped particles, from rods to platelets.[35] The formation mechanism clearly cannot involve complete dissolution of the precursor, as that would imply loss of the shape memory, but must instead involve some heterogeneous pathways with diffusion of Ba^{2+} into the solid precursor, corresponding to the '*in situ* mechanism' proposed earlier by Eckert *et al.*[36] Cao *et al.* used 'nano-whiskers' of $K_2Ti_4O_9$ and proposed that ion-exchange of K^+ by Ba^{2+} initially occurs, followed by recrystallisation, such that the anisotropic particle morphology is first retained; this is then followed by secondary growth of nanoparticles, leading to coated rods and then ultimately dispersed nanoparticles as the rods are completely consumed, Figure 4.[37]

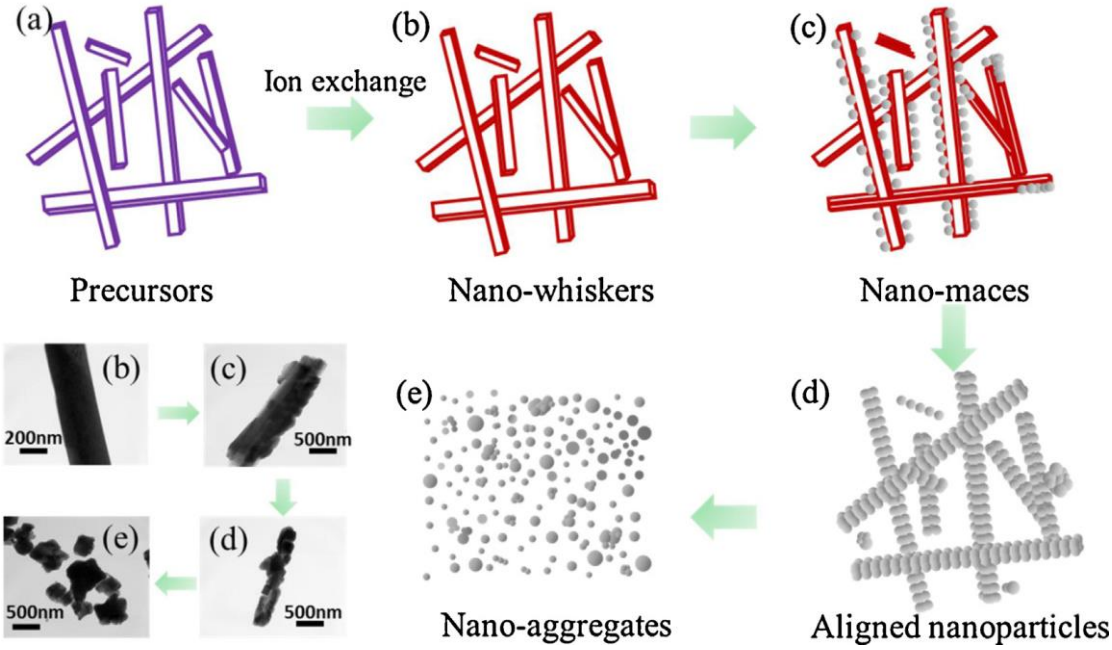

Figure 4: Proposed mechanism for the hydrothermal formation of $BaTiO_3$ nanostructures from a $K_2Ti_4O_9$ precursor with different alkaline concentration (a) 0.2 M (b), 0.4 M (c), 0.6 M (d), 0.8 M (e). Reprinted from *Materials Research Bulletin*, Vol 57, Y. Cao, K. J. Zhu, Q. L. Wu, Q. L. Gu, J. H. Qiu, Hydrothermally synthesized barium titanate nanostructures from $K_2Ti_4O_9$ precursors: Morphology evolution and its growth mechanism, Pages 162-169, Copyright (2014), with permission from Elsevier."

Lamberti *et al.* exploited the shape memory effect to convert aligned arrays of TiO_2 nanotubes into arrays of $BaTiO_3$, and measured their ferroelectric properties.[38] Using hollow TiO_2 spheres as precursors was shown to yield 'nano-torus' crystals of $BaTiO_3$, that were shown to have enhanced microwave absorption compared to solid $BaTiO_3$ nanoparticles, suggesting promise as effective microwave absorbers.[39] Ye *et al.* used intricately shaped TiO_2 precursors prepared from ZnO templates for the hydrothermal formation of various $ATiO_3$ materials (A=Sr, Pb or Ba) from acetate precursors $A(CH_3COO)_2$: the complex flower-shaped precursor yielded a 'garden' of crystal morphologies with superior photocatalytic activity for the degradation of methyl blue.[40]

Another method of shape control of crystals is to use solution additives that may coordinate to the surface of growing crystals, adjusting their final morphology, or may complex with solution species, controlling their release to the growing crystals. Maxim *et al.* surveyed a range of such additives, poly(acrylic acid) (PAA),

poly(vinylpyrrolidone) (PVP), sodium dodecylsulfate (SDS), hydroxypropylmethylcellulose (HPMC), and D-fructose and found that PAA prompted oriented attachment secondary growth, PVP, SDS and HMPC acted as growth inhibitors to yield nanoscale crystallites, while D-fructose increased the activation energy for nucleation.[41] Ma *et al.* used a highly water-soluble Ti precursor, bis(ammonium lactate) titanium dihydroxide, $Ba(OH)_2$, and additives tert-butylamine and oleic acid to form 25-nm cubes of $BaTiO_3$ from NaOH solutions, finding that the addition of oleic acid produced roughened, facetted surfaces, Figures 5a and 5b.[42] Monodisperse hollow perovskite $BaTiO_3$ nanostructures were prepared by a sol gel hydrothermal method using acetylacetone as a modifier in the initial TiO_2 sol itself prepared from hydrolysis of tetrabutyl titanate, Figure 5c and 5d.[43] Zhan *et al.* performed synthesis in polyethyleneglycol-20 and proposed a reaction mechanism by which colloidal TiO_2 initially forms and nucleation of $BaTiO_3$ occurs at the surface, followed by orientated connection and crystal extension *via* an Ostwald ripening process; this ultimately lead to dodecahedral crystals with {110} crystal faces.[44]

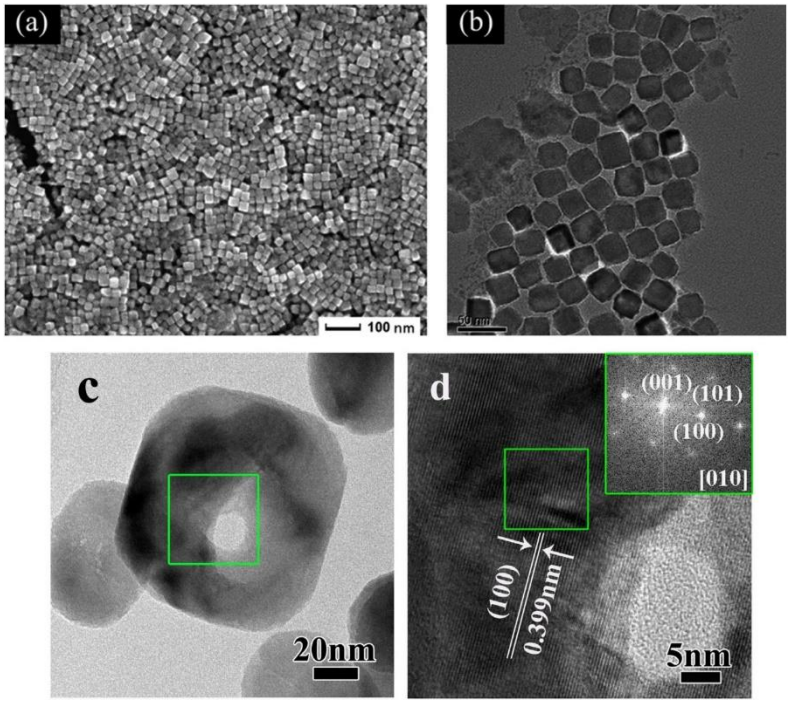

Figure 5: Examples of shapes of $BaTiO_3$ produced by hydrothermal synthesis: (a) and (b) Cubes shown by scanning electron microscopy and transmission electron microscopy images, respectively. Reprinted from Journal of Alloys and Compounds, Vol 655, Q. Ma, K. Mimura, K. Kato, Tuning shape of barium titanate nanocubes by combination of oleic acid/tert-butylamine through hydrothermal process, Pages 71-78,

Copyright (2016), with permission from Elsevier. (c) and (d) Hollow nanocubes shown by TEM at two magnifications with the green boxes indicating the higher magnification areas. Reprinted from Ceramics International, Vol 40, X. Yang, Z. H. Ren, G. Xu, C. Y. Chao, S. Jiang, S. Q. Deng, G. Shen, X. Wei, G. R. Han, Monodisperse hollow perovskite $BaTiO_3$ nanostructures prepared by a sol–gel–hydrothermal method, Pages 9663-9670, Copyright (2014), with permission from Elsevier

Similar principles have been applied to the synthesis of various other $ATiO_3$ perovskite powders. For example, Yang *et al.* produced hollow cubes of $CaTiO_3$ from poly(ethylene glycol) (PEG-200)-water mixed solutions.[45] In the absence of water agglomerates of 40 nm primary particles were observed, but with increasing water content hollow cube-shaped particles of several hundred nanometres in dimension were found, and a mechanism of oriented aggregation was proposed, aided by the polymer additives, Figure 6.[45] Such hollow nanocrystals were later shown to possess useful photocatalytic properties.[46]

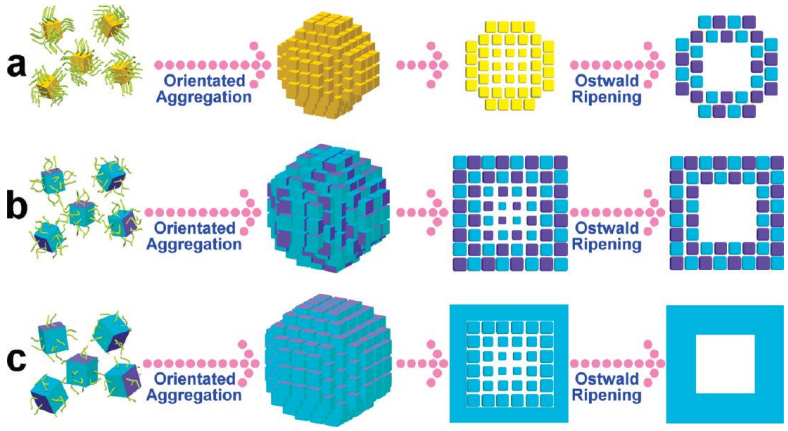

Figure 6: Formation mechanisms proposed for the hydrothermal formation of $CaTiO_3$ hollow crystals in the presence of poly(ethylene glycol) with different microstructures in (a) water-free, (b) 1.25 vol % water, and (c) 5 vol % water. Reprinted with permission from X. F. Yang, J. X. Fu, C. J. Jin, J. A. Chen, C. L. Liang, M. M. Wu, W. Z. Zhou, *J. Am. Chem. Soc.* **2010**, *132*, 14279-14287. Copyright (2010) American Chemical Society.

Many other shapes of $CaTiO_3$ nanoparticles have now been reported from solvothermal reactions depending on the combination of the choice of starting materials, solvents, pH and reaction time and temperature, and some examples are shown in Figure 7. This

includes cross-shaped,[47] solid cuboid,[48] solid spheres,[48a] tubular,[49] rod-shaped,[50] concave-faced cubes,[50a] spheres of agglomerated nanosheets,[51] as well as more complex dendritic morphologies,[52] and intergrowths of primary particles.[53]

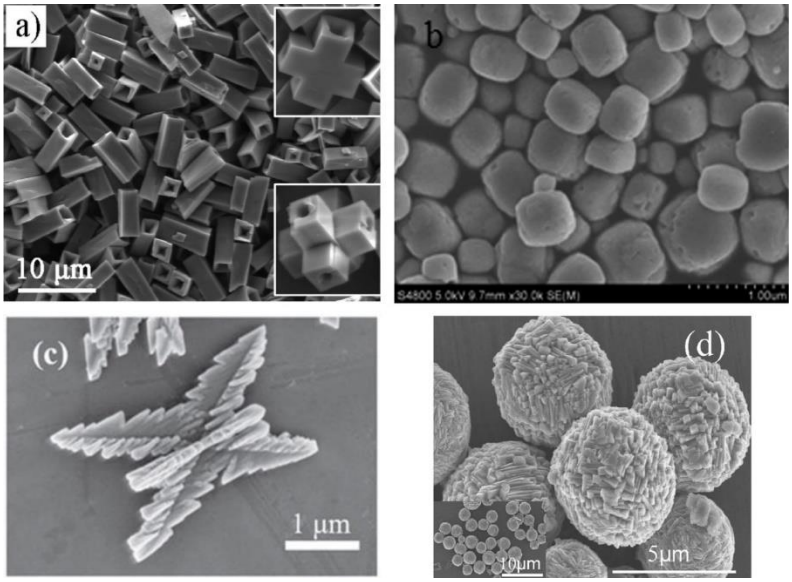

Figure 7: Various shapes of $CaTiO_3$ crystals from solvothermal synthesis. (a) Tubular from aqueous sodium hydroxide. Reprinted with permission from D. B. Yu, J. H. Zhang, F. Wang, M. H. Zhao, K. Du, S. W. Shu, J. W. Zou, Y. Wang, *Cryst. Growth Des.* **2013**, *13*, 3138-3143.. Copyright (2013) American Chemical Society. (b) Cuboid from water. Reproduced from Ref. 48a with permission from the Centre National de la Recherche Scientifique (CNRS) and The Royal Society of Chemistry. (c) Dendritic from ethanolic tetramethylammonium hydroxide. Reproduced from reference [52d], © IOP Publishing. Reproduced with permission. All rights reserved. (d) Microspheres of agglomerated sheets from water-ethanol-NaOH. Reprinted from Applied Surface Science, Vol 349, W. X. Dong, B. Song, W. J. Meng, G. L. Zhao, G. R. Han, A simple solvothermal process to synthesize $CaTiO_3$ microspheres and its photocatalytic properties, Pages 272-278, Copyright (2015), with permission from Elsevier

In the case of $SrTiO_3$, formed under solvothermal conditions in mixed PEG-200/water, Zhan *et al.* showed the photocatalytic activity for dye degradation was correlated with the growth stage of the nanocrystals, being related to the surface morphology and defect chemistry.[54] This suggests that a fine tailoring of bulk material properties for such perovskites should be possible dependent on precise crystal architecture on the nanoscale. For the distorted perovskite $PbTiO_3$, hydrothermal synthesis yielded

nanosheets by use of employing layered $K_2Ti_6O_{13}$ nanofibres as titanium sources,[55] but the nanosheet morphology could also be obtained when using KNO_3 as a solution additive, which was attributed to the interaction of the alkali cations with the growing crystal faces.[56] These results imply that the shape-memory effect may be more complex and that the role of counter-ions is also important to consider.

The quaternary titanate $Na_{0.5}Bi_{0.5}TiO_3$, which contains a randomised distribution of Na^+ and Bi^{3+} on its A-site, is another oxide of interest for its ferroelectricity, and its complex phase transitions.[57] The synthesis of this material by conventional solid-state synthesis can be challenging since bismuth and its oxides are rather volatile and so when using high temperatures, achieving the desired composition can be difficult, leading to defective materials. By hydrothermal synthesis the material crystallises directly,[58] although several competing phases must be avoided by choice of pH and alkali reaction medium.[59] Morphology control is possible from spherical agglomerates of primary nanocubes, nanowires and microcubes, depending on NaOH concentration and reaction temperature,[60] and Zhou *et al.* used piezoresponse force microscopy to analyse the ferroelectric response of individual crystallites, Figure 8.[61]

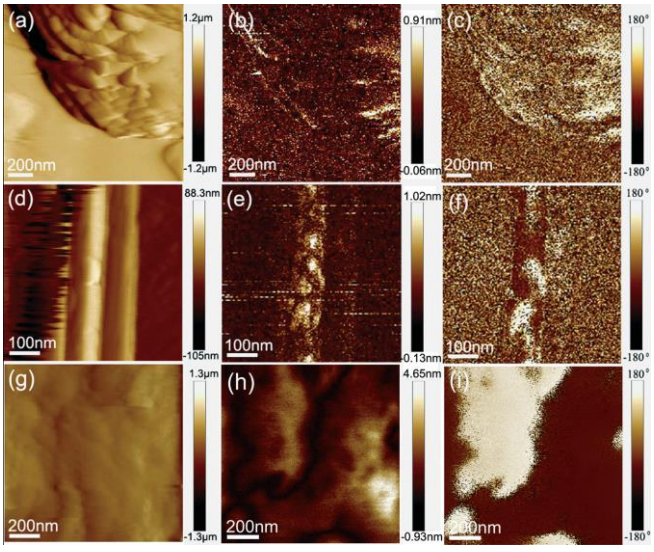

Figure 8: Atomic force microscopy images of $Na_{0.5}Bi_{0.5}TiO_3$: topographic images, piezoresponse force microscopy (PFM) amplitude images and PFM phase images from left to right, of spherical agglomerates, nanowires and microcubes, from top to bottom. Reproduced from Ref. 61 with permission from The Royal Society of Chemistry.

The fine powders of $Na_{0.5}Bi_{0.5}TiO_3$, and $K_{0.5}Bi_{0.5}TiO_3$, produced hydrothermally can be processed more easily than those prepared using conventional solid-state synthesis into

densified ceramics,[62] although as noted above the presence of defects may diminish bulk electronic properties upon annealing into ceramics.[31] The photocatalytic properties of $Na_{0.5}Bi_{0.5}TiO_3$ nanocubes from hydrothermal synthesis have also been studied, and degradation of nitric oxide proved possible, more efficiently than a reference TiO_2 catalyst.[63] A low level of Zr-substitution in $Na_{0.5}Bi_{0.5}TiO_3$ has also been proven possible by a direct hydrothermal reaction, and densified ceramics from the fine powder of $Na_{0.5}Bi_{0.5}Ti_{0.99}Zr_{0.01}O_3$ showed lower remnant polarisation and enhanced piezoelectric response.[64]

More complex perovskite-related structures are found for titanates and some of these have been accessed by hydrothermal routes. $K_2La_2Ti_3O_{10}$ belongs to the Ruddlesden–Popper family of layered perovskites that can be considered as intergrowths of perovskite-type and rocksalt-type slabs; hydrothermal synthesis provided micron-sized crystallites with enhanced photocatalytic activities over solid-state samples.[65]

Zirconate and hafnate perovskites, $AZrO_3$ and $AHfO_3$, have also been prepared by solvothermal routes for A = Ca, Sr, Ba, Pb, Zn. Microwave synthesis has been particularly effective for the formation of $BaZrO_3$: Longo and co-workers produced the material as micron-sized decaoctahedron-shaped crystallites at 140°C in just 40 minutes, [66] and proposed a crystallisation mechanism based on the mesoscale self-assemblies of nanoparticles, which was dependent on the surfactant used as a solution additive, Figure 9. The samples were shown to have photoluminescence properties, which were rationalised on the basis of defects using computation.[67] Borja-Urby used the method to form Bi/Si doped samples for use in photocatalysis.[68] In general it is found that the microwave method offers the best prospect for synthesis of fine powders with narrow particle size distribution.[69] Conventional heating does not necessitate long reaction times, however, or very high temperatures for the formation of crystalline $BaZrO_3$: Boschini *et al.* showed that precipitation of the solid occurs below 100 °C in only 15 minutes with sufficiently high concentration of NaOH,[70] while Yamaguchi *et al.* showed that $BaZrO_3$ and $BaHfO_3$ crystallised at only 50 °C from a zirconia or hafnia gel and barium hydroxide after 10 days.[71] More typically, however, higher temperatures have been applied: for example, Dong *et al.* heated aqueous KOH solutions of salt precursors at 200 °C for 24 hours to yield hollow spherical particles of $BaZrO_3$.[72] Kanie *et al.* used a seeding approach, by heating zirconium oxyacetate and

barium hydroxide for 200 °C in methanol for 24 hours to yield seed crystals that were returned to hydrothermal conditions with a barium hydroxide and a Zr-triethanolamine complex at 250 °C to finally produce $BaZrO_3$ as monodisperse spherical crystallites.[73] The same group have also investigated control of particle shape by changing metal ion concentrations, to give spherical, rhombic dodecahedral, and flower-shaped $BaZrO_3$ particles; this also allowed Eu^{3+}-doped samples to be prepared that had modified photoluminescence properties.[74] Ce^{4+}-substituted $BaZr_{1-x}Ce_xO_3$ materials were prepared by Zhang *et al.* directly from aqueous NaOH, who used the powders as a sonocatalyst for the degradation of a model organic pollutant,[75] while Yb^{3+}-doped samples were studied for their photoluminescence.[76] Using EDTA as a solvent gave hollow $BaZrO_3$ nanocrystals that were shown to have a high concentration of oxygen vacancies that gave photocatalysis properties for hydrogen evolution from water.[77]

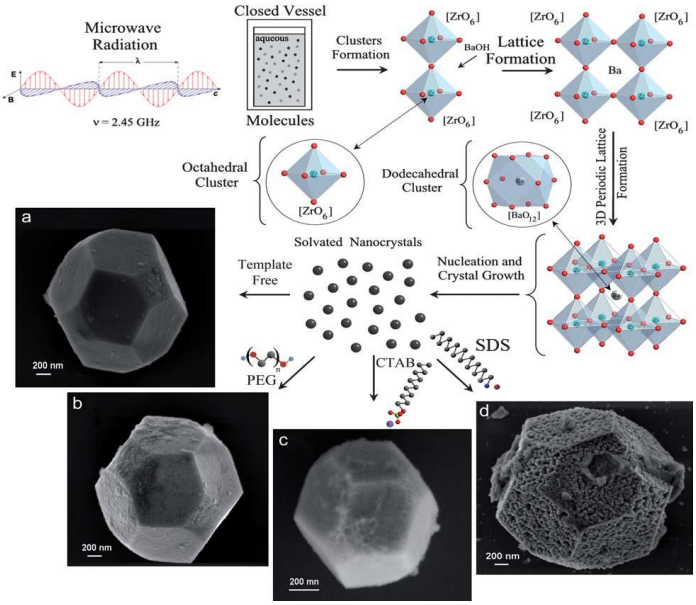

Figure 9: Formation mechanism of $BaZrO_3$ in microwave hydrothermal reactions in the presence of surfactants proposed by Macario *et al.* Reproduced from Ref. 6 with permission from The Royal Society of Chemistry.

In the case of $SrZrO_3$, $SrHfO_3$ and $BaZrO_3$, aggregation of primary particles led to hollow nanocubes in the absence of any template from $Sr(NO_3)_2$ and $HfCl_4$ as the starting materials in aqueous KOH: these nanostructures showed enhanced photoluminescence properties.[78] Thin films, around 5 μm thickness, of $PbZrO_3$ were grown directly onto NiTi alloy substrates using an ultrasonic-assisted hydrothermal

method.[79] The material $ZnZrO_3$ has also been produced directly via hydrothermal crystallisation.[80]

In this section we also consider the hydrothermal synthesis of PZT, *i.e.* $Pb(Zr_{1-x}Ti_x)O_3$ that contains mixed B-site Group 4 cations. This is another well-studied dielectric material that finds common application in electronic devices, despite the push to remove lead from commercial products.[81] Compositions close to $x \approx 0.47$ are particularly relevant since these lie close to the morphotropic phase boundary, the boundary between the tetragonal and the rhombohedral phases, where maximum values of dielectric permittivity, piezoelectric coefficients and electromechanical coupling factors of PZT are found at room temperature.[82] Early work on hydrothermal synthesis of PZT investigated the formation of both polycrystalline powders and thin films from hydrothermal chemistry using various precursors in KOH solution up to 180 °C.[83] As with $BaTiO_3$, in the past decade, work on the synthesis of PZT from solution has focussed on the control of crystal form. This includes the formation of powders of well-dispersed, sub-micron particles,[84] intricate microstructures,[85] and arrays of nanowires.[86] Direct growth of films on various substrates has proved possible, [14b, 87] and hydrothermally grown particles have been used to form composites, for example, by embedding in polymer host matrices.[88] In many cases favourable electronic properties were reported, either from ceramics formed from sintered powders or from the layers deposited. Bian *et al.* concluded that that A-site deficiency may degrade the sinterability of PZT powders, and showed how hydrothermal synthesis of PZT powders with appropriate Pb excess was a useful method to increase sinterability, lower sintering temperature and lessen the loss of Pb by volatilisation during the fabrication of ceramics.[89] Datta *et al.* produced nanoparticles of PZT by pulsed laser deposition on a strontium titanate substrate and then by hydrothermal treatment converted these to hierarchically ordered surface structures to allow the fabrication of capacitors with symmetric ferroelectric hysteresis loops and a high remnant polarisation, Figure 10.[90] Takada *et al.* formed plate-like particles using oleic acid as a solution additive and then could align these on a substrate to give a layer that was conveniently annealed into a film at low temperature (600 °C) and from which local piezoelectric properties were measured *via* piezoresponse force microscopy.[91]

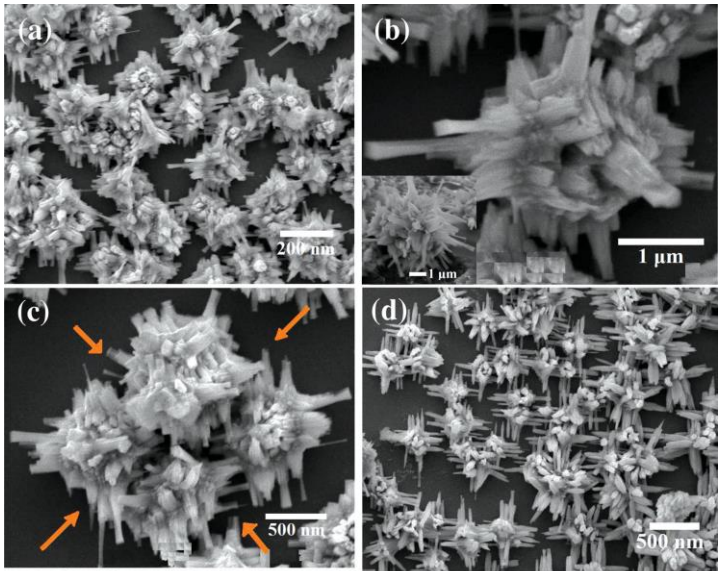

Figure 10: SEM images of the hierarchical growth of PZT (a,b,c) 10 h and (d) 12 hour of hydrothermal treatment on PZT seeds on a strontium titanate substrate. Reproduced from Datta *et al.*[90]

3.2 Niobates and tantalates

$ANbO_3$ and $ATaO_3$ perovskites (A = Na, K) are of great interest as parent members of solid solutions that have been intensely studied as ferroelectric materials to replace the lead-containing PZT materials that find widespread use in electronic devices.[81, 92] The hydrothermal synthesis of the ternary end members is now well established, following on from a body of work more than 15 years ago, in which the direct reaction between Nb_2O_5 (or Ta_2O_5) and aqueous solutions of NaOH or KOH yielded the perovskites directly as fine polycrystalline powders.[93] The simplicity of the synthesis could easily be adapted to allow epitaxial growth of films of the perovskite on suitable substrates.[94]

The early studies of $NaNbO_3$ crystallisation pointed out that the formation of the polyoxometallate anion $[Nb_6O_{19}]^{8-}$ (the hexaniobate Lindqvist ion) was commonly observed as a competing product in these reactions, especially at short reaction times, lower temperatures or as a function of solution pH.[93a, 93d, 95] The Lindqvist ion is structurally unrelated to the perovskite product so cannot be considered an intermediate in the sense of structure formation. It is rather a metastable phase that redissolves on continued reaction time to yield ultimately the dense product, following Ostwald's rule of successive crystallisations. In fact other phases are observed at early times in the

hydrothermal formation of $NaNbO_3$, including the tunnel-structured $Na_2Nb_2O_6{\cdot}nH_2O$.[93d, 96] Our own *in situ* X-ray diffraction study of the hydrothermal crystallisation of $NaNbO_3$ showed the transient presence of these, and other crystalline phases, at reaction temperature (and pressure), *i.e.* not just upon quenching.[97] This work also revealed that by how adjusting the pH, a second polymorph of $NaNbO_3$ could be isolated, with the rhombohedral ilmenite structure instead of the perovskite structure. Kong *et al.* subsequently used the potassium salt of the hexaniobate $[Nb_6O_{19}]^{8-}$ as a reagent in hydrothermal reactions to isolate various niobates, depending on pH and temperature, including polymorphs of the perovskite $KNbO_3$.[98] The crystallisation of $KNbO_3$ in supercritical water has also been investigated and proposed to occur by rearrangements of connectivity of $[NbO_6]$ octahedra *via* the intermediate phase $K_4Nb_6O_{17}$.[99]

More recently Skjaervø *et al.* studied the kinetics of the hydrothermal growth of $NaNbO_3$ and $KNbO_3$ using time-resolved *in situ* X-ray diffraction with high intensity synchrotron X-rays.[100] This work showed how $KNbO_3$ crystallises directly from dissolved Nb_2O_5 precursor at 250°C-300°C and 250 bar, whereas $NaNbO_3$ forms *via* crystalline intermediate phases at 225°C-325°C and 250 bar.[100a]. At higher temperatures a sequence of transient phases were observed on very short-timescales, Figure 11.[100b] These experiments illustrate how reaction conditions often must be chosen carefully to isolate the desired product phase as a pure sample.

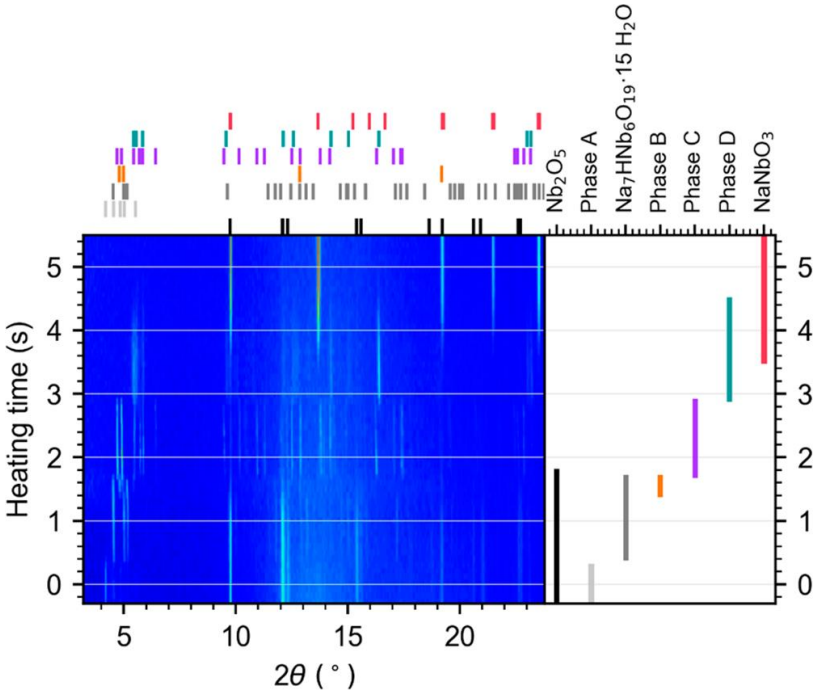

Figure 11: 2D contour plot of the evolution of phases in the Na-Nb-O system during hydrothermal synthesis in 9 M NaOH during rapid heating approaching supercritical conditions (423°C and 250 bar), including a schematic showing the phase development. Reprinted with permission from S. L. Skjaervø, K. H. Wells, S. Sommer, T. D. Vu, J. R. Tolchard, W. van Beek, T. Grande, B. B. Iversen, M. A. Einarsrud. Copyright (2018) American Chemical Society.

It should also be noted that the hydrothermal crystal growth method can be exploited to grow large crystals of $KNbO_3$ and $KTaO_3$ when more extreme temperatures are used: Mann *et al.* used silver ampoules containing concentrated aqueous KOH and powders of the perovskite as precursors, heated to 400-600 °C and produced high quality millimetre-sized crystals.[101] They noted that these conditions avoided problems of imperfections in conventionally-grown crystals, such as inhomogeneity, non-stoichiometry, and crystal cracking which occur from resulting from phase transitions. In particular, hydroxide defects were reduced at high temperature compared to in nanocrystalline materials formed at lower temperature, where their presence could influence phase transition behaviour.[102]

In the past decade, a huge attention has been focussed on control of crystal form for alkali niobates and tantalates, and the effect that this has on the resulting properties of the material. The majority of these studies have focussed on the formation of polycrystalline powders containing submicron crystallites. Song *et al.* found that a low concentration of Nb_2O_5 leads to nanorods or nanoplates of $NaNbO_3$, while a lower concentration of NaOH yields $NaNbO_3$ cubes, but all samples possessed an orthorhombic perovskite crystal structure.[96a] Crystallite morphology of $NaNbO_3$ can also be influenced by the choice of niobium oxide precursor,[103] the pH of solution,[104] and the choice of solvent, for example composition of water-methanol mixtures.[105] The fast synthesis offered by microwaves allowed the material to be formed as highly agglomerated micron-sized cubes in just 15 minutes at 180 °C using 6 M NaOH as the reaction medium.[106] All of these studies interpret the powder X-ray diffraction patterns as an orthorhombic distorted perovskite, which is expected for $NaNbO_3$, although it should be noted that other polymorphs do exist, resulting from different tilting patterns of the perovskite,[107] and that high resolution diffraction studies, or

NMR spectroscopy,[108] are needed to assign properly the true crystal symmetry of many samples. Only in one case was such detailed characterisation of hydrothermal $NaNbO_3$ made, and this showed the presence of a polar polymorph (space group $P2_1ma$) alongside the expected *Pbcm* polymorph.[109]

As with titanates, the hydrothermal route allows the growth of niobates with morphological control from choice of precursors. Wu *et al.* used directed the formation of arrays of $NaNbO_3$ nanorods by first crystallising a Nb_2O_5 rod-like array on niobium foil, which was then exposed to NaOH solutions along with ethylenediamine and treated hydrothermally.[110] This uses a similar idea to that discussed above for titanate synthesis and gave intricate microstructures, as illustrated in Figure 12. On the other hand, Joung *et al.* found that $KNbO_3$ nanowires formed directly from KOH solution at rather low temperatures of 120 °C,[111] and Kim *et al.* produced nanowires using metallic Nb as reagent, which they found to be a more reactive precursor than Nb_2O_5.[112] $NaTiO_3$ was grown using Ta metal foil as precursor in the form of films on the foil, with crystal morphology adjusted by the addition of hydrogen peroxide to the reaction solution.[113]

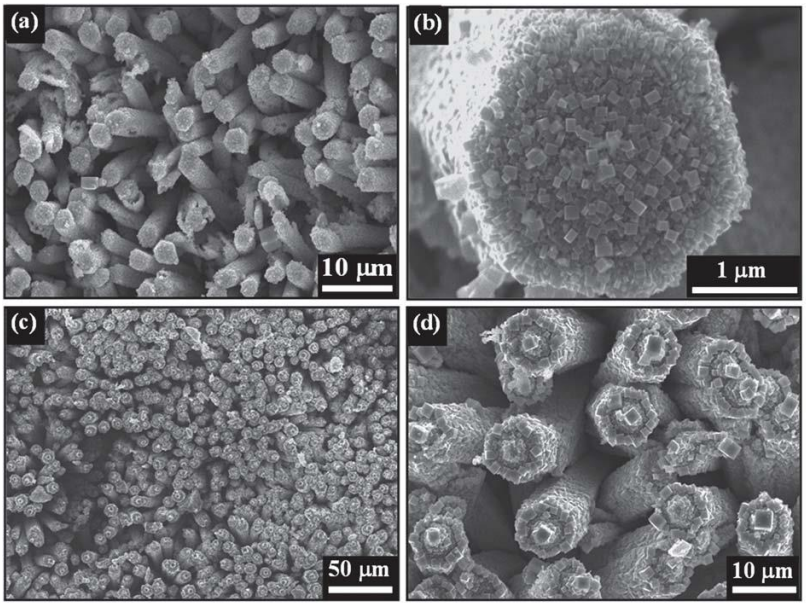

Figure 12: Views of $NaNbO_3$ hierarchical structures derived from hydrothermal treatment of arrays of Nb_2O_5 rods in aqueous ethylenediamine-NaOH solutions. Reproduced from Ref. 110 with permission from The Royal Society of Chemistry.

It may be noted here that the hydrothermal synthesis of the metastable rhombohedral ilmenite form of $NaNbO_3$ has also been studied by various groups, and this material typically forms as hexagonal plate-like crystals, a reflection of its underlying crystal symmetry.[114]

Piezoelectric ceramics formed from hydrothermally prepared alkali niobates and tantalates have shown characteristics comparable to ceramics made by conventional methods, but with the advantage of lower sintering temperatures to achieve densification.[115] Jung *et al.* prepared nanowires of $NaNbO_3$ from hydrothermal reactions and then used them to form a polymer composite to construct piezoelectric devices, making use of the fact that the nanowires crystallised in the polar *P*21*ma* structure.[116] Others have made composites from nanorods of $NaNbO_3$ and polyvinylidene fluoride to prepare capacitors[117] and to modify the polymorph of the polymer itself to enhance piezoelectric properties.[118] The growth of films or arrays of nanoparticles also allows the measurement of electronic properties directly, as well as the fabrication of devices. $KNbO_3$ thick films (tens of microns) have been grown epitaxially at 240 °C onto $(100)_cSrRrO_3//(100)SrTiO_3$ substrates, but measured ferroelectric and piezoelectric responses suggest the presence of contaminants.[119] Piezoelectrically active hydrothermal $KNbO_3$ thin films were produced by Goh and co-workers that could be rendered free of lattice hydroxyls and they reduced the concentration of oxygen vacancies by a post growth O_2 plasma treatment and thermal annealing,[120] while Shiraishi *et al.* grew $KNbO_3$ onto flexible polysulfone substrates that had been sputtered with $LaNiO_3$, and recorded ferroelectric and piezoelectric properties.[121] In contrast, a nanorod array of $KNbO_3$ was produced when Nb:$SrTiO_3$ was used as a substrate at 150 °C for 12 hours using Nb metal and an aqueous KOH solution, Figure 13; this was tested as a piezoelectric energy harvester and second harmonic generator.[122] Tu *et al.* have produced high-aspect-ratio potassium niobate ferroelectric crystals by use of MXene Nb_2C as a reagent in KOH: this uses the idea of crystal growth by morphological control dictated by the precursor, similar to the idea used in titanates described above, and ferroelectric loops of the anisotropic particles were measured directly using piezoresponse force microscopy. [123]

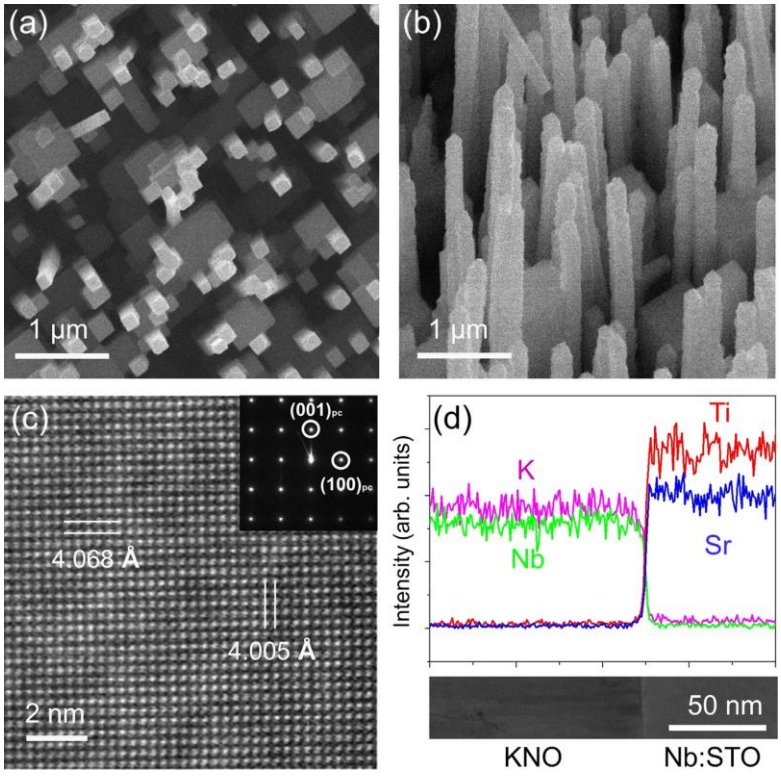

Figure 13: Vertically aligned single-crystalline $KNbO_3$ nanorod array on a Nb:$SrTiO_3$ (Nb:STO) substrate. Scanning electron microscopy images of (a) top and (b) 45° tilt views, (c) high-resolution transmission electron microscopy image with inset showing selected area electron diffraction, (d) spatial distribution of chemical elements near the interface. Reprinted from Nano Energy, Vol 17, P. G. Kang, T. K. Lee, C. W. Ahn, I. W. Kim, H. H. Lee, S. B. Choi, K. D. Sung, J. H. Jung, Vertically aligned epitaxial $KNbO_3$ nanorod array for piezoelectric energy harvester and second harmonic generator, Pages 261-268, Copyright (2015), with permission from Elsevier.

Photocatalytic properties of the alkali niobates and tantalates have been the focus of much attention for environmental and energy-related applications and hydrothermally grown materials demonstrate the possibility of tuneable properties either by adjustment of crystal morphology or by formation of composite materials. Relevant literature is summarised in Table 1. In the case of $NaNbO_3$, the surface area is important: Shi *et al.* prepared nanocubes (surface area 4.8 m^2g^{-1}) and compared them with nanowires formed by calcination of fibrous $Na_2Nb_2O_6{\cdot}H_2O$ (surface area 12 m^2g^{-1}), as well as literature data, and found a correlation with photocatalytic activity for hydrogen evolution from water/methanol.[124] Gu *et al.* produced nanowires directly by fluctuation the

solvothermal synthesis temperature in ethylene glycol and produced materials with activity for hydrogen evolution.[125] Jiang *et al.* found that agglomerates of oriented cuboids were effective for photocatalytic methane oxidation, as well as the degradation of rhodamine B.[126] Using $LaAlO_3$(111) and $NaNbO_3$/$LaAlO_3$(111) as substrates, triangular pyramidal crystals of $NaNbO_3$ could be grown hydrothermally that showed photocatalytic degradation of organics.[127]

Table 1: Summary of photocatalysis studies of alkali-metal niobate and tantalate perovskites from hydrothermal synthesis

Perovskite	Synthesis	Crystal morphology	Co-Catalyst	Light Source	Photocatalytic Reaction(s)	Reference
$NaNbO_3$	$Nb(OC_2H_5)_5$ + NaOH in water/polyethylene glycol 200°C for 24 h	Cubes	Pt	400 W high-pressure Hg lamp	Hydrogen evolution from water/methanol	[124]
	Nb_2O_5 + NaOH in water 200°C for 24 h	Agglomerate of cuboids	Pt	300 W Xe lamp	Degradation of rhodamine B Oxidation of methane	[126]
	Nb_2O_5 + NaOH in ethylene glycol 200°C for 4 h with temperature fluctuation	Intergrown nanowires, 10 nm diameter	Pt	300 W Xe lamp	Hydrogen evolution from water/methanol	[125]

	Nb_2O_5 + NaOH in water 200°C for 12 h	Cubes, micron sized	Cu_2O	250 W Xe lamp	Degradation of methyl orange	[128]
	Nb_2O_5 + NaOH in water 180°C for 3 h $LaAlO_3$(111) and $NaNbO_3/LaAlO_3$(111) substrates	Triangular pyramids, micron sized	-	300 W Xe lamp	Decomposition of 2,4-dichlorophene and rhodamine B	[127]
	Nb_2O_5 + NaOH in water 200°C for 2-3 hours	Nanowires (2 hour reaction) Agglomerated cuboids (3 hour reaction)	Pt	300 W Xe lamp	Hydrogen evolution from water/methanol Degradation of rhodamine B	[129]
	Nb_2O_5 + NaOH in water 200°C for 24 hours	Intergrown cuboids ~ 10 nm	Ru or Ag	500 W Xe lamp (420 nm< λ <800 nm)	Hydrogen evolution from water/methanol	[130]

$KNbO_3$	Nb_2O_5 + KOH in water 200°C for 12 h	Aggregated nanowires, 10 - 20 nm diameter (low KOH concentration) Agglomerated cubes (high KOH concentration)	-	300 W Xe lamp	Degradation of rhodamine B	[131]
	Nb_2O_5 + KOH in water and sodium dodecyl sulfate 180°C for 24 h	Rod shaped (orthorhombic polymorph)	Pt	250 W Xe lamp	Hydrogen evolution from water/methanol	[132]
	Nb_2O_5 + KOH in water 160°C for 12 h	Cube (cubic polymorph)	Pt	250 W Xe lamp	Hydrogen evolution from water/methanol	[132]

	$NbCl_5$ + KOH + H_2O_2 in ethanol 160°C for 16 hours	Nanowires (self doped)	Pt	300 W Xe lamp with 420 nm cut-off filter (simulated visible light)	Hydrogen evolution from water/methanol	[133]
	$NbCl_5$ + KOH in water 180°C for 24 h + vermiculite support	Needles ~ 2 μm long	-	300 W Xe lamp	Degradation of methyl blue	[134]
	$NbCl_5$ + KOH in water 160 °C or 260 °C for 24 h	Submicron cuboids	Ag	300 W Xe lamp with 420 nm cut-off filter (simulated visible light)	Photocatalytic N_2 fixation H_2 evolution Degradation of rhodamine B	[135]
	Nb_2O_5 + KOH in water 200 °C for 30	Agglomerated cuboids/cubes	-	Not specified	Degradation of rhodamine B	[136]

	minutes (2600 W microwaves)	dependent on KOH concentration				
$NaTaO_3$	Impregnation of Ta(*n*-OBu)$_5$, into mesoporous carbon followed by calcination in air and hydrothermal treatment in aqueous NaOH/ethylene glycol/ polyvinylpyrrolidone at 120 ºC for 3 days	array of spheres 20-100 nm diameter	NiO	450 W high-pressure Hg lamp	Total water splitting	[137]
	Ta_2O_5 (ball milled) + NaOH in water at 100-220 °C 20 minutes (1600 W microwaves)	Submicron cubes	NiO	450 W high-pressure Hg lamp	Total water splitting	[138]

	$TaCl_5$ + NaOH + H_2O_2 in ethanol at 110 °C for 24 hours	Nanospheres ~ 1 nm diameter (self doped)	-	300 W Xe lamp with 420 nm cut-off filter (simulated visible light)	Water splitting Degradation of Safranine O	[139]
	$Ta(OEt)_5$ + NaOH in water at 200 °C for 16 hours	Micron-sized cubes	-	700 W Hg mid-pressure immersion lamp	Hydrogen evolution from water/methanol	[140]
	$TaCl_5$ + NaOH + glucose in water/ethylene glycol at 110 °C for 24 hours	Interconnected 20 nanocrystals; carbon modified mesostructures	-	300 W simulated solar light	Destruction of NO_x	[141]
$KaTO_3$	Ta_2O_5 + KOH in water + ethanol or hexane at 160 °C 24 hours	Cubes (from ethanol) Flakes (from hexane)	Pt or Ag	300 W Xe lamp	CO_2 reduction	[142]

	Ta_2O_5 + KOH in water + PEG-400 at 200 °C 24 hours	Micron-sized cubes	Au, Ag, Pt, Pd, Rh, Ru, Au/Pt, Ag/Pd,Rh/Ru	1000 W Xe lamp (with UV filter to simulate visible light)	Degradation of phenol and toluene Hydrogen evolution from aqueous formic acid	[143]

$KNbO_3$ has been similarly explored for its photocatalytic activity.[131-132, 136] Wang *et al.* used vermiculite as a substrate on which to grow $KNbO_3$ needles that showed photoactivity for degradation of methyl blue,[134] while nitrogen-doping of $KNbO_3$ prepared hydrothermally was possible by heat treatment in the presence of urea to tune photocatalytic properties.[144] Using ethanol as solvent and $NbCl_5$ as precursor, Nb^{4+}-containing $KNbO_3$ was prepared with improved water splitting properties; these could also be readily nitrided in a second step with ammonia to give a surface modified with Nb_4N_5 that showed enhanced photocatalysis properties, ascribed to the introduction of some Nb^{4+}, and the junction between the oxide and nitride.[133]

In the case of $NaTaO_3$, hydrothermal reaction between NaOH and Ta_2O_5 in the pores of a three-dimensional mesoporous carbon gave a colloidal array of $NaTaO_3$ nanoparticles 20 nm in size, whose photocatalytic performance for overall water splitting under UV irradiation was evaluated after loading of a NiO cocatalyst: these showed higher activity than a bulk sample of $NaTaO_3$.[137] Microwave synthesis provides a rapid route to $NaTaO_3$, and if the Ta_2O_5 precursor is milled prior to use, the materials are effective for photocatalytic water splitting.[138] Wang *et al.* showed that by use of ethanol as solvent and $TaCl_5$ as precursor, self-doped (*i.e.*, Ta^{4+}-containing) nanocrystalline samples could be produced with smaller band-gaps and enhanced photocatalytic properties than stoichiometric samples.[139] The formation of the defect-pyrochlore $Na_2Ta_2O_6$ is found at lower KOH concentrations, but mixed $Na_2Ta_2O_6$-$NaTaO_3$ samples provide photoactive phase-junctions for water splitting in the absence of a co-catalyst.[140] Addition of glucose to ethylene glycol/water mediated reactions yields mesostructures of agglomerates of primary $NaTaO_3$ crystallites bound by carbonaceous material, that were tested for NOx destruction under visible light.[141] Pt- or Ag-loaded $KTaO_3$ was tested for photocatalytic CO_2 reduction and nanoflakes prepared *via* solvothermal reaction in hexane,[142] while a systematic study of various metallic co-catalysts has been made on micron cubes (Figure 14) with 0.5 Au/1.5 Pt-$KTaO_3$ showing the highest rate of hydrogen evolution from splitting of water.[143]

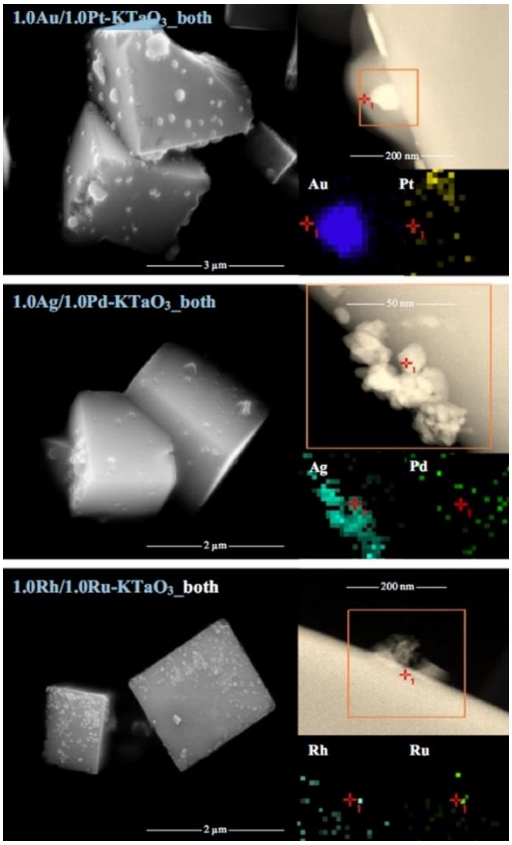

Figure 14. Cubes of $KTaO_3$ decorated with nanoparticles of precious metals used as photocatalysts for water splitting. The insets show expanded regions studied by EDS mapping. Reprinted from Applied Surface Science, Vol 441, A. Krukowska, G. Trykowski, M. J. Winiarski, T. Klimczuk, W. Lisowski, A. Mikolajczyk, H. P. Pinto, A. Zaleska-Medynska, Mono- and bimetallic nanoparticles decorated $KTaO_3$ photocatalysts with improved Vis and UV–Vis light activity, Pages 993-1011, Copyright (2018), with permission from Elsevier.

Other properties of hydrothermally-prepared niobates and tantalates that have been measured include the second harmonic generation response of $KNbO_3$ nanoneedles,[145] sonocatalytic degradation of organic dyes over $KNbO_3$, [146] and humidity sensing on nanocrystalline $NaTaO_3$.[147] Recent work has investigated further modification of the properties of niobate perovskites *via* the hydrothermal synthesis of composites: for example, nanowires of hydrothermally prepared $KNbO_3$ were modified by a second hydrothermal reaction with thiocarbamide dissolved in 20 mL oxalic acid to give a surface coating of flakes of MoS_2 and the composites showed enhanced photocatalytic H_2 production and organic pollutant degradation, compared to the individual

components.[148] Hu *et al.* have recently used hydrothermally prepared $NaNbO_3$ as a support for Ru nanoparticles *via* surface functionalisation with a silane, to produce a heterogeneous catalyst for selective hydrogenation of α-pinene.[149]

As well as ternary niobates and tantalates, solid-solutions $(K,Na)(Nb,Ta)O_3$ have also been proven possible to access directly *via* hydrothermal synthesis, providing atomically homogeneous samples. $(K,Na)NbO_3$ has been the focus of much attention and this includes polycrystalline samples[150] that have been sintered into ceramics,[151] [152] grown directly as epitaxial films on suitable substrates,[153] or as arrays of nanostructures.[154] Skjaervo *et al.* used *in situ* X-ray diffraction to follow the crystallisation of $K_xNa_{1-x}NbO_3$ and observed directly the formation of an intermediate mixed sodium-potassium hexaniobate (analogous to those seen in studies of $NaNbO_3$) and showed that using a water-ethanol mixture prolonged the reaction time by stabilising the intermediate phase and gave a smaller final crystallite size for the perovskite.[155] Toyama *et al.* developed a synthesis of $K_{1-x}Na_xNbO_3$ nanoparticles using a supercritical water flow at 480 °C and 25 MPa.[156] Most recently, Park *et al.* investigated the crystal symmetry of $(K_{1-x}Na_x)NbO_3$ and found that while conventional hydrothermal synthesis yields the orthorhombic perovskite, a monoclinic polymorph was isolated when high-intensity ultrasound irradiation was used for mixing and cubic materials were formed when ethylene glycol was used as a co-solvent, Figure 15.[157] This work illustrates the possibility of control of polymorphism *via* solution-mediated reactions; each phase was formed *via* intermediate layered structures and the particles were used to form polymer nanocomposites for use as piezoelectric harvesters.

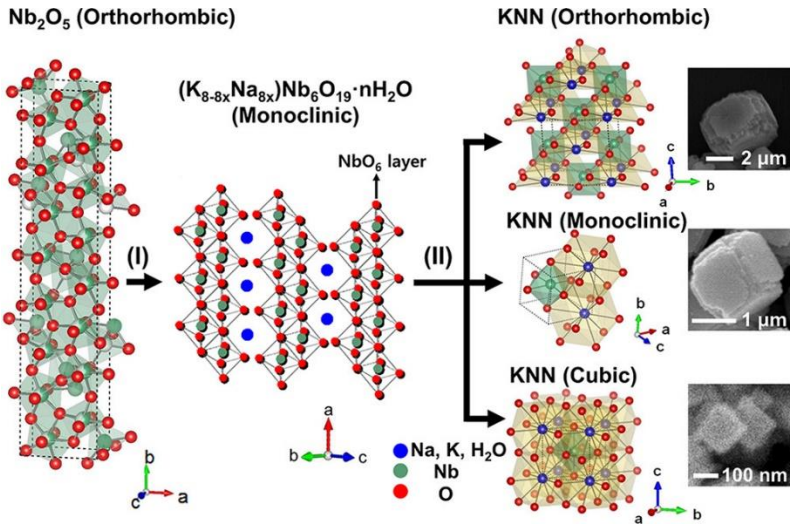

Figure 15. Structures of niobates found during the hydrothermal conversion of Nb_2O_5 to $(K_{1-x}Na_x)NbO_3$ (KNN), depending on reaction conditions (see text). Reprinted with permission from (S. Park, M. Peddigari, J. H. Kim, E. Kim, G.-T. Hwang, J.-W. Kim, C.-W. Ahn, J.-J. Choi, B.-D. Hahn, J.-H. Choi, W.-H. Yoon, D.-S. Park, K.-I. Park, C. K. Jeong, J. W. Lee, Y. Min, *Inorg. Chem.* **2020**, *59*, 3042-3052). Copyright (2020) American Chemical Society

Mixed tantalate-niobates have also been prepared using hydrothermal approaches.[158] Other substitutions in the this family of perovskites include lithium, in $(Na,K)NbO_3$-$LiTaO_3$ thin films,[159] and also epitaxial $(K,Na,Li)NbO_3$ films which were grown hydrothermally on (100)-La:$SrTiO_3$ substrates to give layers that showed ferroelectric hysteresis loops,[160] and sulfur-containing $NaTaO_3$ produced directly by use of $Na_2S_2O_3{\cdot}5H_2O$ as a hydrothermal reagent.[161]

Other niobates whose hydrothermal synthesis has been studied include $AgNbO_3$, whose photocatalytic properties have been studied,[162] and $Pb(Mg_{1/3}Nb_{2/3}O_3)$, which was formed at high KOH concentrations in preference to a pyrochlore phase.[163] The hexagonal niobate perovskite $Ba_5Nb_4O_{15}$[164] and the layered Dion-Jacobson-type perovskite $CsSr_2Nb_3O_{10}$[165] have also been prepared by direct hydrothermal routes.

3.3 Chromites

Early work on the hydrothermal synthesis of chromite perovskites, $ACrO_3$ (A = trivalent cation, such as a rare-earth) in the 1980s, used high temperatures and hence high autogeneous pressures to bring about crystal growth: using 400 °C and 100 MPa to form $LaCrO_3$, for example.[166] Sr-substituted lanthanum chromite powders, with partial oxidation of chromium above +3, with two different compositions, $La_{0.9}Sr_{0.1}CrO_3$ and $La_{0.8}Sr_{0.2}CrO_3$ were produced by similar high temperature/pressure methods,[167] Ca-substituted $LaCrO_3$ was prepared by Rivas-Vazquez *et al.* above 350 °C,[168] while Zheng *et al.* found that the temperature of synthesis of $LaCrO_3$ could be lowered to 260 °C if high KOH concentrations were used as reaction medium.[169] In our own work we found that temperatures above 300 °C were needed to induce crystallisation of $ACrO_3$ perovskites, from an initial precipitate of an amorphous mixed-metal hydroxide, but this then led to highly crystalline specimens for A = La, Pr, Sm, Gd, Dy, Ho, Yb, Lu and Y),[170] for which a detailed Raman spectroscopic study was

made to provide benchmark spectra for the family of materials.[171] Materials were all formed as rather large crystals, up to a micron in dimension. The formation of the mixed A-site chromites $La_{1-x}Sm_xCrO_3$ and $La_{1-x}Tb_xCrO_3$ by the same method also proved possible.[172] These materials show some structural subtleties, seen by use of high resolution TEM methods: in the case of $La_{0.5}Sm_{0.5}CrO_3$ the La and Sm cations are apparently homogeneously dispersed on the nanoscale, but in $La_{0.5}Tb_{0.5}CrO_3$ there is evidence for separation of La and Tb into layers, Figure 16. Although this layering does not propagate through the crystallites, and hence in not seen using diffraction methods, the magnetic properties are distinct from an annealed sample in which the La and Tb become randomised. Attempts to make the same composition by conventional solid-state synthesis methods lead to phase-separation, suggesting that the local segregation is a metastable arrangement and hence a kinetic phenomenon, most likely driven by the large size miss-match between large La^{3+} and smaller Tb^{3+} which leads to local ordering in their distribution.

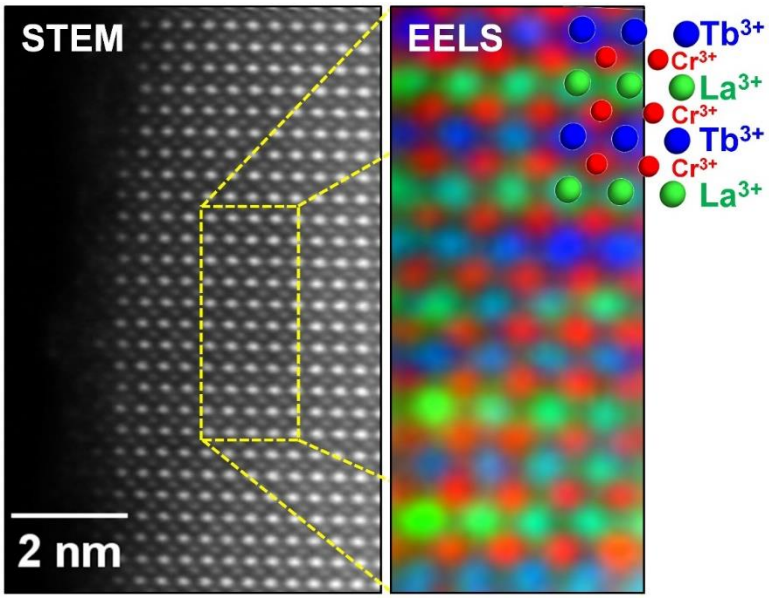

Figure 16: Local atomic structure seen by EELS mapping of the mixed rare-earth perovskite $La_{0.5}Tb_{0.5}CrO_3$ produced by hydrothermal crystallisation illustrating local layering of the A-site cations. The left image shows a scanning transmission electron microscopy image. Reproduced from Daniels *et al.*[172b]

The group of Feng have also produced samples of rare-earth chromites by hydrothermal reactions: $La_{0.9}Sr_{0.1}CrO_3$ and $La_{0.8}Sr_{0.2}CrO_3$ were prepared at 260 °C as micron-sized cubes and were shown to have composition-dependent magnetism and conductivity,[173] while $LaCrO_3$ was shown to have crystallite shape modulated by use of urea as an additive in synthesis.[174] Other groups have now reported high quality samples of a range of $ACrO_3$ materials, using temperatures as low as 260 °C, thus verifying the synthesis route as reliable.[175] [176] Wang *et al.*, showed how addition of urea allowed crystal shape to be tuned for $LaCrO_3$, $PrCrO_3$ and $NdCrO_3$, Figure 17.[177]

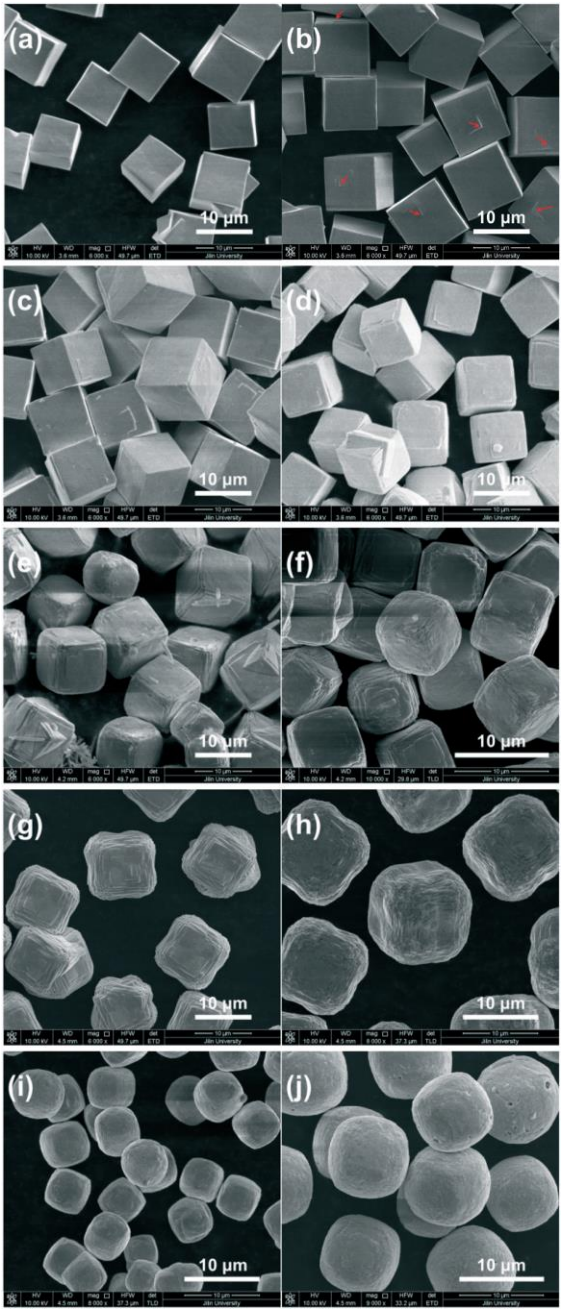

Figure 17: Shape-tuning of $LaCrO_3$ synthesised hydrothermally with different masses of urea at 260°C: (a) 0 g, (b) 0.2 g, (c) 0.4 g, (d) 0.6 g, (e) 0.8 g, (f) 1.0 g, (g) 1.2 g, (h) 1.4 g, (i) 1.6 g and (j) 1.8 g. The arrows in (b) show the initial effect of addition of urea on crystal shape. Reproduced from Ref. 177 with permission from The Royal Society of Chemistry.

Girish used a different approach to the hydrothermal formation of $LaCrO_3$, by first preparing $LaCrO_4$ and then treating it in supercritical water at 700 °C to reduce the precursor to the desired product.[178] The use of supercritical conditions has also allowed a continuous flow synthesis of the same material and this provided fine powders for fabrication into dual-phase oxygen transport membranes for solid-oxide fuel cells.[179] The higher temperatures needed for the formation of chromites, compared to the titanates already discussed, and the manganite discussed below, may in part be due to kinetically limited ligand substitution of Cr^{3+} in solution.

3.4 Manganites

Manganese-containing perovskites introduce further complexity into synthesis since the Mn may be present in either the +3 or +4 oxidation state, or in mixtures of both. These materials have long been of attention for their exotic magnetic and electronic properties, and the interplay between the two, such as magnetoresistive behaviour.[180] In our earlier review article we highlighted the successful hydrothermal synthesis of $A_{1-x}A'_xMnO_3$ perovskites, where A = trivalent rare-earth cation and A' = divalent alkali-earth cation.[15] These syntheses, first reported by Feng's group at Jilin University,[181] use a comproportionation reaction between $KMnO_4$ and Mn^{2+} to target the desired oxidation state in the oxide product. This proved a versatile method to prepare some unusual phases, such as $La_{0.5}Ba_{0.5}MnO_3$ in which the La^{3+} and Ba^{2+} show ordering such that they are arranged in layers.[182]

The manganese-containing $AMnO_3$ perovskites also provide examples of hexagonal structures. For example, $BaMnO_3$ and $SrMnO_3$ crystallise as 2H and 4H structures, respectively, Figures 2c and 2d, and these Mn(IV) phases form directly from solution under alkali hydrothermal conditions.[183] The case of $YMnO_3$, which possess a layered hexagonal structure, Figures 2a and 2b, is particularly interesting because of the

physical properties of the material. $YMnO_3$ has been widely studied for its multiferroic properties, showing a combination of magnetic order; antiferromagnetism below 74 K and spontaneous polarisation that persists up to 1270 K.[184] Typically, synthesis is performed using high temperature annealing of binary oxides in oxygen gas at 1100 °C,[185] well above the polar ordering temperature, but *via* hydrothermal chemistry, crystallisation can be brought about directly from solution at 240 °C.[186] High resolution TEM of the micron-sized platey crystals formed, shows the spontaneous formation of polar domains, even at this low temperature, Figure 18. Interestingly, Zheng *et al.* produced $YMnO_3$, apparently in the absence of hydroxide,[187] while Kumar and Jayavel prepared nanorods of $YMnO_3$ using hydrothermal synthesis in dilute NaOH (0.5 M) and using Mn(II) acetate as a precursor:[188] these results illustrate how change in mineraliser and precursor salts can influence the product form under hydrothermal conditions. $YMnO_3$ also has an orthorhombic perovskite polymorph and this was accessed as single crystals by hydrothermal treatment of a polycrystalline sample of hexagonal $YMnO_3$ in aqueous KCl at 5.5 GPa up to 1280 °C to give high quality specimens for magnetic and electrical polarisation measurements.[189]

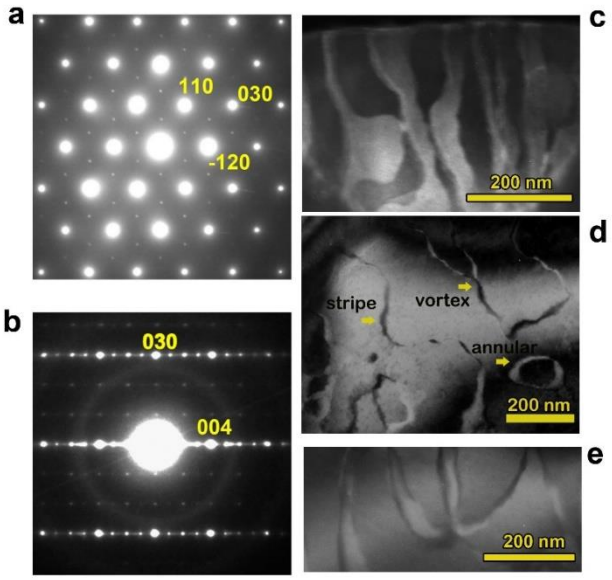

Figure 18: Electron microscopy of hydrothermally produced $YMnO_3$ Electron diffraction patterns along (a) the [001], (b) the [100] zone-axis directions, showing the triple superlattice reflection spots correlated with the trimerisation of MnO_5 polyhedra and the buckling of Y layers. Superlattice dark-field TEM images showing (c) the

typical curved stripe domain pattern, (d) the coexistence of curved stripe, cloverleaf patterns and annular domains in one area, and (e) a typical cloverleaf pattern domain. Reprinted from M. H. Harunsani, J. Li, Y. B. Qin, H. T. Tian, J. Q. Li, H. X. Yang, R. I. Walton, *Appl. Phys. Lett.* **2015**, *107*, 062905 with the permission of AIP Publishing

Since the initial reports of the hydrothermal synthesis of perovskite manganites, work in the past decade has focussed on the study of the properties and applications of the materials, in particular those that might take advantage of the low temperature synthesis approach and the unusual crystal forms. This includes magnetic properties, for example, Chu *et al.* prepared hollow $La_{0.7}Sr_{0.3}MnO_3$ microspheres formed from aggregates of primary cube-shaped particles with room temperature ferromagnetism (T_C = 301 K).[190] Datta *et al.* produced nanowires of $La_{0.5}Sr_{0.5}MnO_3$, from which as well as magnetisation, they were able to measure resistivity from focussed ion beam attachment of electrodes.[191] Composition-dependent magnetic properties of $Y_{1-x}Ca_xMnO_3$ (x= 0, 0.07, 0.55, 0.65) have been studied, with the x = 0.55 and 0.56 materials found to show a low temperature antiferromagnetic state that is stabilised by charge ordering. [192] The magnetic order and dielectric properties of $TbMnO_3$ platelets prepared by hydrothermal crystallisation were studied to prove its multiferroic character.[193] Other applications of manganite fine powders prepared by hydrothermal crystallisation include $La_{0.5}Sr_{0.5}MnO_3$ as a cathode material for solid-oxide fuel cells,[194] $La_{0.77}Sr_{0.23}MnO_3$ for magnetic nanohyperthermia cancer treatment, where biocomptability was tested,[195] and $La_{0.5}Sr_{0.5}MnO_3$ for electrocatalytic oxygen reduction, where properties were shown to depend on the crystal morphology.[196]

Size and shape control of manganite crystallites has also been the focus of continued study. Makovec *et al.* produced dendrites of $La_{1-x}Sr_xMnO_3$ directly from hydrothermally treated solutions with no additive.[197] Huang *et al.* used NH_4^+ to control the shape of the same materials and proposed that the ammonium ion interacted directly with octahedral MnO_6 units and with increasing concentration hindered propagation of crystal growth in certain directions to give rise to various crystal morphologies, Figure 19.[198]

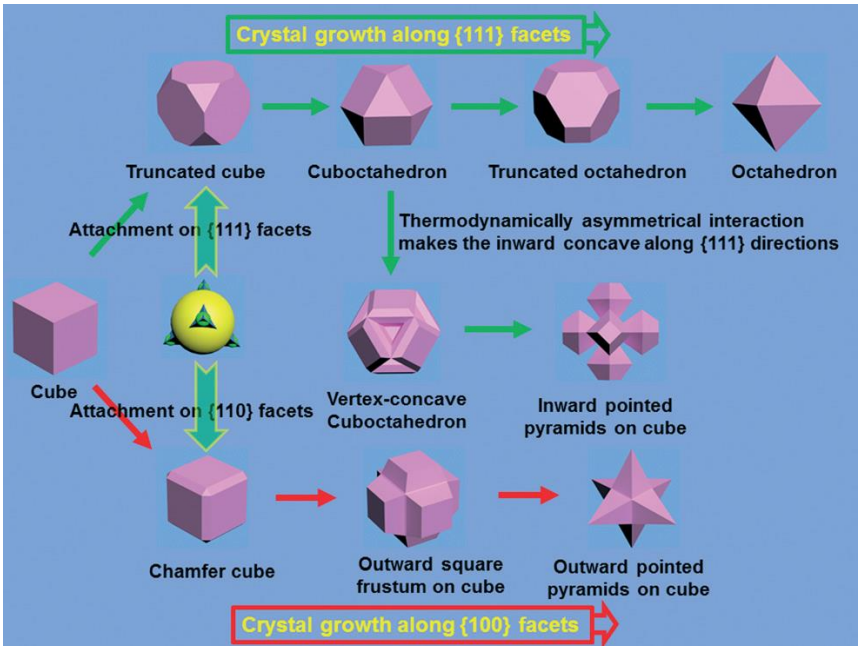

Figure 19: Proposed model for the shape evolution of $La_{0.5}Sr_{0.5}MnO_3$ crystal shape evolution in aqueous NH_4^+. Reproduced from Ref. 198 with permission from The Royal Society of Chemistry.

Finally, it is worth pointing out that a continuous flow synthesis of $La_{1-x}Sr_xMnO_3$ at 390-410 °C and 30 MPa provided access to high surface area powders, suggesting that practical application of the solids should prove possible.[199]

3.5 Ferrites and ruthenates

In a forthcoming review article innovative synthesis routes to mixed-metal iron oxides will be surveyed, including the solvothermal synthesis of ferrite perovskites,[200] and here only the key findings in the case of the perovskites will be summarised. Extensive work has been carried out in the past decade on the solvothermal synthesis of the perovskite $BiFeO_3$, and this has been driven by first its multiferroic properties, where the coexistence of magnetism and polar properties has emerged of being importance,[201] and second its potential use in photocatalysis, where its band gap is appropriate for solar light activation, and it has been widely studied for the degradation of organics.[202] The hydrothermal synthesis of $BiFeO_3$ was established independently by Chen *et al.*[203] and Han *et al.*[204] in 2006 who produced the material in alkali hydrothermal conditions, showing crystallite-shape dependence on pH and temperature, along with the competitive formation of other bismuth iron oxides, including $Bi_{25}FeO_{40}$ and $Bi_2Fe_4O_9$, that are structurally unrelated to the desired

perovskite. Numerous other reports of solvothermal synthesis of $BiFeO_3$ have followed, and the ease of its formation has led to extensive exploration of the use of solution additives, such as NH_4Cl,[205] and Na_2CO_3,[206] the use of non-aqueous solvents such as acetone,[207] 2-methoxy ethanol,[208] triethanolamine,[209] polyethylene glycols,[210], polyvinylalcohol,[211] and use of microwaves instead of conventional heating.[206, 212] All of these works have been focussed on optimising synthesis parameters for precise size and shape control of particle morphology, and some examples are shown in Figure 20.

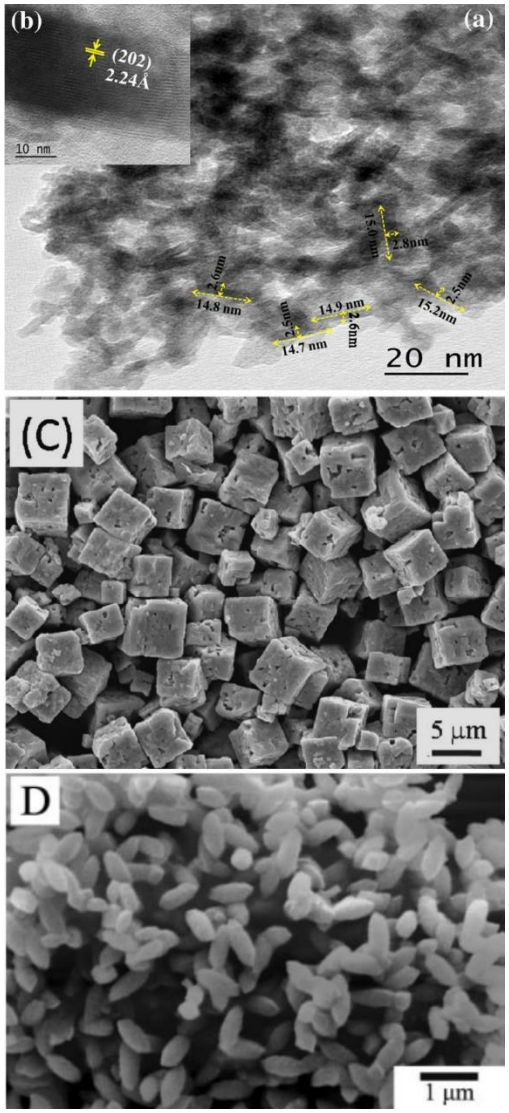

Figure 20: Examples of particle morphologies of $BiFeO_3$ from solvothermal synthesis: (a) and (b) Rods from Dhanalakshmi *et al.* prepared in 2-methoxy ethanol. Reprinted by permission from Springer-Verlag, Applied Physics A, Materials Science &

Processing, Enhanced photocatalytic activity of hydrothermally grown $BiFeO_3$ nanostructures and role of catalyst recyclability in photocatalysis based on magnetic framework, R. Dhanalakshmi, M. Muneeswaran, P. R. Vanga, M. Ashok, N. V. Giridharan (2016). (c) Microcubes of assembled submicron primary particles from Li using polyethylene glycol. Reprinted with permission from (S. Li, Y. H. Lin, B. P. Zhang, Y. Wang, C. W. Nan, *J. Phys. Chem. C* **2010**, *114*, 2903-2908). Copyright (2010) American Chemical Society (d) Spindle-shaped crystallites formed in aqueous NaOH, reproduced from Han *et al.*[204]

The properties of $BiFeO_3$ prepared from solvothermal routes can depend upon crystal form: for example, the rod-shape nanocrystallites produced by Dhanalakshmi *et al.* showed enhanced photocatalytic properties,[208] and Li *et al.* also produced nanorods with favourable photocatalytic properties *via* a polyvinylpyrrolidone-assisted hydrothermal route.[213] You *et al.* prepared nanosheets *via* ammonia-mediated hydrothermal crystallisation that showed mechanically-activated catalytic properties for water splitting and dye-degradation,[214] while Huang *et al.* performed epitaxial growth of the material on orientated surfaces of $SrTiO_3$ to give micron-thick films with favourable dielectric properties.[215]

Mi *et al.* produced $BiFeO_3$ nanocrystals in rapid reactions at temperature of up to 350 °C at 250 bar from $Fe(NO_3)_3{\cdot}9H_2O$ and $Bi(NO_3)_3{\cdot}5H_2O$ and followed the reaction using *in situ* X-ray diffraction, observing Bi_2O_3 under reactions conditions which they proposed reacted with an amorphous iron hydroxide phase.[216]

In contrast to $BiFeO_3$, whose solvothermal synthesis appears straightforward and so allows for the wide exploration of reaction condition and control of crystal form, the solution synthesis of the rare-earth ferrites, $REFeO_3$ (RE = lanthanide or Y) has been rather less studied. Early work by Yoshimura *et al.* found that the direct hydrothermal synthesis of $LaFeO_3$ from KOH solution required temperatures above 300 °C from lanthanum oxide and hydrated iron oxide as reagents with optimum reaction temperatures around 450 – 500 °C,[217] and although more recently nitrates have been used as precursors, still reactions temperature of 450 °C were needed.[218] In fact the synthesis of $LaFeO_3$ at more moderate temperatures, less than 300 °C, has only proved possible if sodium carbonate[219] or urea[174] [220] is added as a crystallising agent at high

KOH concentration. The materials then formed consist of highly crystalline particles with highly facetted morphologies, Figure 21.

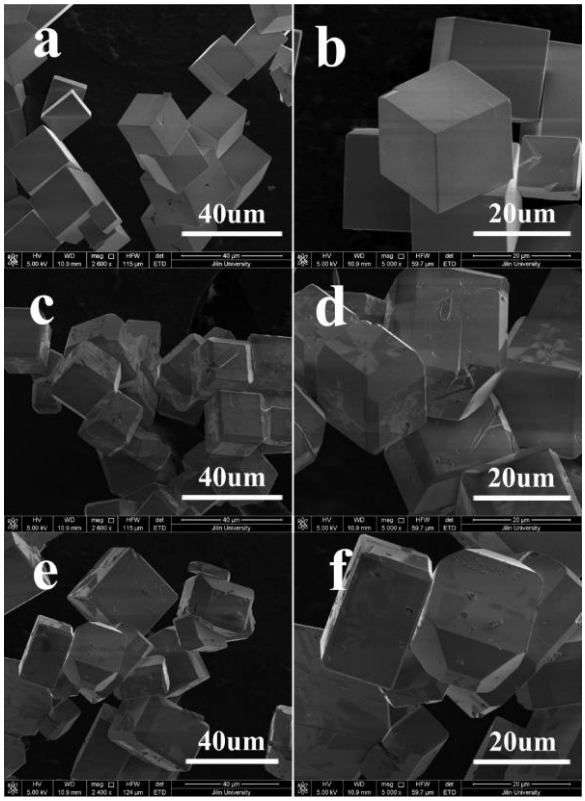

Figure 21: $LaFeO_3$ from urea-aided hydrothermal synthesis showing the effect of mineraliser concentration on crystal size and shape from addition of different masses of KOH: 4.5 g (a, b), 5.0 g (c, d), 5.5 g (e, f). Reprinted with permission from L. Yuan, K. K. Huang, S. Wang, C. M. Hou, X. F. Wu, B. Zou, S. H. Feng, *Cryst. Growth Des.* **2016**, *16*, 6522-6530. Copyright (2016) American Chemical Society.

Feng and co-workers have proposed that the role of urea is to release ammonium ions into solution upon decomposition, which coordinate to the $[FeO_6]$ octahedra at the surface of the growing perovskite crystals leading to a modulation of their morphology.[220a, 221] It was found that urea could then be used to control the crystal shape of the materials $REFeO_3$ (RE = La, Pr, Sm, Dy, Er, and Y).[220a] For $YbFeO_3$, the choice of base, NaOH or KOH, or the addition of NH_4^+, could be used to adjust the crystal shape to give a wide range of morphologies.[222] In fact, a body of work has showed how the rare-earth ferrites of other lanthanides are more readily synthesised: those of all of the elements Pr–Lu (except Pm) crystallise at 240 °C from aqueous KOH in 24 hours without the need for solution additives;[223] the as-made materials are

polycrystalline powders and their magnetic behaviour corresponds to solids prepared by conventional synthesis routes.

The rare-earth ferrite $YFeO_3$ also crystallises directly from solution and although some groups have reported that temperatures of 300 °C are required,[224] others have used 240 °C with concentrated aqueous KOH as reaction medium.[225] The ferrites of the smaller rare-earth cations may adopt a hexagonal perovskite structure, like $YMnO_3$ already discussed, and this may be formed selectively by solvothermal synthesis instead of the orthorhombic polymorph. Using rare-earth (RE) acetates (RE= Tm-Lu) and iron acetylacetonate in 1,4-butanediol at 300 °C gave hexagonal $REFeO_3$ materials, which irreversibly transformed into the orthorhombic perovskite on subsequent heating to around 980 °C. [226] The choice of reagents can have a subtle effect on which polymorph initially crystallises: the solvothermal reaction between $YbCl_3$ and iron acetylacetonate in 1,4-butanediol in the presence of 1,6-hexanediamine gave the orthorhombic perovskite $YbFeO_3$ directly, in contrast to the hexagonal polymorph prepared when using the prior method.[227]

As yet, there are few reports of the hydrothermal crystallisation of perovskites that contain the other Group 8 metals, Ru and Os. In our own work we discovered a novel phase $Ba_4Ru_3O_{10.2}(OH)_{1.8}$, a member of the cation deficient hexagonal perovskite $A_nB_{n-\delta}O_{3n}$ series, which contains partial replacement of some oxide by hydroxide and partially ordered Ru vacant sites to give a complex and not-before-seen variant of the 8H hexagonal perovskite structure.[228] As with other ruthenium(V) oxides prepared hydrothermally, the material collapses on heating in air at around 500 °C,[229] which suggests that other new metastable phases may yet be discovered by exploration of hydrothermal chemistry.

3.6 Main group perovskite oxides

There are various possible perovskite oxides that contain a main-group metal cation as the B-site metals. The lanthanide aluminates $LnAlO_3$ (Ln=La, Sm and Gd) were prepared by a hydrothermal supercritical fluid technique using a co-precipitated gel as a precursor using sealed gold capsules at 600–700 °C and 100–200 MPa,[230] and $LaAlO_3$ was separately reported as forming at 450 °C and 30 MPa from nitrates in aqueous KOH.[218] The method was applied to include Nd^{3+}, $Eu^{3+}$and Er^{3+} dopants in

$YAlO_3$,[231] but still the phases are only directly accessible under hydrothermal conditions when high temperature and pressures are used.

In contrast to aluminates the formation of $ASnO_3$ stannates, with A^{2+} a variety of partner cations, occurs readily under mild hydrothermal conditions. Note that the composition $ZnSnO_3$, whose hydrothermal synthesis has been extensively studied, usually has $LiNbO_3$-type structure with both metals octahedrally coordinated,[232] although under specific conditions the perovskite polymorph can apparently be prepared.[233] $CaSnO_3$ has been prepared using various reactive solutions for hydrothermal reactions, and investigated for applications in photocatalysis,[234] and as an anode material for lithium-ion batteries,[235] while materials doped with lanthanide cations formed by one-step hydrothermal crystallisation have been shown to have upconversion luminescence properties.[236] Similar investigations have been made on $SrSnO_3$ and $BaSnO_3$,[234b, 234c, 237] and the magnetic properties of Fe-doped $CaSnO_3$ were characterised as room temperature ferromagnetism.[238] Hu *et al.* prepared carbon-coated nanotubes of $CaSnO_3$ by used of nanotubes of a $CaSn(OH)_6$ precursor that were solvothermally treated in water-ethanol in the presence of glucose; calcination gave the perovskite product with carbonisation of glucose having occurred at the surface and the materials were assessed for use as anodes in lithium batteries.[239]

The Group 15 perovskites whose hydrothermal synthesis has been developed include the double perovskites Ba_2MSbO_6 (M = Pr, Nd, Sm, Eu, In and Fe) that contain Sb^{5+} as one of the B-site cations. These materials are superstructures of the classical perovskite with ordering of the B-site cations driven by their differing charges and coordination preferences. For Ba_2InSbO_6[240] and Ba_2SbLnO_6 (Ln = Pr, Nd, Sm, Eu),[241] the Sb^{3+}-containing precursor Sb_2O_3 was used as a reagent with oxidising conditions provided by hydrogen peroxide and the presence of Sb^{5+} in the perovskite was confirmed using ^{121}Sb Mössbauer spectroscopy: this combination of reagents provided impurity-free samples. For Ba_2FeSbO_6, dielectric properties were measured.[242]

The hydrothermal chemistry of bismuth oxides provides some striking examples of novel perovskites with interesting properties: the group of Kumada have produced a number of perovskites that contain mixed-valent Bi^{3+}/Bi^{5+} on the B-site and that show superconductivity characterised by the characteristic transition to diamagnetism upon

cooling. These have complex chemical compositions, with multiple A-site cations, in some cases also including water, and in some cases also mixed B-site cations. Table 2 shows the compositions, synthesis conditions and critical superconductivity temperature measured for these novel materials. The reagent in the synthesis of all of these perovskites is the Bi^{5+}-containing $NaBiO_3.nH_2O$ (or $KBiO_3$), which under alkali hydrothermal conditions is known to reduce, wholly or partially, to Bi^{3+}-containing species, depending on the pH of solution and the temperature used.[11e] Some of the perovskites shown in Table 2 were proven to show order of the A-site cations to give superstructure evident in powder neutron and X-ray diffraction measurements. For example, the material $(K_{1.00})(Ba_{1.00})_3(Bi_{0.89}Na_{0.11})_4O_{12}$ shows ordering of the A-site K and Ba, while the B-site Bi and Na share the same crystallographic position to give a body-centred cubic unit cell with edge length double the conventional perovskite structure, Figure 22.[243] In the case of $(Ba_{0.62}K_{0.38})(Bi_{0.92}Mg_{0.08})O_3$, the A-site and B-site cations show no ordering,[244] and the metallic nature of the material was verified using first-principles calculations.[245] For several of these materials the onset of superconductivity was measured by detecting the characteristic diamagnetism in a polycrystalline powder, but also from resistivity measurements of pressed pellets. Zhang *et al.* also reported two sets of materials $Ba_{1-x}K_xBiO_3$ (x = 0.06, 0.35, 0.5, 0.55) and $Ba_{1-x}K_xBi_{1-y}Na_yO_3$ (x=0 y=0.25, and x=0.15 y=0.17) using similar hydrothermal reactions, and for the former superconductivity was detected.[246]

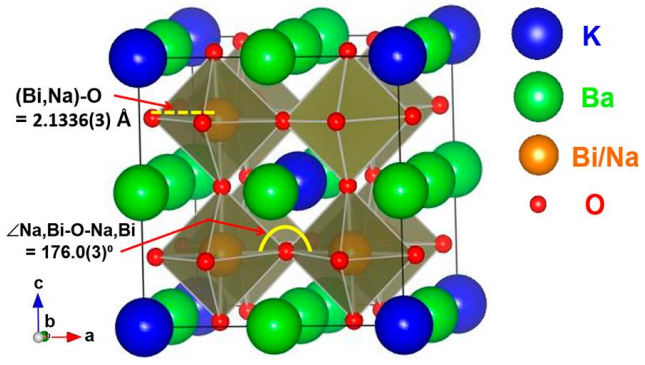

Figure 22: Crystal structure of $(K_{1.00})(Ba_{1.00})_3(Bi_{0.89}Na_{0.11})_4O_{12}$ double perovskite showing ordering of A-site K and Ba. Reprinted with permission from M. H. K. Rubel, T. Takei, N. Kumada, M. M. Ali, A. Miura, K. Tadanaga, K. Oka, M. Azuma, M. Yashima, K. Fujii, E. Magome, C. Moriyoshi, Y. Kuroiwa, J. R. Hester, M. Aydeev, *Chem. Mater.* **2016**, *28*, 459-465. Copyright (2016) American Chemical Society

Table 2: Superconducting bismuthate perovskites prepared using hydrothermal chemistry by Kumada and co-workers, with the superconducting critical temperature T_C indicated.

Material	**Synthesis**	T_C	**Reference**
$(Ba_{0.75}K_{0.14}H_{0.11})BiO_3{\cdot}nH_2O$	$NaBiO_3.nH_2O$, $Ba(OH)_2.8H_2O$, and KOH 180 °C for 2 days.	8 K (increased to 15 K upon heat treatment to dehydrate at 500 °C).	[247]
$Ba_{0.96}Bi_{0.86}O_{2.59}(OH)_{0.41}$	$NaBiO_3{\cdot}nH_2O$ and $Ba(OH)_2{\cdot}8H_2O$ at 180 °C for 2 days	None detected above 4 K	[248]
$(Na_{0.25}K_{0.45})(Ba_{1.00})_3(Bi_{1.00})_4O_{12}$	$NaBiO_3.nH_2O$,$Ba(OH)_2.8H_2O$, and KOH 220 °C	27 K	[249]
$(Ba_{0.82}K_{0.18})(Bi_{0.53}Pb_{0.47})O_3$	$PbBi_2O_5.9{\cdot}H_2O$,* $Ba(OH)_2{\cdot}8H_2O$ and KOH at 240 °C for 2 days	22.8 K	[250]
$(K_{1.00})(Ba_{1.00})_3(Bi_{0.89}Na_{0.11})_4O_{12}$	$NaBiO_3.nH_2O$,$Ba(OH)_2.8H_2O$, and KOH 240 °C for 2 days	~31.5 K	[243]
$(Ba_{0.62}K_{0.38})(Bi_{0.92}Mg_{0.08})O_3$	$MgBi_2O_6$**, $Ba(OH)_2{\cdot}8H_2O$ and KOH 220 °C for 2 days	~ 30 K	[244-245]
$(Ba_{0.54}K_{0.46})_4Bi_4O_{12}$	$KBiO_3$, $Ba(OH)_2{\cdot}8H_2O$, and KOH 240 °C for 2 days	~ 30 K	[251]

* $PbBi_2O_5{\cdot}9H_2O$ was synthesised in a separate reaction from $NaBiO_3{\cdot}nH_2O$ and $Pb(NO_3)_2$ in water at 10 °C.
** $MgBi_2O_6$ was synthesised in a separate hydrothermal reaction using $NaBiO_3{\cdot}nH_2O$ and $MgCl_2{\cdot}6H_2O$ at 130 °C.

3.7 Substitutional chemistry and solid-solutions of perovskites

As well as the ternary $ATiO_3$ and quaternary $(A,A')TiO_3$ and $A(Ti,Zr)O_3$ materials already discussed above in Section 3.1, and the mixed tantalate-niobate materials in Section 3.2, in the past 10 years hydrothermal synthesis of complex solid-solutions of perovskites has been increasingly studied, coupled with in depth investigation of the atomic-scale structure and nanoscale characteristics. In this section we consider mixed B-site materials containing elements from different groups of Periodic Table, often with different charges and so requiring mixtures of A-site cations for charge compensation. This includes substitutional chemistry on both the A-site and the B-site of the prototype ferroelectric $BaTiO_3$ to give atomically homogeneous phases, and also compositionally inhomogeneous phases, where the concentration gradient of elements varies across the particles.

The solid-solution $0.5BaTiO_3$-$0.5BiFeO_3$ was produced directly from hydrothermal reactions in aqueous KOH at a reaction temperature of 200 °C, with lower temperatures or low KOH concentrations giving impurity bismuth ferrites.[252] Wada *et al.* used $BaTiO_3$ powders to prepare a $BaTiO_3$-$KNbO_3$ composite *via* an ethanolic solvothermal synthesis of the second perovskite;[253] this gave nanostructured ceramics with a heteroepitaxial interface structure, Figure 23, that showed enhanced dielectric properties that were ascribed to the strained interface.

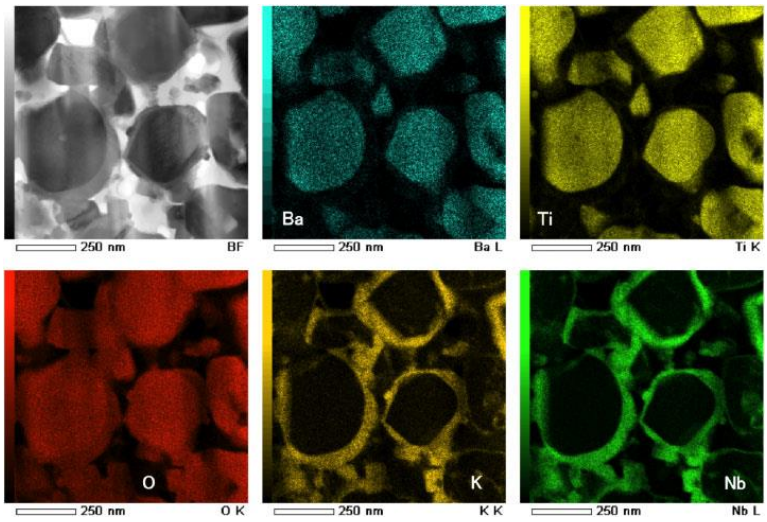

Figure 23: Chemical composition distribution from EDS maps of $BaTiO_3$-$KNbO_3$ (BT–KN) nanostructured ceramics with KN/BT molar ratio of 0.5 illustrating the $KNbO_3$ shell. Reproduced from Wada *et al.*[254] Copyright (2012) The Japan Society of Applied Physics.

Within the titanate perovskite family, gradient core-shell structured nanoparticles of $BaTiO_3$-$Ba_{1-x}Sr_xTiO_3$ have been prepared using $BaTiO_3$ seed particles that were first acid-treated to leach Ba from the surface before being hydrothermally treated in aqueous $Sr(OH)_2{\cdot}8H_2O$ at 200 °C.[255] Other substituted titanate perovskites whose hydrothermal synthesis has proved possible include, $(Bi_{0.5}K_{0.5})(Zr_xTi_{1-x})O_3$ with $x \leq 0.1$,[256] and Fe^{3+}-containing $SrFe_xTi_{1-x}O_{3-\delta}$ with $x \leq 0.1$ that showed photocatalytic activity for NO oxidation.[257] Co-doping of Bi and Co into strontium titanate gave materials with photocatalytic properties under visible light irradiation,[258] and La/Cr co-doping of hollow $CaTiO_3$ cubes allowed for efficient photocatalytic hydrogen production.[259] The solid solution $Na_{0.5}La_{0.5}TiO_3$-$LaCrO_3$ produced by hydrothermal crystallisation gave materials of high purity, and $(Na_{0.5}La_{0.5}TiO_3)_{1.00}(LaCrO_3)_{0.08}$ was produced with few defects, and regulated morphology in which solely Ti^{4+} and Cr^{3+} were present; this supressed the recombination of photogenerated carriers to enhance photocatalytic H_2 evolution from water.[260] Widening the solid solution showed that with higher amounts of $LaCrO_3$, Cr^{6+} was found with resulting defects that decreased the photocatalytic activity.[261] Hydrothermal synthesis of $(1\text{-}x)K_{0.5}Na_{0.5}NbO_3$-$xBi_{0.5}Na_{0.5}TiO_3$ was investigated and depending on composition, phase separation was often found, and piezoelectric properties of ceramics formed from the powders were not optimal.[262] Enhanced piezoresponse and electric field induced relaxor-ferroelectric

phase transition was found in NBT-0.06BT ceramics prepared from hydrothermally synthesised nanoparticles.[263]

Zirconate solid solutions have similarly been prepared: for example, $BaZr_{1-x}Hf_xO_3$ from microwave-heated hydrothermal reactions,[264] and growth of $Ba_{1-x}Sr_xZrO_3$ ($0 \leq x \leq 1$) nanoparticles in supercritical water [265]

As well as solid-solutions and substitutional variants of titanate perovskites, some focus has been made on the preparation of heterostructures of $ATiO_3$ perovskites and TiO_2 prepared *via* hydrothermal synthesis. TiO_2 nanofibres have been used as a host to grow surface cubic particles of $SrTiO_3$ that show photocatalytic activity, which may be due to the heterostructure junction effect.[266] Yang *et al.* produced TiO_2-$BaTiO_3$ core-shell nanowires, by two separate hydrothermal syntheses, first preparing TiO_2 nanowires and then growing $BaTiO_3$ surface coatings to fabricate photoelectrochemical photoanodes for water splitting, Figure 24.[267]

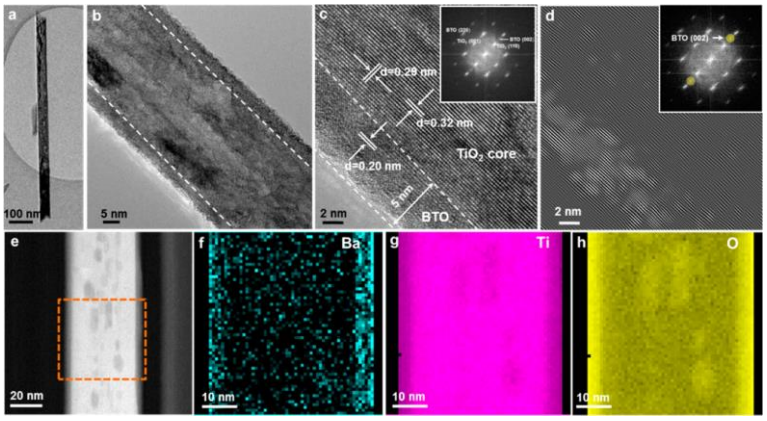

Figure 24: $TiO_2/BaTiO_3$ core/shell nanowires: (a,b) Representative TEM images and (c) high-resolution TEM image of an individual nanowire synthesised with an inset of the corresponding FFT image, (d) Selected inverse FFT image obtained from the marked FFT spots in the inset, which corresponds to (002) and $(00\bar{2})$ planes of $BaTiO_3$. The bright area represents the $BaTiO_3$ composition. (e) STEM image of the $TiO_2/BaTiO_3$ NWs. (f–h) EELS elemental mapping of the dashed-square marked region in panel e for (f) Ba, (g) Ti, and (h) O. Reprinted (adapted) with permission from W. G. Yang, Y. H. Yu, M. B. Starr, X. Yin, Z. D. Li, A. Kvit, S. F. Wang, P. Zhao, X. D. Wang, *Nano Lett.* **2015**, *15*, 7574-7580. Copyright (2015) American Chemical Society

Other perovskite solid-solutions whose hydrothermal synthesis has been studied include (1-x)$K_{0.5}Na_{0.5}NbO_3$-x$LiSbO_3$,[268] $REFe_{0.5}Cr_{0.5}O_3$ (RE = La, Tb, Ho, Er, Yb, Lu and Y), [269] $LaCr_{1-x}Mn_xO_3$ (x=0.1, 0.2, and 0.3).[270] In the niobate and tantalate family, the $Na(Bi_xTa_{1-x})O_3$ solid-solution (x = 0–0.10) has been prepared from hydrothermal reactions,[271] and the formation of the $(K,Na)(Nb,Sb)O_3$ solid solution was studied.[272] La-doping in $NaTaO_3$ was investigated at low La levels,[273], and similarly Sr-substitution in $NaTaO_3$,[274] and La in $KaTaO_3$ have been reported.[275] While low levels of the substituent metal modify properties, such as for photocatalysis, the distribution of the additional metal and the charge-balancing mechanisms needs careful consideration. Co-substitution in $BiFeO_3$ has been reported by direct hydrothermal reaction to give $Bi_{0.95}Sr_{0.05}Fe_{0.95}Co_{0.05}O_3$ as well as singly substituted $Bi_{0.95}Sr_{0.05}FeO_3$ and $BiFe_{0.95}Co_{0.05}O_3$ and this allowed a significant reduction in the band gap to provide enhanced photocatalytic properties.[276] In the case of B-site manganese perovskites, substitutional variants of both orthorhombic $RMn_{0.5}Fe_{0.5}O_3$ (R = Tb, Dy, and Ho)[277] and hexagonal $RMn_{1-x}Fe_xO_3$ (R = Er, Tm, Yb and Lu; x = 0, 0.1, 0.3 and 0.5)[278] materials have been reported using similar solution redox chemistry to the manganites discussed above in Section 3.4.

In addition to the titanate-TiO_2 composite materials already mentioned there have been reports of other oxide heterostructures from hydrothermal reactions. For photocatalysis the aim has been to generate heterojunctions that may modify optical properties, such as minimising charge recombination and this has been investigated for $NaNbO_3$/ZnO [279] and $NaNbO_3$/CeO_2, the latter case CeO_2 added to hydrothermally prepared $NaNbO_3$ by a precipitation-calcination approach.[280] Other properties that have been investigated by such approaches, include electrical and magnetic anisotropy in grain-oriented $Bi_4Ti_3O_{12}$–$La_{0.5}Sr_{0.5}MnO_3$ ceramics produced from powders formed under hydrothermal conditions.[281] Magnetoelectric properties of (1-x)$Pb(Zr_{0.52}Ti_{0.48})O_3$-(x)$CoFe_2O_4$ composites were studied from samples made from fine powders of PZT annealed with the cobalt ferrite spinel.[282]

4. Summary and Outlook

The past decade has seen a rapid growth of interest in the use of solvothermal routes to perovskite oxides, expanding upon earlier work on prototypical materials such as

$BaTiO_3$, $NaNbO_3$ and rare-earth manganites, to explore almost all possible compositional variants of B-site perovskites. This has been further expanded to include solid solutions containing up to five different cations, and also heterostructures that contain interfaces between a perovskite and a different structure type. A large focus of this work has emphasised control of product form, with crystal size and shape being dictated not only by choice of chemical reagents, but also temperature and time of reaction. In some cases intricate crystal morphology results in apparently 'template free' conditions, while in others, solution additives have been purposely introduced that affect the pathways of crystallisation, or non-aqueous solvents used that can influence the resultant crystal form. Despite the large body of work in this respect, and the success in growing complex crystal forms, it remains difficult at present to predict the effect of the balance of reaction conditions on the crystal morphology. It is most likely the case that one set of reagents and conditions cannot be applied to another perovskite family, bearing in mind the different solubilities of cations, and, in some cases, the redox chemistry at play during the crystallisation. The group of Feng have reviewed some of the aspects of faceting in the formation of perovskite crystals and have proposed crystal growth mechanisms for some families, such as chromites and ferrites;[221] this provides a basis for control of crystal growth, but at the same time highlights the need for a greater fundamental understanding.

The ability to control crystal form is nevertheless having implications on the properties of the resulting materials: examples discussed above include the production of fine powders of titanates than can be easily sintered, at lower temperatures than otherwise, into dense electroceramics, or with oriented grains, and how shape of crystals can influence photocatalytic properties of $BiFeO_3$ or $NaNbO_3$. Particularly relevant for the applications of materials is the growth of layers or coatings, which may be continuous films, or arrays of attached and oriented particles, and there is clearly increased effort in this area for formation of devices.

To put crystal growth mechanism on a more quantitative basis, much experimental work is still needed, and the challenges here lie in the need to develop methods for following crystallisation *in situ* from within reaction vessels to track the formation of crystalline products from reactive solutions. Reviews of the progress of such methods have appeared in the past few years,[283] [284] and as illustrated above, some striking results have been obtained from study of niobate perovskites where a sequence of

crystalline phases appears.[155] This occurrence of transient, metastable phases, emphasises the need to understand the solution chemistry, in order to translate laboratory preparative chemistry to reliable, reproducible, and scalable manufacture of materials. The use of *in situ* studies is heavily reliant on access to powerful radiation sources such as synchrotrons, but continued developments at such central facilities mean that availability of such methods is increasing, and new techniques are emerging that can provide fine detail about the assembly of matter. For example, the pair distribution function method has been applied to follow crystallisation of oxides from hydrothermal solutions,[285] and kinetics of formation of $BaZrO_3$ nanoparticles from supercritical water have been followed on the millisecond timescale using *in situ* X-ray diffraction.[286] The quality of data obtained in these *in situ* experiments means that, for example, the evolution of lattice parameters and crystallite domain size can be tracked by refinement against diffraction profiles, as shown for $BaTiO_3$ formation.[287] The combination of spectroscopy and diffraction measurements is especially powerful and Philippot *et al.* used IR, Raman and X-ray photoelectron spectroscopy to rationalise the observations made by *in situ* diffraction on the growth of $Ba_xSr_{1-x}TiO_3$ in supercritical water, to reveal that the density of surface –OH groups strongly influenced particle growth.[288]

It is also useful to consider how computational modelling may contribute to understanding, and then predicting, new hydrothermal reactions. In the case of perovskites, in the 1990s Riman and co-workers used tabulated standard-state thermodynamic data for solid and aqueous species to generate phase stability diagrams for the hydrothermal formation of the perovskites $PbTiO_3$ and $BaTiO_3$ as a function of pH,[289] and similar methods have been used for other oxides.[290] This approach has, however, not been adopted for other perovskites, which may be due to the additional complexity of studying redox-active metal cations, but could be worth reinvestigating with the large number of synthetic parameters now reported. Another predictive approach for materials synthesis that has recently emerged is based on machine-learning: Raccuglia *et al.* used a database of synthesis variables for the solvothermal crystallisation of organic–inorganic hybrid materials that parameterised conditions for not only successful but also failed reactions, to predict reaction conditions for new materials with a statistically significant success rate.[291] Kim and co-workers have used machine-learning to search published experimental details to derive a collection of

synthesis parameters for oxides[292], and more recently, Ceder and co-workers have also created a database of reaction conditions for solid-state materials synthesis by text-mining of literature: this includes more than 19,000 entries;[293] although these approaches do not necessarily allow prediction of new conditions, these methods could provide another way to guide the synthesis of perovskites and could conceivably include synthesis parameters that related to crystal morphology

In terms of scaling laboratory preparations for materials manufacture, the hydrothermal synthesis is already known in industry, where large batch reactors are used to manufacture, for example, zeolites[294] and quartz crystals[295] on a commercial scale. More recently, a large effort has been made on developing continuous-flow reactors for the efficient production of large volumes of polycrystalline material in hydrothermal conditions, and, on various scales, mixed-metal oxide materials have been produced with particular emphasis on nanostructured powders.[296] This includes perovskites, such as $BaZrO_3$,[297] $BaTiO_3$,[298] $Ba_{1-x}Sr_xTiO_3$,[299] with the last being produced at pilot scale of 80 g h^{-1}, as well as the already-mentioned cases of $LaCrO_3$[179] and $La_{1-x}Sr_xMnO_3$.[199] These works illustrate the possibilities of scaling laboratory chemistry to make functional materials for applications in industry and technology, and this is an area that will undoubtedly be of future attention, given the need to develop energy-efficient and environmentally benign ways of manufacturer. Related to the use of materials in real applications is the issue of structural defects and how these affect bulk properties: for example, as highlighted above, the presence of even low levels of hydroxide ions in the perovskite structure, with associated charge-balancing vacancies, may diminish certain electronic properties. This must be a consideration in future research and synthetic chemistry optimised to minimise or control defects should be developed.

Returning to point of view of fundamental chemistry, it is especially important to note that in some cases the hydrothermal method has allowed access to new perovskite compositions not seen under conventional synthesis conditions. This is exemplified by the work of Kumada and co-workers (Section 3.6) who have prepared a set of bismuthate perovskites that show superconductivity but whose synthesis at elevated temperature is impossible due to phase collapse, probably due to the volatility of bismuth and its binary oxides. It is also pertinent to note that while many perovskite compositions are accessible under solvothermal conditions, for certain materials

synthesis appears impossible, or at least has not yet been achieved, suggesting that precise conditions of stability for certain phases may be narrow. For example, in contrast to the now extensive work on ferrite perovskites, there is very little evidence for the direct hydrothermal, or solvothermal synthesis of cobaltite, $ACoO_3$, or nickelate, $ANiO_3$, perovskites. Only the formation of $BiCoO_3$ has been reported as occurring directly from solution, in this case with poly(vinylpyrrolidone) as additive in aqueous NaOH at 120 °C, giving distinctive ribbon-shaped crystallites, Figure 25, from which a bipolar resistive switching property was measured.[300] $BiCoO_3$ possesses a highly distorted variant of the perovskite structure ($PbTiO_3$-type) in which the Co is shifted far from the centre of the octahedra to reside in five-coordinate sites. It may be the case that the difficulty in oxidising Co and Ni to the +3 oxidation state (especially for the latter) makes the solution synthesis of cobaltites and nickelates challenging, but this could be an interesting area for future investigation.

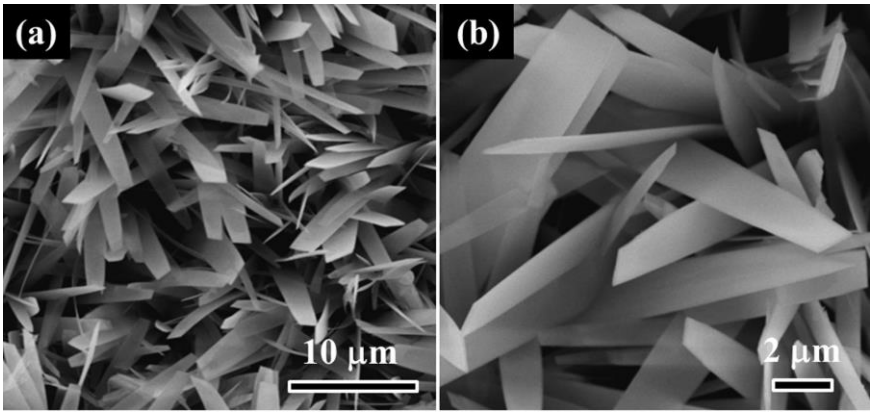

Figure 25: Ribbons of $BiCoO_3$ at two magnifications prepared by hydrothermal crystallisation. Reprinted from Chemical Physics Letters, Vol 613, B. Sun, W. X. Zhao, H. W. Li, L. J. Wei, P. Chen, Reversible resistive switching behaviors of multiferroic single-crystalline $BiCoO_3$ microribbons, Pages 100-103, Copyright (2014), with permission from Elsevier

In earlier work we examined the possible relationship between perovskite tolerance factor and accessibility of various manganite perovskites under mild hydrothermal conditions.[183a] This showed that hydrothermal synthesis was possible for materials with Goldschmidt tolerance factor of close to 1 and whose variance of A-site radii in multi-element systems was close to zero: *i.e.*, the least structurally distorted materials could be isolated under mild reaction conditions. Earlier work by others had proved by

calorimetry that the least distorted (A,A')MnO_3 perovskites possessed the largest enthalpy of formation (albeit from solid-state synthesis using the constituent binary oxides),[301] providing a possible link between crystal structure energetics and synthetic accessibility. Yamaguchi *et al.* suggested a similar relationship between tolerance factor and successful low temperature synthesis for $BaZrO_3$ and $BaHfO_3$, by a gel conversion route.[71] To update these ideas, Figure 26, shows a plot of tolerance factor *vs* synthetic accessibility for various manganite and chromite perovskites prepared in our own work,[170, 172, 182b, 302] and from others' work. [181, 303] This is simply a scatter graph to represent successful synthesis or not (under otherwise identical conditions), but illustrates a principle concerning the relationship between crystal chemistry and possibility of synthesis. This could provide a semi-quantitative guide to future solvothermal synthesis of perovskites and could provide a starting point for computer simulations to lead to the deeper understanding of materials synthesis.

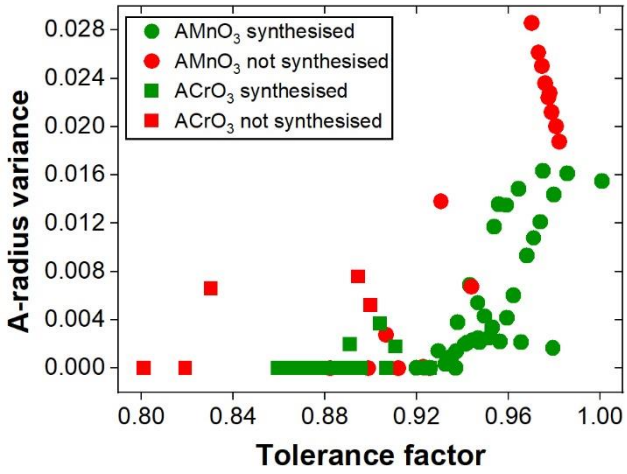

Figure 26: Scatter plot of tolerance factor and A cation radius variance for $AMnO_3$ and $ACrO_3$ perovskites with successful and unsuccessful hydrothermal synthesis indicated at T < 300 ^oC for manganites and T < 450 ^oC for chromites. This contains materials with two or more A-site cations, as well as ternary phases, and Table S1 contains the chemical compositions for the data points.

Acknowledgements

The author is grateful to the Royal Society for funding an industry fellowship with Johnson Matthey 2015-2019 during which some of the ideas in this article were developed. Numerous collaborators and research students whose work has contributed

to developing solvothermal synthesis of inorganic materials are thanked and the PhD thesis work of Dr Jeroen Spooren and Dr Luke Daniels is especially acknowledged.

Conflict of Interest

There are no conflicts of interest to declare.

References

[1] Y. Zhou, G. R. Patzke, *Chimia* **2010**, *64*, 252-258.
[2] a) C. K. Mavrokefalos, G. R. Patzke, *Inorganics* **2019**, *7*; b) D. K. Lee, D. Lee, M. A. Lumley, K. S. Choi, *Chem. Soc. Rev.* **2019**, *48*, 2126-2157.
[3] a) S. Martha, P. C. Sahoo, K. M. Parida, *RSC Adv.* **2015**, *5*, 61535-61553; b) C. P. Xu, P. R. Anusuyadevi, C. Aymonier, R. Luque, S. Marre, *Chem. Soc. Rev.* **2019**, *48*, 3868-3902.
[4] F. F. Abdi, S. P. Berglund, *J. Phys. D* **2017**, *50*.
[5] M. Jansen, *Angew. Chem., Int. Ed.* **2002**, *41*, 3747-3766.
[6] Y. B. Mao, T. J. Park, S. S. Wong, *Chem. Commun.* **2005**, 5721-5735.
[7] a) G. Demazeau, *J. Mater. Chem.* **1999**, *9*, 15-18; b) G. Demazeau, *J. Mater. Sci.* **2008**, *43*, 2104-2114; c) G. Demazeau, *Z. Natur. Sect. B* **2010**, *65*, 999-1006.
[8] C. S. Cundy, P. A. Cox, *Chem. Rev.* **2003**, *103*, 663-701.
[9] R. A. Laudise, *Chem. Eng. News.* **1987**, *65*, 30-&.
[10] A. Rabenau, *Angew. Chem., Int. Ed.* **1985**, *24*, 1026-1040.
[11] a) S. Sōmiya, R. Roy, *Bull. Mater. Sci.* **2000**, *23*, 453-460; b) R. E. Riman, W. L. Suchanek, M. M. Lencka, *Ann. Chim. - Sci. Mater.* **2002**, *27*, 15-36; c) S. Komarneni, *Current Science* **2003**, *85*, 1730-1734; d) M. Yoshimura, K. Byrappa, *J. Mater. Sci.* **2008**, *43*, 2085-2103; e) N. Kumada, *J. Ceram. Soc. Jpn.* **2013**, *121*, 135-141.
[12] M. Niederberger, G. Garnweitner, N. Pinna, G. Neri, *Prog. Solid State Chem.* **2005**, *33*, 59-70.
[13] C. I. Hiley, R. I. Walton, *CrystEngComm* **2016**, *18*, 7656-7670.
[14] a) K. Kajiyoshi, K. Yanagisawa, M. Yoshimura, *J. Euro. Ceram. Soc.* **2006**, *26*, 605-611; b) T. Morita, *Materials* **2010**, *3*, 5236-5245; c) J. Ortiz-Landeros, C. Gomez-Yanez, R. Lopez-Juarez, I. Davalos-Velasco, H. Pfeiffer, *J. Adv. Ceram.* **2012**, *1*, 204-220; d) L. J. Li, L. Miao, Z. Zhang, X. H. Pu, Q. Feng, K. Yanagisawa, Y. Fan, M. J. Fan, P. H. Wen, D. W. Hu, *J. Mater. Chem. A* **2019**, *7*, 16046-16067.
[15] D. R. Modeshia, R. I. Walton, *Chem. Soc. Rev.* **2010**, *39*, 4303-4325.
[16] a) A. S. Bhalla, R. Y. Guo, R. Roy, *Mater. Res. Innov.* **2000**, *4*, 3-26; b) R. H. Mitchell, *Perovskites Modern and Ancient*, Almaz Press, Thunder Bay, Ontario **2002**.
[17] J. J. Zhu, H. L. Li, L. Y. Zhong, P. Xiao, X. L. Xu, X. G. Yang, Z. Zhao, J. L. Li, *ACS Catal.* **2014**, *4*, 2917-2940.
[18] a) J. W. Shi, L. J. Guo, *Prog. Nat. Sci.* **2012**, *22*, 592-615; b) E. Grabowska, *Appl. Catal. B-Environ.* **2016**, *186*, 97-126.

[19] a) P. M. Rorvik, T. Grande, M. A. Einarsrud, *Adv. Mater.* **2011**, *23*, 4007-4034; b) N. Nuraje, K. Su, *Nanoscale* **2013**, *5*, 8752-8780; c) H. Wu, W. R. Xia, P. J. Xue, X. H. Zhu, *Ferroelectrics* **2017**, *518*, 127-136.
[20] a) M. M. Vijatovic, J. D. Bobic, B. A. Stojanovic, *Sci. Sinter.* **2008**, *40*, 155-165; b) M. M. Vijatovic, J. D. Bobic, B. D. Stojanovic, *Sci. Sinter.* **2008**, *40*, 235-244.
[21] J. H. Peterson, *Process for Producing Insoluble Titanates United States Patent 2218655*, **1940**.
[22] S. S. Flaschen, *J. Am. Chem. Soc.* **1955**, *77*, 6194-6194.
[23] B. B. Jiang, J. Iocozzia, L. Zhao, H. F. Zhang, Y. W. Harn, Y. H. Chen, Z. Q. Lin, *Chem. Soc. Rev.* **2019**, *48*, 1194-1228.
[24] J. Su, J. Zhang, *J. Mater. Sci.-Mater. Electron.* **2019**, *30*, 1957-1975.
[25] Y. Feng, W. L. Li, Y. F. Hou, Y. Yu, W. P. Cao, T. D. Zhang, W. D. Fei, *J. Mater. Chem. C* **2015**, *3*, 1250-1260.
[26] L. Tu, Y. You, C. Y. Liu, C. H. Zhan, Y. J. Wang, M. Z. Cheng, R. B. Wei, X. B. Liu, *Ceram. Int.* **2019**, *45*, 22841-22848.
[27] G. Busca, V. Buscaglia, M. Leoni, P. Nanni, *Chem. Mater.* **1994**, *6*, 955-961.
[28] a) P. K. Dutta, J. R. Gregg, *Chem. Mater.* **1992**, *4*, 843-846; b) E. Ciftci, M. N. Rahaman, M. Shumsky, *J. Mater. Sci.* **2001**, *36*, 4875-4882.
[29] M. Inada, N. Enomoto, K. Hayashi, J. Hojo, S. Komarnen, *Ceram. Int.* **2015**, *41*, 5581-5587.
[30] K. Hongo, S. Kurata, A. Jomphoak, M. Inada, K. Hayashi, R. Maezono, *Inorg. Chem.* **2018**, *57*, 5413-5419.
[31] A. O'Brien, D. I. Woodward, K. Sardar, R. I. Walton, P. A. Thomas, *Appl. Phys. Lett.* **2012**, *101*, 142902.
[32] M. H. Harunsani, D. I. Woodward, M. D. Peel, S. E. Ashbrook, R. I. Walton, *J. Solid State Chem.* **2013**, *207*, 117-125.
[33] Y. Sato, M. Aoki, R. Teranishi, K. Kaneko, M. Takesada, H. Moriwake, H. Takashima, Y. Hakuta, *ACS Appl. Nano. Mater.* **2019**, *2*, 5761-5768.
[34] B. Xie, H. B. Zhang, H. Kan, S. S. Liu, M. Y. Li, Z. Y. Li, S. Zhu, S. Y. Qiu, S. L. Jiang, *Ceram. Int.* **2017**, *43*, 2969-2973.
[35] a) Y. Ohara, K. Koumoto, H. Yanagida, *J. Am. Ceram. Soc.* **1994**, *77*, 2327-2331; b) Q. Feng, M. Hirasawa, K. Yanagisawa, *Chem. Mater.* **2001**, *13*, 290-296.
[36] J. O. Eckert, C. C. HungHouston, B. L. Gersten, M. M. Lencka, R. E. Riman, *J. Am. Ceram. Soc.* **1996**, *79*, 2929-2939.
[37] Y. Cao, K. J. Zhu, Q. L. Wu, Q. L. Gu, J. H. Qiu, *Mater. Res. Bull.* **2014**, *57*, 162-169.
[38] A. Lamberti, N. Garino, K. Bejtka, S. Bianco, S. Stassi, A. Chiodoni, G. Canavese, C. F. Pirri, M. Quaglio, *New. J. Chem.* **2014**, *38*, 2024-2030.
[39] F. Xia, J. W. Liu, D. Gu, P. F. Zhao, J. Zhang, R. C. Che, *Nanoscale* **2011**, *3*, 3860-3867.
[40] M. D. Ye, M. Y. Wang, D. J. Zheng, N. Zhang, C. J. Lin, Z. Q. Lin, *Nanoscale* **2014**, *6*, 3576-3584.
[41] F. Maxim, P. Ferreira, P. M. Vilarinho, A. Aimable, P. Bowen, *Cryst. Growth Des.* **2010**, *10*, 3996-4004.
[42] Q. Ma, K. Mimura, K. Kato, *J. Alloy. Compd.* **2016**, *655*, 71-78.
[43] X. Yang, Z. H. Ren, G. Xu, C. Y. Chao, S. Jiang, S. Q. Deng, G. Shen, X. Wei, G. R. Han, *Ceram. Int.* **2014**, *40*, 9663-9670.

[44] H. Q. Zhan, X. F. Yang, C. M. Wang, J. Chen, Y. P. Wen, C. L. Liang, H. F. Greer, M. M. Wu, W. Z. Zhou, *Cryst. Growth Des.* **2012**, *12*, 1247-1253.
[45] X. F. Yang, J. X. Fu, C. J. Jin, J. A. Chen, C. L. Liang, M. M. Wu, W. Z. Zhou, *J. Am. Chem. Soc.* **2010**, *132*, 14279-14287.
[46] J. D. Zhuang, Q. F. Tian, S. Lin, W. B. Yang, L. H. Chen, P. Liu, *Appl. Catal. B-Environ.* **2014**, *156*, 108-115.
[47] J. Yang, B. Y. Geng, Y. X. Ye, X. Yu, *CrystEngComm* **2012**, *14*, 2959-2965.
[48] a) H. Y. Zhao, Y. W. Duan, X. Sun, *New. J. Chem.* **2013**, *37*, 986-991; b) Y. X. Yan, H. Yang, X. X. Zhao, H. M. Zhang, J. L. Jiang, *J. Electron. Mater.* **2018**, *47*, 3045-3050.
[49] D. B. Yu, J. H. Zhang, F. Wang, M. H. Zhao, K. Du, S. W. Shu, J. W. Zou, Y. Wang, *Cryst. Growth Des.* **2013**, *13*, 3138-3143.
[50] a) T. Kimijima, K. Kanie, M. Nakaya, A. Muramatsu, *CrystEngComm* **2014**, *16*, 5591-5597; b) T. Z. Chen, L. Bao, Y. R. Zheng, X. Yang, L. Y. Ruan, Y. Liu, G. Xu, G. R. Han, *CrystEngComm* **2019**, *21*, 4763-4770.
[51] W. X. Dong, B. Song, W. J. Meng, G. L. Zhao, G. R. Han, *Appl. Surf. Sci.* **2015**, *349*, 272-278.
[52] a) W. X. Dong, G. L. Zhao, B. Song, G. Xu, J. Zhou, G. R. Han, *CrystEngComm* **2012**, *14*, 6990-6997; b) W. X. Dong, B. Song, G. L. Zhao, G. R. Han, *Mater. Res. Bull.* **2013**, *48*, 4633-4640; c) W. X. Dong, Q. F. Bao, X. Y. Gu, G. L. Zhao, *J. Ceram. Soc. Jpn.* **2015**, *123*, 643-648; d) T. Z. Chen, Y. R. Zheng, Z. H. Lu, T. Xu, Y. Liu, X. D. Meng, G. Xu, G. R. Han, *Nanotechnology* **2019**, *30*, 9.
[53] J. Y. Pei, J. Meng, S. Y. Wu, Q. Y. Lin, J. X. Li, X. Wei, G. R. Han, Z. Zhang, *J. Alloy. Compd.* **2019**, *806*, 889-896.
[54] H. Q. Zhan, Z. G. Chen, J. L. Zhuang, X. F. Yang, Q. L. Wu, X. P. Jiang, C. L. Liang, M. M. Wu, J. Zou, *J. Phys. Chem. C* **2015**, *119*, 3530-3537.
[55] S. Q. Deng, G. Xu, H. W. Bai, L. L. Li, S. Jiang, G. Shen, G. R. Han, *Inorg. Chem.* **2014**, *53*, 10937-10943.
[56] G. Xu, X. Q. Huang, V. Krstic, S. Q. Chen, X. Yang, C. Y. Chao, G. Shen, G. R. Han, *CrystEngComm* **2014**, *16*, 4373-4376.
[57] a) T. Takenaka, K. Maruyama, K. Sakata, *Jpn. J. Appl. Phys.* **1991**, *30*, 2236-2239; b) G. O. Jones, P. A. Thomas, *Acta Crystallogr. Sect. B* **2002**, *58*, 168-178.
[58] a) T. L. Lu, J. H. Dai, J. T. Tian, W. W. Song, X. Z. Liu, L. Lai, H. J. Chu, X. Huang, X. Y. Liu, *J. Alloy. Compd.* **2010**, *490*, 232-235; b) T. Setinc, M. Spreitzer, M. Logar, D. Suvorov, *J. Am. Ceram. Soc.* **2011**, *94*, 3793-3799; c) H. Z. Zhang, M. K. Zhu, Y. D. Hou, R. Z. Wang, H. Yan, L. Y. Liu, *Int. J. Appl. Ceram. Technol.* **2016**, *13*, 569-578.
[59] K. Sardar, R. I. Walton, *J. Solid State Chem.* **2012**, *189*, 32-37.
[60] X. Ma, W. X. Zhang, L. H. Xue, S. M. Yin, L. Wan, Y. W. Yan, *J. Mater. Sci.* **2013**, *48*, 6878-6884.
[61] X. F. Zhou, C. Jiang, C. Chen, H. Luo, K. C. Zhou, D. Zhang, *CrystEngComm* **2016**, *18*, 1302-1310.
[62] a) K. Kanie, Y. Numamoto, S. Tsukamoto, T. Sasaki, M. Nakaya, J. Tani, H. Takahashi, A. Muramatsu, *Mater. Trans.* **2011**, *52*, 1396-1401; b) X. P. Jiang, M. Lin, N. Tu, C. Chen, S. L. Zhou, H. Q. Zhan, *J. Alloy. Compd.* **2011**, *509*, 9346-9350; c) B. Li, M. S. Cao, J. Liu, D. W. Wang, *J. Am. Ceram. Soc.* **2016**, *99*, 2316-2326.
[63] Z. H. Ai, G. Lu, S. C. Lee, *J. Alloy. Compd.* **2014**, *613*, 260-266.

[64] M. H. Harunsani, D. I. Woodward, P. A. Thomas, R. I. Walton, *Dalton Trans.* **2015**, *44*, 10714-10720.
[65] Y. F. Huang, J. H. Wu, Y. L. Wei, J. M. Lin, M. L. Huang, *J. Alloy. Compd.* **2008**, *456*, 364-367.
[66] a) M. L. Moreira, J. Andres, J. A. Varela, E. Longo, *Cryst. Growth Des.* **2009**, *9*, 833-839; b) L. R. Macario, M. L. Moreira, J. Andres, E. Longo, *CrystEngComm* **2010**, *12*, 3612-3619.
[67] R. A. Gouvea, E. M. Flores, S. D. Cava, M. L. Moreira, *J. Lumines.* **2016**, *180*, 73-80.
[68] R. Borja-Urby, L. A. Diaz-Torres, I. Garcia-Martinez, D. Bahena-Uribe, G. Casillas, A. Ponce, M. Jose-Yacaman, *Catal. Today* **2015**, *250*, 95-101.
[69] K. De Keukeleere, J. Feys, M. Meire, J. De Roo, K. De Buysser, P. Lommens, I. Van Driessche, *J. Nanopart. Res.* **2013**, *15*, 12.
[70] F. Boschini, A. Rulmont, R. Cloots, B. Vertruyen, *J. Euro. Ceram. Soc.* **2009**, *29*, 1457-1462.
[71] Y. Yamaguchi, M. Fukushima, S. Ito, K. Fujimoto, *Chem. Lett.* **2016**, *45*, 226-228.
[72] Z. H. Dong, T. N. Ye, Y. N. Zhao, J. G. Yu, F. Q. Wang, L. L. Zhang, X. B. Wang, S. K. Guo, *J. Mater. Chem.* **2011**, *21*, 5978-5984.
[73] K. Kanie, Y. Seino, M. Matsubara, A. Muramatsu, *Adv. Powder Technol.* **2017**, *28*, 55-60.
[74] K. Kanie, Y. Seino, M. Matsubara, M. Nakaya, A. Muramatsu, *New. J. Chem.* **2014**, *38*, 3548-3555.
[75] H. B. Zhang, J. Qiao, G. S. Li, S. Y. Li, G. W. Wang, J. Wang, Y. T. Song, *Ultrason. Sonochem.* **2018**, *42*, 356-367.
[76] L. L. Zhang, J. L. Wang, D. J. Peng, F. Long, S. Y. Mo, Y. Wu, Z. G. Zou, *J. Phys. Chem. Solids* **2017**, *104*, 1-7.
[77] T. Chen, J. Meng, Q. Y. Lin, X. Wei, J. X. Li, Z. Zhang, *J. Alloy. Compd.* **2019**, *780*, 498-503.
[78] a) T. N. Ye, Z. H. Dong, Y. N. Zhao, J. G. Yu, F. Q. Wang, S. K. Guo, Y. C. Zou, *Langmuir* **2011**, *27*, 8878-8884; b) T. N. Ye, Z. H. Dong, Y. N. Zhao, J. G. Yu, F. Q. Wang, S. K. Guo, Y. C. Zou, *CrystEngComm* **2011**, *13*, 3842-3847; c) T. N. Ye, Z. H. Dong, Y. N. Zhao, J. G. Yu, F. Q. Wang, L. L. Zhang, Y. C. Zou, *Dalton Trans.* **2011**, *40*, 2601-2606.
[79] F. Schiedeck, T. Morita, *J. Electroceram.* **2012**, *28*, 45-52.
[80] X. H. Zhu, J. Zhou, J. M. Zhu, Z. G. Liu, Y. Y. Li, T. Al-Kassab, *J. Am. Ceram. Soc.* **2014**, *97*, 1987-1992.
[81] P. K. Panda, B. Sahoo, *Ferroelectrics* **2015**, *474*, 128-143.
[82] S. A. Mabud, *J. Appl. Cryst.* **1980**, *13*, 211-216.
[83] K. Shimomura, T. Tsurumi, Y. Ohba, M. Daimon, *Jpn. J. Appl. Phys.* **1991**, *30*, 2174-2177.
[84] a) G. Xu, W. Jiang, M. Qian, X. X. Chen, Z. B. Li, G. R. Han, *Cryst. Growth Des.* **2009**, *9*, 13-16; b) Z. C. Qiu, J. P. Zhou, G. Q. Zhu, P. Liu, X. B. Bian, *Bull. Mater. Sci.* **2009**, *32*, 193-197; c) S. H. Kim, S. Komarneni, *Ceram. Int.* **2011**, *37*, 1101-1107; d) K. J. Zhu, R. Q. Zhu, N. N. Dong, H. H. Gu, J. H. Qiu, H. L. Ji, *J. Inorg. Mater.* **2012**, *27*, 507-512; e) C. A. Oliveira, E. Longo, J. A. Varela, M. A. Zaghete, *Ceram. Int.* **2014**, *40*, 1717-1722; f) H. L. Huang, G. Z. Cao, I. Y. Shen, *Sens. Actuator A-Phys.* **2014**, *214*, 111-119.
[85] a) G. F. Teixeira, G. Gasparotto, E. C. Paris, M. A. Zaghete, E. Longo, J. A. Varela, *J. Lumines.* **2012**, *132*, 46-50; b) G. Xu, X. Yang, C. X. Hua, J. H. He,

Z. H. Ren, W. J. Weng, P. Y. Du, G. Shen, G. R. Han, *CrystEngComm* **2012**, *14*, 6783-6787; c) G. F. Teixeira, M. A. Zaghete, G. Gasparotto, M. G. S. Costa, J. W. M. Espinosa, E. Longo, J. A. Varela, *J. Alloy. Compd.* **2012**, *512*, 124-127; d) J. Wang, A. Durussel, C. S. Sandu, M. G. Sahini, Z. B. He, N. Setter, *J. Cryst. Growth* **2012**, *347*, 1-6; e) C. F. Chen, A. D. Wang, X. L. Han, C. Y. Ni, J. Liu, *Sci. Adv. Mater.* **2012**, *4*, 749-752; f) S. Bai, Q. Xu, L. Gu, F. Ma, Y. Qin, Z. L. Wang, *Nano Energy* **2012**, *1*, 789-795; g) Q. X. Peng, W. B. Luo, C. G. Wu, X. Y. Sun, P. Li, X. Y. Chen, *J. Mater. Sci.-Mater. Electron.* **2014**, *25*, 1627-1632; h) C. Glass, W. Ahmed, J. van Ruitenbeek, *Mater. Lett.* **2014**, *125*, 71-74; i) J. Wang, J. Trodahl, C. Sandu, I. Gregora, N. Setter, *J. Euro. Ceram. Soc.* **2014**, *34*, 2311-2316; j) X. Zhang, J. F. Chen, Y. Wang, *ACS Appl. Nano. Mater.* **2018**, *1*, 1461-1466; k) Y. Takada, K. Mimura, K. Kato, *J. Ceram. Soc. Jpn.* **2018**, *126*, 326-330.

[86] a) Y. R. Lin, Y. T. Liu, H. A. Sodano, *Appl. Phys. Lett.* **2009**, *95*, 122901; b) A. Datta, D. Mukherjee, M. Hordagoda, S. Witanachchi, P. Mukherjee, R. V. Kashid, M. A. More, D. S. Joag, P. G. Chavan, *ACS Appl. Mater. Interfaces* **2013**, *5*, 6261-6267; c) C. G. Wu, Q. X. Peng, X. Y. Sun, J. Meng, S. Yao, W. B. Luo, W. L. Zhang, *Jpn. J. Appl. Phys.* **2015**, *54*, 04dh16; d) Q. L. Zhao, G. P. He, J. J. Di, W. L. Song, Z. L. Hou, P. P. Tan, D. W. Wang, M. S. Cao, *ACS Appl. Mater. Interfaces* **2017**, *9*, 24696-24703; e) W. C. Jin, Z. Wang, H. Huang, X. K. Hu, Y. H. He, M. Li, L. Y. Li, Y. H. Gao, Y. M. Hu, H. S. Gu, *RSC Adv.* **2018**, *8*, 7422-7427.

[87] a) B. P. Zhu, Q. F. Zhou, J. Shi, K. K. Shung, S. Irisawa, S. Takeuchi, *Appl. Phys. Lett.* **2009**, *94*, 102901; b) H. Nii, A. Kunishige, H. Nakagawa, T. Koyanagi, *Jpn. J. Appl. Phys.* **2011**, *50*, 091501; c) S. H. Kim, S. Komarneni, *Ceram. Int.* **2011**, *37*, 3211-3216; d) K. Ohta, G. Isobe, P. Bornmann, T. Hemsel, T. Morita, Ieee, in *2012 IEEE International Ultrasonics Symposium*, IEEE, New York, **2012**, pp. 186-189; e) T. Hasegawa, M. Ishikawa, M. K. Kurosawa, S. Takeuchi, *Electr. Commun. Jpn.* **2012**, *95*, 1-8; f) K. Bi, Z. L. He, Y. G. Wang, *Thin Solid Films* **2012**, *520*, 5575-5578; g) K. Ohta, G. Isobe, P. Bornmann, T. Hemsel, T. Morita, *Ultrasonics* **2013**, *53*, 837-841; h) T. Abe, S. Ozeki, M. K. Kurosawa, S. Takeuchi, *Jpn. J. Appl. Phys.* **2015**, *54*, 07hb06; i) B. P. Zhu, J. Xu, Y. Li, T. Wang, K. Xiong, C. Lee, X. F. Yang, M. Shiiba, S. Takeuchi, Q. F. Zhou, K. K. Shung, *AIP Adv.* **2016**, *6*, 6; j) K. Saigusa, T. Morita, *Jpn. J. Appl. Phys.* **2016**, *55*, 07kc05; k) D. L. Wang, J. Ou-Yang, W. E. Guo, X. F. Yang, B. P. Zhu, *Ceram. Int.* **2017**, *43*, 9573-9576; l) G. H. Feng, K. Y. Lee, *R. Soc. Open Sci.* **2017**, *4*, 14.

[88] a) C. Andrews, Y. R. Lin, H. X. Tang, H. A. Sodano, *J. Intell. Mater. Syst. Struct.* **2011**, *22*, 1879-1886; b) W. W. Xu, H. L. Huang, Y. F. Liu, C. Luo, G. Z. Cao, I. Y. Shen, *Sens. Actuator A-Phys.* **2016**, *246*, 102-113; c) Y. Zhang, W. L. Zhu, C. K. Jeong, H. J. Sun, G. Yang, W. Chen, Q. Wang, *RSC Adv.* **2017**, *7*, 32502-32507.

[89] K. Bian, Q. L. Gu, K. J. Zhu, R. Q. Zhu, J. Wang, J. S. Liu, J. H. Qiu, *J. Mater. Sci.-Mater. Electron.* **2016**, *27*, 8573-8579.

[90] A. Datta, D. Mukherjee, S. Witanachchi, P. Mukherjee, *Adv. Funct. Mater.* **2014**, *24*, 2638-2647.

[91] Y. Takada, K. Mimura, Z. Liu, K. Kato, *Jpn. J. Appl. Phys.* **2019**, *58*, Sllb08.

[92] a) K. Wang, J. F. Li, *J. Adv. Ceram.* **2012**, *1*, 24-37; b) J. F. Li, K. Wang, F. Y. Zhu, L. Q. Cheng, F. Z. Yao, *J. Am. Ceram. Soc.* **2013**, *96*, 3677-3696.

[93] a) I. Santos, L. H. Loureiro, M. F. P. Silva, A. M. V. Cavaleiro, *Polyhedron* **2002**, *21*, 2009-2015; b) G. K. L. Goh, F. F. Lange, S. M. Haile, C. G. Levi, *J. Mater. Res.* **2003**, *18*, 338-345; c) E. Vasco, A. Magrez, L. Forro, N. Setter, *J. Phys. Chem. B* **2005**, *109*, 14331-14334; d) H. Y. Zhu, Z. F. Zheng, X. P. Gao, Y. N. Huang, Z. M. Yan, J. Zou, H. M. Yin, Q. D. Zou, S. H. Kable, J. C. Zhao, Y. F. Xi, W. N. Martens, R. L. Frost, *J. Am. Chem. Soc.* **2006**, *128*, 2373-2384.

[94] a) G. K. L. Goh, C. G. Levi, F. F. Lange, *J. Mater. Res.* **2002**, *17*, 2852-2858; b) G. K. L. Goh, C. G. Levi, J. H. Choi, F. F. Lange, *J. Cryst. Growth* **2006**, *286*, 457-464.

[95] S. Y. Wu, W. Zhang, X. M. Chen, *J. Mater. Sci.-Mater. Electron.* **2010**, *21*, 450-455.

[96] a) H. W. Song, W. H. Ma, *Ceram. Int.* **2011**, *37*, 877-882; b) A. Yu, J. S. Qian, L. Liu, H. Pan, X. F. Zhou, *Appl. Surf. Sci.* **2012**, *258*, 3490-3496; c) S. Z. Ji, H. Liu, Y. H. Sang, W. Liu, G. W. Yu, Y. H. Leng, *CrystEngComm* **2014**, *16*, 7598-7604.

[97] D. R. Modeshia, R. J. Darton, S. E. Ashbrook, R. I. Walton, *Chem. Commun.* **2009**, 68-70.

[98] X. G. Kong, D. W. Hu, P. H. Wen, T. Ishii, Y. Tanaka, Q. Feng, *Dalton Trans.* **2013**, *42*, 7699-7709.

[99] K. Kaseda, M. Takesue, T. M. Aida, M. Watanabe, H. Hayashi, R. L. Smith, *J. Supercrit. Fluids* **2011**, *58*, 279-285.

[100] a) S. L. Skjaervø, S. Sommer, P. Norby, E. D. Bojesen, T. Grande, B. B. Iversen, M. A. Einarsrud, *J. Am. Ceram. Soc.* **2017**, *100*, 3835-3842; b) S. L. Skjaervø, K. H. Wells, S. Sommer, T. D. Vu, J. R. Tolchard, W. van Beek, T. Grande, B. B. Iversen, M. A. Einarsrud, *Cryst. Growth Des.* **2018**, *18*, 770-774.

[101] M. Mann, S. Jackson, J. Kolis, *J. Solid State Chem.* **2010**, *183*, 2675-2680.

[102] B. K. Yun, Y. S. Koo, J. H. Jung, M. Song, S. Yoon, *Physica B* **2010**, *405*, 4866-4870.

[103] N. Kumada, Q. Dong, Y. Yonesaki, T. Takei, N. Kinomura, *J. Ceram. Soc. Jpn.* **2011**, *119*, 483-485.

[104] G. D. Shi, J. H. Wang, H. L. Wang, Z. J. Wu, H. P. Wu, *Ceram. Int.* **2017**, *43*, 7222-7230.

[105] K. Nakashima, Y. Toshima, Y. Kobayashi, Y. Ishikawa, M. Kakihana, *J. Asian Ceram. Soc.* **2019**, *7*, 544-550.

[106] R. Lopez-Juarez, R. Castaneda-Guzman, M. E. Villafuerte-Castrejon, *Ceram. Int.* **2014**, *40*, 14757-14764.

[107] a) C. N. W. Darlington, K. S. Knight, *Acta Crystallogr.* **1999**, *55*, 495-495; b) Y. Shiratori, A. Magrez, J. Dornseiffer, F. H. Haegel, C. Pithan, R. Waser, *J. Phys. Chem. B* **2005**, *109*, 20122-20130; c) K. E. Johnston, C. C. Tang, J. E. Parker, K. S. Knight, P. Lightfoot, S. E. Ashbrook, *J. Am. Chem. Soc.* **2010**, *132*, 8732-8746.

[108] K. E. Johnston, J. M. Griffin, R. I. Walton, D. M. Dawson, P. Lightfoot, S. E. Ashbrook, *Phys. Chem. Chem. Phys.* **2011**, *13*, 7565-7576.

[109] S. E. Ashbrook, L. Le Polles, R. Gautier, C. J. Pickard, R. I. Walton, *Phys. Chem. Chem. Phys.* **2006**, *8*, 3423-3431.

[110] J. S. Wu, D. F. Xue, *CrystEngComm* **2011**, *13*, 1966-1975.

[111] M. R. Joung, I. T. Seo, J. S. Kim, H. Xu, G. Han, M. G. Kang, C. Y. Kang, S. J. Yoon, S. Nahm, *Acta Mater.* **2013**, *61*, 3703-3708.

[112] S. Kim, J. H. Lee, J. Lee, S. W. Kim, M. H. Kim, S. Park, H. Chung, Y. I. Kim, W. Kim, *J. Am. Chem. Soc.* **2013**, *135*, 6-9.
[113] X. F. Zhou, Y. Chen, H. Mei, Z. L. Hu, Y. Q. Fan, *Appl. Surf. Sci.* **2008**, *255*, 2803-2807.
[114] a) K. J. Zhu, Y. Cao, X. H. Wang, L. Bai, J. H. Qiu, H. L. Ji, *CrystEngComm* **2012**, *14*, 411-416; b) M. Boukriba, F. Sediri, N. Gharbi, *Mater. Res. Bull.* **2013**, *48*, 574-580; c) Q. L. Gu, K. J. Zhu, J. S. Liu, J. Wang, P. C. Liu, Q. M. Sun, J. H. Qiu, *J. Am. Ceram. Soc.* **2014**, *97*, 3360-3362; d) Y. Lu, T. Karaki, T. Fujii, *Ceram. Int.* **2015**, *41*, S174-S179.
[115] a) K. Kanie, Y. Numamoto, S. Tsukamoto, H. Takahashi, H. Mizutani, A. Terabe, M. Nakaya, J. Tani, A. Muramatsu, *Mater. Trans.* **2011**, *52*, 2119-2125; b) H. Pan, G. S. Zhu, X. L. Chao, L. L. Wei, Z. P. Yang, *Mater. Chem. Phys.* **2011**, *126*, 183-187; c) M. Fukada, K. Shibata, T. Imai, S. Yamazoe, S. Hosokawa, T. Wada, *J. Ceram. Soc. Jpn.* **2013**, *121*, 116-119.
[116] J. H. Jung, M. Lee, J. I. Hong, Y. Ding, C. Y. Chen, L. J. Chou, Z. L. Wang, *ACS Nano* **2011**, *5*, 10041-10046.
[117] Z. B. Pan, L. M. Yao, G. L. Ge, B. Shen, J. W. Zhai, *J. Mater. Chem. A* **2018**, *6*, 14614-14622.
[118] A. Anand, M. C. Bhatnagar, *Mater. Res. Express* **2019**, *6*, 10.
[119] M. Ishikawa, H. Einishi, M. Nakajima, T. Hasegawa, T. Morita, Y. Saijo, M. Kurosawa, H. Funakubo, *Jpn. J. Appl. Phys.* **2010**, *49*, 07hf01.
[120] A. D. Handoko, G. K. L. Goh, R. X. Chew, *CrystEngComm* **2012**, *14*, 421-427.
[121] T. Shiraishi, N. Kaneko, M. Ishikawa, M. Kurosawa, H. Uchida, H. Funakubo, *Jpn. J. Appl. Phys.* **2014**, *53*, 09pa10.
[122] P. G. Kang, T. K. Lee, C. W. Ahn, I. W. Kim, H. H. Lee, S. B. Choi, K. D. Sung, J. H. Jung, *Nano Energy* **2015**, *17*, 261-268.
[123] S. B. Tu, F. W. Ming, J. W. Zhang, X. X. Zhang, H. N. Alshareef, *Adv. Mater.* **2019**, *31*, 7.
[124] H. F. Shi, X. K. Li, D. F. Wang, Y. P. Yuan, Z. G. Zou, J. H. Ye, *Catal. Lett.* **2009**, *132*, 205-212.
[125] Q. L. Gu, K. J. Zhu, N. S. Zhang, Q. M. Sun, P. C. Liu, J. S. Liu, J. Wang, Z. S. Li, *J. Phys. Chem. C* **2015**, *119*, 25956-25964.
[126] L. Q. Jiang, Y. H. Zhang, Y. Qiu, Z. G. Yi, *RSC Adv.* **2014**, *4*, 3165-3170.
[127] Q. N. Yu, F. Zhang, G. Q. Li, W. F. Zhang, *Appl. Catal. B-Environ.* **2016**, *199*, 166-169.
[128] M. S. Fan, B. Hu, X. Yan, C. J. Song, T. J. Chen, Y. Feng, W. D. Shi, *New. J. Chem.* **2015**, *39*, 6171-6177.
[129] Q. Q. Liu, Y. Y. Chai, L. Zhang, J. Ren, W. L. Dai, *Appl. Catal. B-Environ.* **2017**, *205*, 505-513.
[130] W. Chen, Y. Hu, M. W. Ba, *Appl. Surf. Sci.* **2018**, *435*, 483-493.
[131] L. Q. Jiang, Y. Qiu, Z. G. Yi, *J. Mater. Chem. A* **2013**, *1*, 2878-2885.
[132] L. S. Yan, J. Zhang, X. M. Zhou, X. X. Wu, J. Y. Lan, Y. S. Wang, G. Liu, J. G. Yu, L. J. Zhi, *Int. J. Hydrog. Energy* **2013**, *38*, 3554-3561.
[133] J. Q. Wang, X. Wang, Z. T. Cui, B. Liua, M. H. Cao, *Phys. Chem. Chem. Phys.* **2015**, *17*, 14185-14192.
[134] Y. W. Wang, X. G. Kong, W. L. Tian, D. Q. Lei, X. D. Lei, *RSC Adv.* **2016**, *6*, 58401-58408.
[135] P. X. Xing, S. J. Wu, Y. J. Chen, P. F. Chen, X. Hu, H. J. Lin, L. H. Zhao, Y. M. He, *ACS Sustain. Chem. Eng.* **2019**, *7*, 12408-12418.

[136] T. B. Wermuth, S. Arcaro, J. Venturini, T. M. H. Ribeiro, A. D. L. Rodriguez, E. L. Machado, T. F. de Oliveirad, S. E. F. de Oliveira, M. N. Baibich, C. P. Bergmann, *Ceram. Int.* **2019**, *45*, 24137-24145.
[137] T. Yokoi, J. Sakuma, K. Maeda, K. Domen, T. Tatsumi, J. N. Kondo, *Phys. Chem. Chem. Phys.* **2011**, *13*, 2563-2570.
[138] J. Y. Shi, G. J. Liu, N. Wang, C. Li, *J. Mater. Chem.* **2012**, *22*, 18808-18813.
[139] J. Q. Wang, S. Y. Su, B. Liu, M. H. Cao, C. W. Hu, *Chem. Commun.* **2013**, *49*, 7830-7832.
[140] T. Grewe, K. Meier, H. Tuysuz, *Catal. Today* **2014**, *225*, 142-148.
[141] X. Y. Wu, S. Yin, B. Liu, M. Kobayashi, M. Kakihana, T. Sato, *J. Mater. Chem. A* **2014**, *2*, 20832-20840.
[142] K. Li, A. D. Handoko, M. Khraisheh, J. W. Tang, *Nanoscale* **2014**, *6*, 9767-9773.
[143] A. Krukowska, G. Trykowski, M. J. Winiarski, T. Klimczuk, W. Lisowski, A. Mikolajczyk, H. P. Pinto, A. Zaleska-Medynska, *Appl. Surf. Sci.* **2018**, *441*, 993-1011.
[144] R. W. Wang, Y. F. Zhu, Y. F. Qiu, C. F. Leung, J. He, G. J. Liu, T. C. Lau, *Chem. Eng. J.* **2013**, *226*, 123-130.
[145] Y. Wang, Z. Chen, Z. Z. Ye, J. Y. Huang, *J. Cryst. Growth* **2012**, *341*, 42-45.
[146] H. B. Zhang, C. S. Wei, Y. Y. Huang, J. Wang, *Ultrason. Sonochem.* **2016**, *30*, 61-69.
[147] Y. Zhang, Y. Chen, Y. P. Zhang, X. Cheng, C. H. Feng, L. H. Chen, J. R. Zhou, S. P. Ruan, *Sens. Actuator B-Chem.* **2012**, *174*, 485-489.
[148] S. F. Jia, Y. P. Su, B. P. Zhang, Z. C. Zhao, S. Li, Y. F. Zhang, P. C. Li, M. Y. Xu, R. Ren, *Nanoscale* **2019**, *11*, 7690-7700.
[149] Y. Hu, W. Chen, M. W. Ba, W. G. Song, *Catal. Lett.* **2019**, *149*, 180-189.
[150] a) L. Bai, K. J. Zhu, L. K. Su, J. H. Qiu, H. L. Ji, *Mater. Lett.* **2010**, *64*, 77-79; b) L. K. Su, K. J. Zhu, J. H. Qiu, H. L. Ji, *J. Mater. Sci.* **2010**, *45*, 3311-3317; c) Z. Wang, H. S. Gu, Y. M. Hu, K. Yang, M. Z. Hu, D. Zhou, J. G. Guan, *CrystEngComm* **2010**, *12*, 3157-3162; d) F. Zhang, S. Bai, T. Karaki, *Phys. Status Solidi A-Appl. Mat.* **2011**, *208*, 1052-1055; e) M. Zhang, M. Guo, Y. Zhou, *Int. J. Appl. Ceram. Technol.* **2011**, *8*, 591-596; f) G. Stavber, B. Malic, M. Kosec, *Green Chem.* **2011**, *13*, 1303-1310; g) Z. Wang, Y. M. Hu, W. Wang, D. Zhou, Y. Wang, H. S. Gu, *Integr. Ferroelectr.* **2013**, *142*, 24-30; h) S. Bai, T. Karaki, *J. Am. Ceram. Soc.* **2013**, *96*, 2515-2518; i) D. Q. Zhang, F. Shin, J. Y. Cheng, Z. J. Cheng, X. Y. Yang, G. P. Zheng, M. S. Cao, *Ceram. Int.* **2015**, *41*, 8837-8842; j) D. Q. Zhang, Z. J. Cheng, J. Y. Cheng, F. Shi, X. Y. Yang, G. P. Zheng, M. S. Cao, *Ceram. Int.* **2016**, *42*, 9073-9078.
[151] a) A. D. Handoko, G. K. L. Goh, *Green Chem.* **2010**, *12*, 680-687; b) T. Maeda, N. Takiguchi, T. Morita, M. Ishikawa, T. Hemsel, *J. Korean Phys. Soc.* **2010**, *57*, 924-928; c) T. Maeda, T. Hemsel, T. Morita, *Jpn. J. Appl. Phys.* **2011**, *50*, 07hc01; d) R. Lopez-Juarez, O. Novelo-Peralta, F. Gonzalez-Garcia, F. Rubio-Marcos, M. E. Villafuerte-Castrejon, *J. Euro. Ceram. Soc.* **2011**, *31*, 1861-1864; e) K. Kanie, H. Mizutani, A. Terabe, Y. Numamoto, S. Tsukamoto, H. Takahashi, M. Nakaya, J. Tani, A. Muramatsu, *Jpn. J. Appl. Phys.* **2011**, *50*, 09nd09; f) D. Y. Jeong, S. H. Lee, H. C. Song, K. H. Choi, J. H. Cho, *J. Korean Phys. Soc.* **2011**, *58*, 663-667.
[152] a) L. A. Ramajo, F. Rubio-Marcos, A. Del Campo, J. F. Fernandez, M. S. Castro, R. Parra, *Ceram. Int.* **2014**, *40*, 14701-14712; b) Y. H. He, Z. Wang,

W. C. Jin, X. K. Hu, L. Y. Li, Y. H. Gao, X. H. Zhang, H. S. Gu, X. L. Wang, *Appl. Phys. Lett.* **2017**, *110*, 5.

[153] a) T. Shiraishi, H. Einishi, S. Yasui, M. Ishikawa, T. Hasegawa, M. Kurosawa, H. Uchida, Y. Sakashita, H. Funakubo, *Jpn. J. Appl. Phys.* **2011**, *50*, 09nd11; b) A. D. Handoko, G. K. L. Goh, *Thin Solid Films* **2011**, *519*, 5156-5160; c) T. Shiraishi, H. Einishi, S. Yasui, M. Ishikawa, T. Hasegawa, M. Kurosawa, H. Uchida, Y. Sakashita, H. Funakubo, *J. Ceram. Soc. Jpn.* **2013**, *121*, 627-631; d) T. Shiraishi, N. Kaneko, H. Einishi, T. Shimizu, M. Kurosawa, H. Uchida, T. Kobayashi, T. Kiguchi, T. J. Konno, H. Funakubo, *Jpn. J. Appl. Phys.* **2013**, *52*, 09ka11; e) T. Shiraishi, H. Einishi, S. Yasui, H. Funakubo, T. Hasegawa, M. Kurosawa, M. Ishikawa, H. Uchida, Y. Sakashita, *J. Korean Phys. Soc.* **2013**, *62*, 1055-1059; f) T. Shiraishi, H. Einishi, T. Shimizu, H. Funakubo, M. Kurosawa, H. Uchida, N. Kumada, T. Kiguchi, T. J. Konno, *J. Mater. Res.* **2016**, *31*, 693-701; g) T. Shiraishi, M. Ishikawa, H. Uchida, T. Kiguchi, M. K. Kurosawa, H. Funakubo, T. J. Konno, *Jpn. J. Appl. Phys.* **2017**, *56*, 10pf04; h) Y. Ito, A. Tateyama, Y. Nakamura, T. Shimizu, M. Kurosawa, H. Uchida, T. Shiraishi, T. Kiguchi, T. J. Konno, M. Ishikawa, H. Funakubo, *J. Ceram. Soc. Jpn.* **2019**, *127*, 478-484; i) Y. Ito, A. Tateyama, Y. Nakamura, T. Shimizu, M. Kurosawa, H. Uchida, T. Shiraishi, T. Kiguchi, T. J. Konno, M. Ishikawa, H. Funakubo, *Jpn. J. Appl. Phys.* **2019**, *58*, Sllb14; j) A. Tateyama, Y. Ito, Y. Nakamura, T. Shimizu, Y. Orino, M. Kurosawa, H. Uchida, T. Shiraishi, T. Kiguchi, T. J. Konno, N. Kumada, H. Funakubo, *J. Cryst. Growth* **2019**, *511*, 1-7.

[154] a) Y. Xu, Q. Yu, J. F. Li, *J. Mater. Chem.* **2012**, *22*, 23221-23226; b) X. H. Meng, W. Wang, H. Ke, J. C. Rao, D. C. Jia, Y. Zhou, *J. Mater. Chem. C* **2017**, *5*, 747-753; c) Y. H. He, Z. Wang, X. K. Hu, Y. X. Cai, L. Y. Li, Y. H. Gao, X. H. Zhang, Z. B. Huang, Y. M. Hu, H. S. Gu, *RSC Adv.* **2017**, *7*, 16908-16915.

[155] S. L. Skjaervø, K. H. Wells, W. van Beek, T. Grande, M. A. Einarsrud, *CrystEngComm* **2018**, *20*, 6795-6802.

[156] S. Toyama, H. Hayashi, M. Takesue, M. Watanabe, R. L. Smith, *J. Supercrit. Fluids* **2016**, *107*, 1-8.

[157] S. Park, M. Peddigari, J. H. Kim, E. Kim, G.-T. Hwang, J.-W. Kim, C.-W. Ahn, J.-J. Choi, B.-D. Hahn, J.-H. Choi, W.-H. Yoon, D.-S. Park, K.-I. Park, C. K. Jeong, J. W. Lee, Y. Min, *Inorg. Chem.* **2020**, *59*, 3042-3052.

[158] a) Y. M. Hu, H. S. Gu, D. Zhou, Z. Wang, H. L. W. Chan, Y. Wang, *J. Am. Ceram. Soc.* **2010**, *93*, 609-613; b) L. Li, Y. Q. Gong, L. J. Gong, H. Dong, X. F. Yi, X. J. Zheng, *Mater. Des.* **2012**, *33*, 362-366; c) P. Jana, V. A. D. O'Shea, C. M. Montero, P. Galvez, P. Pizarro, J. M. Coronado, D. P. Serrano, *Green Chem.* **2015**, *17*, 1735-1743; d) L. P. Chen, G. B. Qiu, B. Peng, M. Guo, M. Zhang, *Ceram. Int.* **2015**, *41*, 13331-13340; e) Y. Muto, T. Shiraishi, Y. Ito, A. Tateyama, H. Uchida, T. Kiguchi, H. Funakubo, T. J. Konno, *Jpn. J. Appl. Phys.* **2019**, *58*, Sllb12.

[159] A. D. Handoko, G. K. L. Goh, *CrystEngComm* **2013**, *15*, 672-678.

[160] T. Shiraishi, Y. Muto, Y. Ito, A. Tateyama, H. Uchida, T. Kiguchi, M. K. Kurosawa, H. Funakubo, T. J. Konno, *J. Ceram. Soc. Jpn.* **2019**, *127*, 388-393.

[161] F. F. Li, D. R. Liu, G. M. Gao, B. Xue, Y. S. Jiang, *Appl. Catal. B-Environ.* **2015**, *166*, 104-111.

[162] a) G. Q. Li, S. C. Yan, Z. Q. Wang, X. Y. Wang, Z. S. Li, J. H. Ye, Z. G. Zou, *Dalton Trans.* **2009**, 8519-8524; b) W. L. Wang, G. Q. Li, Y. Bai, N. Yang, W. F. Zhang, *J. Phys. Chem. Solids* **2011**, *72*, 1457-1461; c) H. B. Chang, M. Y. Shang, C. Y. Zhang, H. M. Yuan, S. H. Feng, *J. Am. Ceram. Soc.* **2012**, *95*, 3673-3677; d) B. F. Gao, D. S. Hu, C. X. Xiao, D. X. Li, B. Z. Lin, Y. L. Chen, Y. Zheng, *J. Phys. Chem. Solids* **2019**, *135*, 7.
[163] X. L. Chen, H. Q. Fan, Y. F. Fu, L. J. Liu, J. Chen, *J. Alloy. Compd.* **2009**, *469*, 322-326.
[164] S. Park, H. J. Song, C. W. Lee, S. W. Hwang, I. S. Cho, *ACS Appl. Mater. Interfaces* **2015**, *7*, 21860-21867.
[165] T. Ban, T. Kaiden, Y. Ohya, *Cryst. Growth Des.* **2019**, *19*, 6903-6910.
[166] a) M. Yoshimura, S. Song, S. Sōmiya, *Yogyo Kyokai shi* **1982**, *90*, 91-95; b) S. T. Song, H. Y. Pan, Z. Wang, B. Yang, *Ceram. Int.* **1984**, *10*, 143-146.
[167] J. C. Rendon-Angeles, K. Yanagisawa, Z. Matamoros-Veloza, M. I. Pech-Canul, J. Mendez-Nonell, S. Diaz-de la Torre, *J. Alloy. Compd.* **2010**, *504*, 251-256.
[168] a) L. R. Rivas-Vazquez, J. C. Rendon-Angeles, J. L. Rodriguez-Galicia, C. A. Gutierrez-Chavarria, K. J. Zhu, K. Yanagisawa, *J. Euro. Ceram. Soc.* **2006**, *26*, 81-88; b) L. P. Rivas-Vazquez, J. C. Rendon-Angeles, J. L. Rodriguez-Galicia, K. Zhu, K. Yanagisawa, *Solid State Ionics* **2004**, *172*, 389-392.
[169] W. J. Zheng, W. Q. Pang, G. Y. Meng, D. K. Peng, *J. Mater. Chem.* **1999**, *9*, 2833-2836.
[170] K. Sardar, M. R. Lees, R. J. Kashtiban, J. Sloan, R. I. Walton, *Chem. Mater.* **2011**, *23*, 48-56.
[171] M. C. Weber, J. Kreisel, P. A. Thomas, M. Newton, K. Sardar, R. I. Walton, *Phys. Rev. B* **2012**, *85*.
[172] a) L. M. Daniels, M. C. Weber, M. R. Lees, M. Guennou, R. J. Kashtiban, J. Sloan, J. Kreisel, R. I. Walton, *Inorg. Chem.* **2013**, *52*, 12161-12169; b) L. M. Daniels, R. J. Kashtiban, D. Kepaptsoglou, Q. M. Ramasse, J. Sloan, R. I. Walton, *Chem.-Eur. J.* **2016**, *22*, 18362-18367.
[173] S. Wang, K. K. Huang, B. N. Zheng, J. Q. Zhang, S. H. Feng, *Mater. Lett.* **2013**, *101*, 86-89.
[174] C. M. Hou, W. C. Feng, L. Yuan, K. K. Huang, S. H. Feng, *CrystEngComm* **2014**, *16*, 2874-2877.
[175] a) Y. J. Zhang, C. P. Yao, Y. Fan, M. Z. Zhou, *Mater. Res. Bull.* **2014**, *59*, 387-393; b) S. Wang, K. K. Huang, C. M. Hou, L. Yuan, X. F. Wu, D. Y. Lu, *Dalton Trans.* **2015**, *44*, 17201-17208.
[176] a) C. P. Yao, Y. J. Zhang, Y. Fan, M. Z. Zhou, H. Wu, *Cryst. Res. Technol.* **2015**, *50*, 566-573; b) S. Wang, C. M. Hou, L. Yuan, M. Y. Qu, B. Zou, D. Y. Lu, *Dalton Trans.* **2016**, *45*, 17593-17597; c) S. Wang, X. F. Wu, T. S. Wang, J. Q. Zhang, C. Y. Zhang, L. Yuan, X. Q. Cui, D. Y. Lu, *Inorg. Chem.* **2019**, *58*, 2315-2329.
[177] S. Wang, X. F. Wu, L. Yuan, C. Y. Zhang, D. Y. Lu, *CrystEngComm* **2017**, *19*, 6436-6442.
[178] H. N. Girish, G. Q. Shao, B. Basavalingu, *RSC Adv.* **2016**, *6*, 79763-79767.
[179] Y. Xu, S. Pirou, P. Zielke, S. B. Simonsen, P. Norby, P. V. Hendriksen, R. Kiebach, *Ind. Eng. Chem. Res.* **2018**, *57*, 2123-2130.
[180] J. M. D. Coey, M. Viret, S. von Molnar, *Adv. Phys.* **2009**, *58*, 567-569.
[181] D. Wang, R. B. Yu, S. H. Feng, W. J. Zheng, G. S. Pang, H. Zhao, *Chem. J. Chin. Univ.* **1998**, *19*, 165-168.

[182] a) J. Spooren, A. Rumplecker, F. Millange, R. I. Walton, *Chem. Mater.* **2003**, *15*, 1401-1403; b) J. Spooren, R. I. Walton, F. Millange, *J. Mater. Chem.* **2005**, *15*, 1542-1551.
[183] a) J. Spooren, R. I. Walton, *J. Solid State Chem.* **2005**, *178*, 1683-1691; b) A. Querejeta, A. Varela, M. Parras, F. del Monte, M. Garcia-Hernandez, J. M. Gonzalez-Calbet, *Chem. Mater.* **2009**, *21*, 1898-1905; c) J. H. Zhang, D. B. Yu, K. Du, F. Wang, D. P. Zhao, Y. Wang, L. L. Chen, M. G. Kong, J. W. Zou, *J. Cryst. Growth* **2013**, *380*, 163-168; d) I. N. Gonzalez-Jimenez, A. Torres-Pardo, M. Garcia-Hernandez, J. M. Gonzalez-Calbet, M. Parras, A. Varela, *Cryst. Growth Des.* **2015**, *15*, 2192-2203.
[184] B. B. Van Aken, T. T. M. Palstra, A. Filippetti, N. A. Spaldin, *Nat. Mater.* **2004**, *3*, 164-170.
[185] D. G. Tomuta, S. Ramakrishnan, G. J. Nieuwenhuys, J. A. Mydosh, *J. Phys.-Condes. Matter* **2001**, *13*, 4543-4552.
[186] M. H. Harunsani, J. Li, Y. B. Qin, H. T. Tian, J. Q. Li, H. X. Yang, R. I. Walton, *Appl. Phys. Lett.* **2015**, *107*, 062905.
[187] H. W. Zheng, Y. F. Liu, W. Y. Zhang, S. J. Liu, H. R. Zhang, K. F. Wang, *J. Appl. Phys.* **2010**, *107*, 053901.
[188] R. D. Kumar, R. Jayavel, *Mater. Lett.* **2013**, *113*, 210-213.
[189] S. Ishiwata, Y. Tokunaga, Y. Taguchi, Y. Tokura, *J. Am. Chem. Soc.* **2011**, *133*, 13818-13820.
[190] X. F. Chu, K. K. Huang, M. Han, S. H. Feng, *Inorg. Chem.* **2013**, *52*, 4130-4132.
[191] S. Datta, S. Chandra, S. Samanta, K. Das, H. Srikanth, B. Ghosh, *J. Nanomater.* **2013**, 6.
[192] Z. Q. Zhou, L. Guo, F. Ye, *J. Alloy. Compd.* **2013**, *571*, 123-131.
[193] S. A. Acharya, S. M. Khule, V. M. Gaikwad, *Mater. Res. Bull.* **2015**, *67*, 111-117.
[194] M. J. Zhi, G. W. Zhou, Z. L. Hong, J. Wang, R. Gemmen, K. Gerdes, A. Manivannan, D. L. Ma, N. Q. Wu, *Ener. Environ. Sci.* **2011**, *4*, 139-144.
[195] M. Aneja, A. Tovstolytkin, G. S. Lotey, *J. Magn. Magn. Mater.* **2017**, *442*, 423-428.
[196] K. K. Huang, L. Yuan, Y. L. Jiang, J. X. Zhang, Z. B. Geng, L. Q. Luo, S. H. Feng, *Inorg. Chem. Front.* **2018**, *5*, 732-738.
[197] D. Makovec, T. Gorsak, K. Zupan, D. Lisjak, *J. Cryst. Growth* **2013**, *375*, 78-83.
[198] K. K. Huang, W. C. Feng, L. Yuan, J. X. Zhang, X. F. Chu, C. M. Hou, X. F. Wu, S. H. Feng, *CrystEngComm* **2014**, *16*, 9842-9846.
[199] N. M. Islam, T. Noguchi, Y. Hakuta, H. Hayashi, *Nanosci. Nanotech. Lett.* **2011**, *3*, 324-327.
[200] S. Diodati, R. I. Walton, S. Mascotto, S. Gross, *in preparation* **2020**.
[201] J. G. Wu, Z. Fan, D. Q. Xiao, J. G. Zhu, J. Wang, *Prog. Mater. Sci.* **2016**, *84*, 335-402.
[202] S. M. Lam, J. C. Sin, A. R. Mohamed, *Mater. Res. Bull.* **2017**, *90*, 15-30.
[203] C. Chen, J. R. Cheng, S. W. Yu, L. J. Che, Z. Y. Meng, *J. Cryst. Growth* **2006**, *291*, 135-139.
[204] J. T. Han, Y. H. Huang, X. J. Wu, C. L. Wu, W. Wei, B. Peng, W. Huang, J. B. Goodenough, *Adv. Mater.* **2006**, *18*, 2145-2148.
[205] Z. C. Qiu, J. P. Zhou, G. Q. Zhu, X. M. Chen, R. L. Yang, Y. H. Song, P. Liu, *J. Nanosci. Nanotechnol.* **2012**, *12*, 6552-6557.

[206] C. Ponzoni, R. Rosa, M. Cannio, V. Buscaglia, E. Finocchio, P. Nanni, C. Leonelli, *J. Alloy. Compd.* **2013**, *558*, 150-159.
[207] Z. W. Chen, W. L. Jin, *J. Mater. Sci.-Mater. Electron.* **2014**, *25*, 4039-4045.
[208] R. Dhanalakshmi, M. Muneeswaran, P. R. Vanga, M. Ashok, N. V. Giridharan, *Appl. Phys. A-Mater. Sci. Process.* **2016**, *122*, 14.
[209] C. M. Cho, J. H. Noh, I. S. Cho, J. S. An, K. S. Hong, J. Y. Kim, *J. Am. Ceram. Soc.* **2008**, *91*, 3753-3755.
[210] a) S. Li, Y. H. Lin, B. P. Zhang, Y. Wang, C. W. Nan, *J. Phys. Chem. C* **2010**, *114*, 2903-2908; b) J. Li, D. Z. Yan, *Ceram. Int.* **2018**, *44*, 18271-18278.
[211] D. R. Cai, J. M. Li, T. Tong, D. R. Jin, S. W. Yu, J. R. Cheng, *Mater. Chem. Phys.* **2012**, *134*, 139-144.
[212] a) U. A. Joshi, J. S. Jang, P. H. Borse, J. S. Lee, *Appl. Phys. Lett.* **2008**, *92*, 3; b) G. Biasotto, A. Z. Simoes, C. R. Foschini, M. A. Zaghete, J. A. Varela, E. Longo, *Mater. Res. Bull.* **2011**, *46*, 2543-2547; c) X. Y. Sun, Z. W. Liu, H. Y. Yu, Z. G. Zheng, D. C. Zeng, *Mater. Lett.* **2018**, *219*, 225-228.
[213] X. Y. Li, Z. X. Tang, H. D. Ma, F. Wu, R. H. Jian, *Appl. Phys. A-Mater. Sci. Process.* **2019**, *125*, 6.
[214] H. L. You, Z. Wu, L. H. Zhang, Y. R. Ying, Y. Liu, L. F. Fei, X. X. Chen, Y. M. Jia, Y. J. Wang, F. F. Wang, S. Ju, J. L. Qiao, C. H. Lam, H. T. Huang, *Angew. Chem., Int. Ed.* **2019**, *58*, 11779-11784.
[215] A. Huang, A. D. Handoko, G. K. L. Goh, P. K. Pallathadka, S. Shannigrahi, *CrystEngComm* **2010**, *12*, 3806-3814.
[216] J. L. Mi, T. N. Jensen, M. Christensen, C. Tyrsted, J. E. Jorgensen, B. B. Iversen, *Chem. Mater.* **2011**, *23*, 1158-1165.
[217] M. Yoshimura, K. Yamasawa, S. Sōmiya, *Yogyo Kyokai shi* **1982**, *90* 521-527.
[218] Y. Abe, I. Satou, T. Aida, T. Adschiri, *Ceram. Int.* **2018**, *44*, 12996-13003.
[219] W. J. Zheng, R. H. Liu, D. K. Peng, G. Y. Meng, *Mater. Lett.* **2000**, *43*, 19-22.
[220] a) L. Yuan, K. K. Huang, S. Wang, C. M. Hou, X. F. Wu, B. Zou, S. H. Feng, *Cryst. Growth Des.* **2016**, *16*, 6522-6530; b) E. M. Kostyukhin, A. L. Kustov, L. M. Kustov, *Ceram. Int.* **2019**, *45*, 14384-14388; c) F. Tong, Y. Zhao, M. H. Wang, *Micro & Nano Letters* **2019**, *14*, 259-262.
[221] K. K. Huang, L. Yuan, S. H. Feng, *Inorg. Chem. Front.* **2015**, *2*, 965-981.
[222] J. Q. Zhang, K. K. Huang, L. Yuan, S. H. Feng, *CrystEngComm* **2018**, *20*, 470-476.
[223] a) Y. J. Zhang, A. Zheng, X. Z. Yang, H. M. He, Y. Fan, C. P. Yao, *CrystEngComm* **2012**, *14*, 8432-8439; b) Z. Q. Zhou, L. Guo, H. X. Yang, Q. Liu, F. Ye, *J. Alloy. Compd.* **2014**, *583*, 21-31; c) M. Zhou, H. Yang, T. Xian, J. Y. Ma, H. M. Zhang, W. J. Feng, Z. Q. Wei, J. L. Jiang, *J. Alloy. Compd.* **2014**, *617*, 855-862; d) Y. Wang, X. C. Yan, J. Chen, J. X. Deng, R. B. Yu, X. R. Xing, *CrystEngComm* **2014**, *16*, 858-862; e) C. Y. Zhang, M. Y. Shang, M. L. Liu, T. S. Zhang, L. Ge, H. M. Yuan, S. H. Feng, *J. Alloy. Compd.* **2016**, *665*, 152-157.
[224] a) V. I. Popkov, O. V. Almjasheva, *Nanosystems: Physics, Chemistry, Mathematics* **2014**, *5*, 703–708; b) A. V. Racu, D. H. Ursu, O. V. Kuliukova, C. Logofatu, A. Leca, M. Miclau, *Mater. Lett.* **2015**, *140*, 107-110; c) V. I. Popkov, O. V. Almjasheva, A. S. Semenova, D. G. Kellerman, V. N. Nevedomskiy, V. V. Gusarov, *J. Mater. Sci.-Mater. Electron.* **2017**, *28*, 7163-7170.

[225] M. Y. Shang, C. Y. Zhang, T. S. Zhang, L. Yuan, L. Ge, H. M. Yuan, S. H. Feng, *Appl. Phys. Lett.* **2013**, *102*, 3.
[226] M. Inoue, T. Nishikawa, T. Nakamura, T. Inui, *J. Am. Ceram. Soc.* **1997**, *80*, 2157-2160.
[227] a) S. Hosokawa, H. J. Jeon, M. Inoue, *Res. Chem. Int.* **2011**, *37*, 291-296; b) S. Hosokawa, H. J. Jeon, S. Iwamoto, M. Inoue, *J. Am. Ceram. Soc.* **2009**, *92*, 2847-2853.
[228] C. I. Hiley, M. R. Lees, D. L. Hammond, R. J. Kashtiban, J. Sloan, R. I. Smith, R. I. Walton, *Chem. Commun.* **2016**, *52*, 6375-6378.
[229] C. I. Hiley, M. R. Lees, J. M. Fisher, D. Thompsett, S. Agrestini, R. I. Smith, R. I. Walton, *Angew. Chem., Int. Ed.* **2014**, *53*, 4423-4427.
[230] H. N. Girish, M. S. V. Kumar, K. Byrappa, B. Basavalingu, *Mater. Res. Innov.* **2015**, *19*, 270-274.
[231] B. Basavalingu, M. S. V. Kumar, H. N. Girish, S. Yoda, *J. Alloy. Compd.* **2013**, *552*, 382-386.
[232] S. D. Sun, S. H. Liang, *J. Mater. Chem. A* **2017**, *5*, 20534-20560.
[233] R. J. Guo, Y. P. Guo, H. A. Duan, H. Li, H. Z. Liu, *ACS Appl. Mater. Interfaces* **2017**, *9*, 8271-8279.
[234] a) W. Wang, J. Bi, L. Wu, Z. Li, X. Fu, *Scr. Mater.* **2009**, *60*, 186-189; b) W. J. Wang, S. J. Liang, K. N. Ding, J. H. Bi, J. C. Yu, P. K. Wong, L. Wu, *J. Mater. Sci.* **2014**, *49*, 1893-1902; c) F. L. Zhong, H. Q. Zhuang, Q. Gu, J. L. Long, *RSC Adv.* **2016**, *6*, 42474-42481.
[235] a) S. Zhao, Y. Bai, W. F. Zhang, *Electrochim. Acta* **2010**, *55*, 3891-3896; b) H. S. Kim, S. S. Park, S. H. Kang, Y. E. Sung, *J. Appl. Electrochem.* **2014**, *44*, 789-796.
[236] a) X. L. Pang, Y. Zhang, L. H. Ding, Z. H. Su, W. F. Zhang, *J. Nanosci. Nanotechnol.* **2010**, *10*, 1860-1864; b) Z. Fu, H. K. Yang, B. K. Moon, B. C. Choi, J. H. Jeong, *J. Nanosci. Nanotechnol.* **2011**, *11*, 1629-1631.
[237] F. A. Guo, G. Q. Li, N. Yang, W. L. Wang, W. F. Zhang, *Appl. Phys. A-Mater. Sci. Process.* **2012**, *107*, 813-817.
[238] S. Sumithra, N. V. Jaya, *J. Mater. Sci.-Mater. Electron.* **2018**, *29*, 4048-4057.
[239] X. Y. Hu, T. Xiao, W. Huang, W. Tao, B. J. Heng, X. Q. Chen, Y. W. Tang, *Appl. Surf. Sci.* **2012**, *258*, 6177-6183.
[240] X. Y. Mei, L. J. Bie, C. H. Ma, H. B. Huang, R. H. Liu, W. J. Zheng, Y. F. Xia, *Chin. J. Inorg. Chem.* **2008**, *24*, 218-224.
[241] L. Y. Wu, J. M. Ma, H. B. Huang, R. F. Tian, W. J. Zheng, Y. F. Hsia, *Materials Characterization* **2010**, *61*, 548-553.
[242] M. Li, H. M. Yuan, W. Xu, M. Han, L. R. Yao, M. Yang, S. H. Feng, *Chem. Res. Chin. Univ.* **2012**, *28*, 788-791.
[243] M. H. K. Rubel, T. Takei, N. Kumada, M. M. Ali, A. Miura, K. Tadanaga, K. Oka, M. Azuma, M. Yashima, K. Fujii, E. Magome, C. Moriyoshi, Y. Kuroiwa, J. R. Hester, M. Aydeev, *Chem. Mater.* **2016**, *28*, 459-465.
[244] M. H. K. Rubel, T. Takei, N. Kumada, M. M. Ali, A. Miura, K. Tadanaga, K. Oka, M. Azuma, E. Magome, C. Moriyoshi, Y. Kuroiwa, *Inorg. Chem.* **2017**, *56*, 3174-3181.
[245] M. H. K. Rubel, M. M. Ali, M. S. Ali, R. Parvin, M. M. Rahaman, M. Hossain, M. I. Hossain, A. Islam, N. Kumada, *Solid State Commun.* **2019**, *288*, 22-27.
[246] G. H. Zhang, G. B. Li, F. Q. Huang, F. H. Liao, K. Li, Y. X. Wang, J. H. Lin, *J. Alloy. Compd.* **2011**, *509*, 9804-9808.

[247] H. Jiang, N. Kumada, Y. Yonesaki, T. Takei, N. Kinomura, M. Yashima, M. Azuma, K. Oka, Y. Shimakawa, *Jpn. J. Appl. Phys.* **2009**, *48*, 010216.
[248] H. Jiang, N. Kumada, Y. Yonesaki, T. Takei, N. Kinomura, *J. Ceram. Soc. Jpn.* **2009**, *117*, 214-216.
[249] M. H. K. Rubel, A. Miura, T. Takei, N. Kumada, M. M. Ali, M. Nagao, S. Watauchi, I. Tanaka, K. Oka, M. Azuma, E. Magome, C. Moriyoshi, Y. Kuroiwa, A. Islam, *Angew. Chem., Int. Ed.* **2014**, *53*, 3599-3603.
[250] M. H. K. Rubel, T. Takei, N. Kumada, M. M. Ali, A. Miura, K. Tadanaga, K. Oka, M. Azuma, E. Magomae, C. Moriyoshi, Y. Kuroiwa, *J. Alloy. Compd.* **2015**, *634*, 208-214.
[251] M. Saiduzzaman, H. Yoshida, T. Takei, S. Yanagida, N. Kumada, M. Nagao, H. Yamane, M. Azuma, M. H. K. Rubel, C. Moriyoshi, Y. Kuroiwa, *Inorg. Chem.* **2019**, *58*, 11997-12001.
[252] H. B. Qin, H. L. Zhang, B. P. Zhang, L. H. Xu, *J. Am. Ceram. Soc.* **2011**, *94*, 3671-3674.
[253] S. Wada, S. Shimizu, K. Yamashita, I. Fujii, K. Nakashima, N. Kumada, Y. Kuroiwa, Y. Fujikawa, D. Tanaka, M. Furukawa, *Jpn. J. Appl. Phys.* **2011**, *50*, 09nc08.
[254] S. Wada, K. Yamashita, I. Fujii, K. Nakashima, N. Kumada, C. Moriyoshi, Y. Kuroiwa, Y. Fujikawa, D. Tanaka, M. Furukawa, *Jpn. J. Appl. Phys.* **2012**, *51*, 09lc05.
[255] J. E. Wang, C. Baek, Y. H. Jung, D. K. Kim, *Appl. Surf. Sci.* **2019**, *487*, 278-284.
[256] M. Ito, M. Hagiwara, S. Fujihara, *J. Ceram. Soc. Jpn.* **2017**, *125*, 454-457.
[257] Q. Zhang, Y. Huang, S. Q. Peng, T. T. Huang, J. J. Cao, W. K. Ho, S. Lee, *Appl. Catal. B-Environ.* **2018**, *239*, 1-9.
[258] M. L. Lv, Y. H. Xie, Y. W. Wang, X. Q. Sun, F. F. Wu, H. M. Chen, S. W. Wang, C. Shen, Z. F. Chen, S. Ni, G. Liu, X. X. Xu, *Phys. Chem. Chem. Phys.* **2015**, *17*, 26320-26329.
[259] R. N. Wang, S. Ni, G. Liu, X. X. Xu, *Appl. Catal. B-Environ.* **2018**, *225*, 139-147.
[260] J. W. Shi, J. H. Ye, Z. H. Zhou, M. T. Li, L. J. Guo, *Chem.-Eur. J.* **2011**, *17*, 7858-7867.
[261] J. W. Shi, S. C. Zong, Y. C. Hu, X. J. Guan, J. Y. Luo, Y. Shang, G. X. Li, D. Y. Liu, X. Wang, P. H. Guo, *RSC Adv.* **2016**, *6*, 51801-51806.
[262] S. T. Li, Y. Yue, X. J. Ning, M. Guo, M. Zhang, *J. Alloy. Compd.* **2014**, *586*, 248-256.
[263] X. F. Zhou, C. Jiang, H. Luo, C. Chen, K. C. Zhou, D. Zhang, *Ceram. Int.* **2016**, *42*, 18631-18640.
[264] R. U. Fassbender, T. S. Lilge, S. Cava, J. Andres, L. F. da Silva, V. R. Mastelaro, E. Longo, M. L. Moreira, *Phys. Chem. Chem. Phys.* **2015**, *17*, 11341-11349.
[265] A. Yoko, M. Akizuki, N. Umezawa, T. Ohno, Y. Oshima, *RSC Adv.* **2016**, *6*, 67525-67533.
[266] a) J. Ng, S. P. Xu, X. W. Zhang, H. Y. Yang, D. D. Sun, *Adv. Funct. Mater.* **2010**, *20*, 4287-4294; b) T. P. Cao, Y. J. Li, C. H. Wang, C. L. Shao, Y. C. Liu, *Langmuir* **2011**, *27*, 2946-2952.
[267] W. G. Yang, Y. H. Yu, M. B. Starr, X. Yin, Z. D. Li, A. Kvit, S. F. Wang, P. Zhao, X. D. Wang, *Nano Lett.* **2015**, *15*, 7574-7580.

[268] W. L. Liu, G. Q. Tan, P. Xiong, X. Xue, H. F. Hao, H. J. Ren, *J. Mater. Sci.-Mater. Electron.* **2014**, *25*, 2348-2354.
[269] L. Yuan, K. K. Huang, C. M. Hou, W. C. Feng, S. Wang, C. P. Zhou, S. H. Feng, *New. J. Chem.* **2014**, *38*, 1168-1172.
[270] S. Wang, X. F. Wu, L. Yuan, C. Y. Zhang, X. Q. Cui, D. Y. Lu, *CrystEngComm* **2018**, *20*, 3034-3042.
[271] Z. G. Li, Y. X. Wang, J. W. Liu, G. Chen, Y. X. Li, C. Zhou, *Int. J. Hydrog. Energy* **2009**, *34*, 147-152.
[272] L. K. Su, K. J. Zhu, L. Bai, J. H. Qiu, H. L. Ji, *J. Alloy. Compd.* **2010**, *493*, 186-191.
[273] X. Li, J. L. Zang, *Catal. Commun.* **2011**, *12*, 1380-1383.
[274] L. J. An, H. Onishi, *ACS Catal.* **2015**, *5*, 3196-3206.
[275] X. Q. Liu, J. J. Lv, S. Wang, X. Li, J. Y. Lang, Y. G. Su, Z. L. Chai, X. J. Wang, *J. Alloy. Compd.* **2015**, *622*, 894-901.
[276] F. L. Wang, Y. Li, N. Wang, L. Zhu, A. Jain, Y. G. Wang, F. G. Chen, *J. Alloy. Compd.* **2019**, *810*, 6.
[277] L. Guo, Z. Q. Zhou, *J. Magn. Magn. Mater.* **2018**, *458*, 164-170.
[278] L. Guo, Z. Q. Zhou, H. M. Yuan, *J. Alloy. Compd.* **2014**, *616*, 454-460.
[279] H. Xua, C. T. Liu, H. M. Li, Y. G. Xu, J. X. Xia, S. Yin, L. Liu, X. Y. Wu, *J. Alloy. Compd.* **2011**, *509*, 9157-9163.
[280] J. Qian, Y. Xue, Y. H. Ao, P. F. Wang, C. Wang, *Chin. J. Catal.* **2018**, *39*, 682-692.
[281] W. Zou, J. L. Wang, Z. Z. Chen, N. Shi, Z. Li, Z. Z. Cui, X. N. Li, X. F. Yin, W. S. Yan, H. L. Huang, R. R. Peng, Z. P. Fu, Y. L. Lu, *J. Mater. Chem. C* **2018**, *6*, 9.
[282] J. H. Peng, M. Hojamberdiev, H. Q. Li, D. L. Mao, Y. J. Zhao, P. Liu, J. P. Zhou, G. Q. Zhu, *J. Magn. Magn. Mater.* **2015**, *378*, 298-305.
[283] N. Pienack, W. Bensch, *Angew. Chem., Int. Ed.* **2011**, *50*, 2014-2034.
[284] a) Y. Zhou, Y. H. Lin, G. R. Patzke, *Prog. Chem.* **2012**, *24*, 1583-1591; b) K. M. Ø. Jensen, C. Tyrsted, M. Bremholm, B. B. Iversen, *ChemSusChem* **2014**, *7*, 1594-1611.
[285] D. Saha, K. M. Ø. Jensen, C. Tyrsted, E. D. Bojesen, A. H. Mamakhel, A. C. Dippel, M. Christensen, B. B. Iversen, *Angew. Chem., Int. Ed.* **2014**, *53*, 3667-3670.
[286] A. Yoko, M. Akizuki, N. Hirao, S. Kohara, M. Kumar, N. Umezawa, T. Ohno, Y. Oshima, *J. Supercrit. Fluids* **2016**, *107*, 746-752.
[287] O. G. Grendal, A. B. Blichfeld, S. L. Skjaervo, W. van Beek, S. M. Selbach, T. Grande, M. A. Einarsrud, *Crystals* **2018**, *8*, 11.
[288] G. Philippot, K. M. Ø. Jensen, M. Christensen, C. Elissalde, M. Maglione, B. B. Iversen, C. Aymonier, *J. Supercrit. Fluids* **2014**, *87*, 111-117.
[289] M. M. Lencka, R. E. Riman, *Chem. Mater.* **1993**, *5*, 61-70.
[290] a) V. S. T. Ciminelli, A. Dias, *Ferroelectrics* **2000**, *241*, 271-278; b) A. Dias, *J. Sol. Chem.* **2011**, *40*, 1126-1139; c) N. K. V. Nadimpalli, R. Bandyopadhyaya, V. Runkana, *Fluid Ph. Equilibria* **2018**, *456*, 33-45.
[291] P. Raccuglia, K. C. Elbert, P. D. F. Adler, C. Falk, M. B. Wenny, A. Mollo, M. Zeller, S. A. Friedler, J. Schrier, A. J. Norquist, *Nature* **2016**, *533*, 73-76.
[292] a) E. Kim, K. Huang, A. Saunders, A. McCallum, G. Ceder, E. Olivetti, *Chem. Mater.* **2017**, *29*, 9436-9444; b) E. Kim, K. Huang, A. Tomala, S. Matthews, E. Strubell, A. Saunders, A. McCallum, E. Olivetti, *Sci. Data* **2017**, *4*; c) E. Kim, K. Huang, S. Jegelka, E. Olivetti, *Npj Comput. Mater.* **2017**, *3*.

[293] O. Kononova, H. Y. Huo, T. J. He, Z. Q. Rong, T. Botari, W. H. Sun, V. Tshitoyan, G. Ceder, *Sci. Data* **2019**, *6*.
[294] O. M. Valuiskaya, B. K. Nefedov, O. A. Kanakova, A. M. Zubkov, *Chem. Tech. Fuels Oils* **1989**, *25*, 340-342.
[295] X. Buisson, R. Arnaud, *J. Phys. IV Coll.* **1994**, *04* C2-25-C22-32.
[296] a) N. Millot, B. Xin, C. Pighini, D. Aymes, *J. Euro. Ceram. Soc.* **2005**, *25*, 2013-2016; b) T. Adschiri, Y. W. Lee, M. Goto, S. Takami, *Green Chem.* **2011**, *13*, 1380-1390; c) P. W. Dunne, A. S. Munn, C. L. Starkey, T. A. Huddle, E. H. Lester, *Phil. Trans. Roy. Soc. A* **2015**, *373*; d) J. A. Darr, J. Y. Zhang, N. M. Makwana, X. L. Weng, *Chem. Rev.* **2017**, *117*, 11125-11238; e) P. Caramazana, P. Dunne, M. Gimeno-Fabra, J. McKechnie, E. Lester, *Curr. Opin. Green Sus. Chem.* **2018**, *12*, 57-62.
[297] a) A. Aimable, B. Xin, N. Millot, D. Aymes, *J. Solid State Chem.* **2008**, *181*, 183-189; b) A. Yoko, M. Akizuki, Y. Oshima, *J. Nanopart. Res.* **2014**, *16*, 9.
[298] G. Philippot, C. Elissalde, M. Maglione, C. Aymonier, *Adv. Powder Technol.* **2014**, *25*, 1415-1429.
[299] P. W. Dunne, C. L. Starkey, A. S. Munn, S. V. Y. Tang, O. Luebben, I. Shvets, A. G. Ryder, Y. Casamayou-Boucau, L. Morrison, E. H. Lester, *Chem. Eng. J.* **2016**, *289*, 433-441.
[300] B. Sun, W. X. Zhao, H. W. Li, L. J. Wei, P. Chen, *Chem. Phys. Lett.* **2014**, *613*, 100-103.
[301] C. Laberty, A. Navrotsky, C. N. R. Rao, P. Alphonse, *J. Solid State Chem.* **1999**, *145*, 77-87.
[302] a) J. Spooren, *Hydrothermal Synthesis of Manganites, PhD Thesis, University of Exeter* **2004**; b) L. M. Daniels, *Structures and Properties of Perovskites and Pyrochlores from Hydrothermal Synthesis, PhD Thesis, University of Warwick* **2015**.
[303] a) J. B. Liu, H. Wang, M. K. Zhu, B. Wang, H. Yan, *Mater. Res. Bull.* **2003**, *38*, 817-822; b) J. J. Urban, L. Ouyang, M. H. Jo, D. S. Wang, H. Park, *Nano Lett.* **2004**, *4*, 1547-1550; c) S. S. Rao, K. N. Anuradha, S. Sarangi, S. V. Bhat, *Appl. Phys. Lett.* **2005**, *87*; d) C. P. Li, T. Li, B. Wang, H. Yan, *J. Cryst. Growth* **2006**, *295*, 137-140; e) F. Teng, W. Han, S. H. Liang, B. G. Gaugeu, R. L. Zong, Y. F. Zhu, *J. Catal.* **2007**, *250*, 1-11; f) S. Liang, F. Teng, G. Bulgan, Y. Zhu, *J. Phys. Chem. C* **2007**, *111*, 16742-16749; g) Y. Chen, H. M. Yuan, G. Tian, G. H. Zhang, S. H. Feng, *J. Solid State Chem.* **2007**, *180*, 167-172; h) J. G. Deng, Y. Zhang, H. X. Dai, L. Zhang, H. He, C. T. Au, *Catal. Today* **2008**, *139*, 82-87; i) J. G. Deng, L. Zhang, H. X. Dai, C. T. Au, *Catal. Lett.* **2009**, *130*, 622-629; j) F. Teng, *Solid State Sci.* **2009**, *11*, 1643-1648.

Biography

Richard Walton is Professor Chemistry at the University of Warwick and his research group is working in the field of inorganic materials, focussed on the use of innovative synthesis methods for functional solids. This spans zeotypes and metal-organic frameworks through to condensed oxides, with an emphasis on solution-based synthesis routes and characterisation using diffraction and spectroscopy including at synchrotron and neutron facilities. Practical applications are explored and exploited through various industrial collaborations including in areas such as heterogeneous catalysis and ionic conductors. He is presently an editor of the *Inorganic Materials Series* published by the Royal Society of Chemistry.

Table of Contents Entry

Crystallisation of perovskite oxides from water or other polar solvents is reviewed, illustrating the scope for control of chemical composition, nanoscale form and crystal structure. This includes solids containing transition-metals and main group elements, extending to solid-solutions and intergrowths. The materials produced have a variety of useful properties from ferroelectricity, magnetism and conductivity to heterogeneous catalysis.